Title
Carbon Nanotube Films for Energy Storage Applications

Author
Kozinda, Alina

Publication Date
2014

Peer reviewed|Thesis/dissertation

Carbon Nanotube Films for Energy Storage Applications

By

Alina Kozinda

A dissertation submitted in partial satisfaction of the

requirements for the degree of

Doctor of Philosophy

in

Engineering - Mechanical Engineering

In the

Graduate Division

of the

University of California, Berkeley

Committee in Charge:

Professor Liwei Lin, Chair
Professor Dorian Liepmann
Professor Roya Maboudian

Fall 2014

Abstract

Carbon Nanotube Films for Energy Storage Applications

by

Alina Kozinda

Doctor of Philosophy in Engineering – Mechanical Engineering

University of California, Berkeley

Professor Liwei Lin, Chair

With the rising demands for small, lightweight, and long-lasting portable electronics, the need for energy storage devices with both large power and large energy densities becomes vitally important. From their usage in hybrid electric vehicles to wearable electronics, supercapacitors and rechargeable batteries have been the focus of many previous works. Electrode materials with large specific surface areas can enhance the charging speed and total amount of stored energy. To this end, vertically self-aligned carbon nanotube (CNT) forests are well suited, as they possess outstanding electrical conductivities as well as high mechanical strength and large specific surface areas. In addition, forests of vertically aligned CNTs allow the ions within an electrolyte to pass freely between the individual CNTs from electrode to electrode. In order to minimize the system resistance of the battery or supercapacitor, a thin molybdenum current collector layer is deposited beneath catalyst of the CNT forest, thus ensuring that when the CNT forest grows from its substrate, each CNT has an innate connection to the current collector. This versatile CNT-Mo film architecture is used in this work as both supercapacitor as well as lithium-ion battery electrodes.

It is desirable to have energy storage devices of adjustable shapes, such that they may conform to the shrinking form factors of modern portable electronics and mechanically flexible electrodes are an attractive prospect. The CNT-Mo film is shown here to easily release from its growth substrate, after which it may be placed onto a number of

surfaces and topographies and densified. Two polymer films, Kapton® and Thermanox™, have been used as substrates for the demonstrations of flexible supercapacitor electrodes. Test results show that the attached active CNT-Mo film can withstand bending to at least as large an angle as 180°. The specific capacitance of a 5 mm by 5 mm area electrode in the K_2SO_4 aqueous electrolyte with an original CNT height of 40 µm is measured to be 7.0 mF/cm^2. To further increase the surface area of the energy storage electrode, a thin, conformal coating of amorphous silicon is deposited onto a vertically aligned carbon nanotube forest using low pressure chemical vapor deposition (LPCVD). Various silicon film thickness depositions are tested as supercapacitor electrodes. A coating of 35 nm is shown to improve the specific capacitance by a factor of 2 as compared to a bare CNT electrode.

For applications in which a larger operating voltage is desirable, the electrochemical window of the supercapacitor devices are increased by tailoring the electrolyte used. Using an ionic liquid electrolyte (1-ethyl-3-methylimidazolium tetrafluoroborate, or EMIM-BF_4) improves the voltage window from 1 V (in aqueous electrolyte) to 4 V, yielding a power density from the range of 19 to 53 kW/kg. In addition, the CNT-Mo film is shown to outperform an activated carbon (AC) electrode in this ionic liquid in terms of volumetric capacitance by a factor of 12 (388 mF/cm^3 versus 31 mF/cm^3 for the CNT-Mo film and the AC, respectively). The cycling life of the film in ionic liquid at a number of current densities is also analyzed, and shown to be stable over 7000 charge-discharge cycles. Finally, the CNT-Mo film architecture is further utilized and tested as a lithium ion battery electrode. The high surface area, excellent CNT conductivities, and the extremely high lithium ion intercalation capacity of silicon all promise long-lived and energy-dense lithium ion electrodes. Preliminary results show high energy density of 4000 mAh/g initially. The value quickly drops to 600 mAh/g after 5 charge/discharge cycles and stay the same until failure after 15 cycles. Further studies into thinner silicon coatings and electrolyte selections may result in better performance and longer cycling life.

Acknowledgements

To all of the amazing colleagues, mentors, and professors that I have had the pleasure to work with and be mentored by, I give my thanks and appreciation. Thank you for your inspiration, your tireless help, and for the many coffee breaks.

To my family, my deepest thanks for always believing in me.

And a special thank you to Liwei for his support and mentorship throughout the years.

Table of Contents

List of Figures

Chapter 1: Introduction to Supercapacitors, Lithium-Ion Batteries, and Carbon Nanotubes

Chapter Summary

This chapter introduces the concept of supercapacitor and lithium-ion battery storage devices, and will lay the groundwork for the following chapters relating to the use of carbon nanotubes in these devices.

Introduction

The demands for better energy storage devices in terms of higher energy density and higher power density have been and will continue to be important research topics. Specifically, the permeation of portable electronics calls for lightweight, small form factor energy storage systems with fast charge and large storage capacities. The latter two qualities are related to power density and energy density, respectively, which are good metrics for describing the performance of various energy storage devices. For

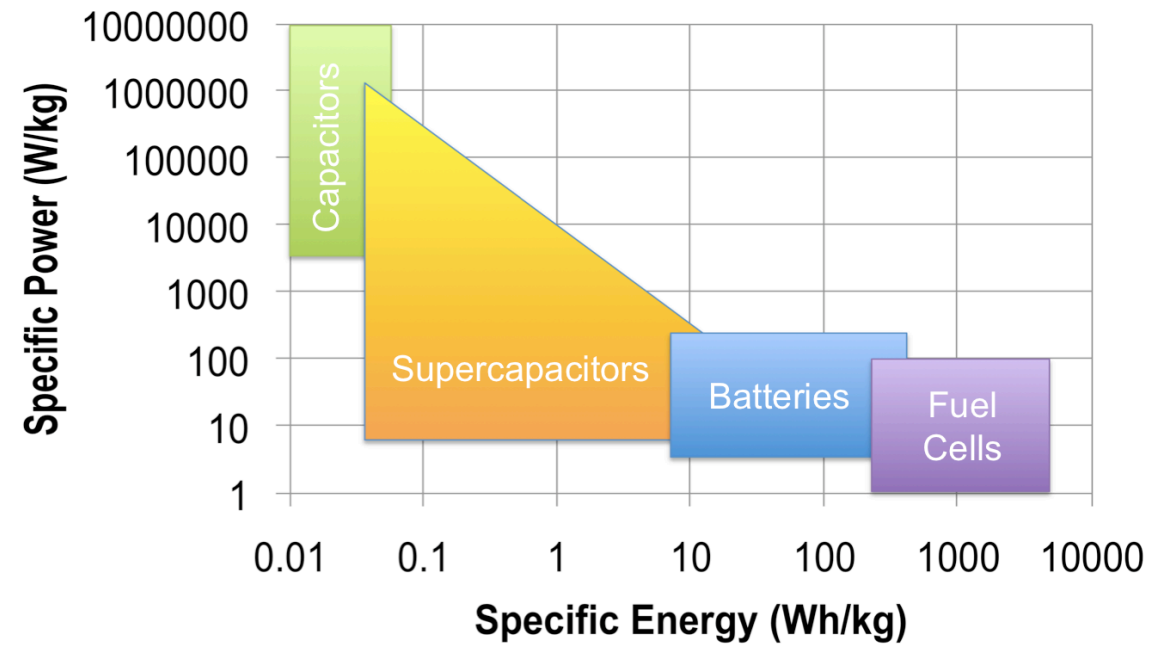

Figure 1-1: Ragone plot comparing various energy storage devices in terms of their specific power values and specific energy values, as extracted from [1].

example, devices such as capacitors have very high specific power, and others such as fuel cells have very high specific energy. It is difficult to manufacture a device that has both of these sought-after characteristics, and increasing one property normally comes at the expense of the other. However, supercapacitors and batteries live in the realm between capacitors and fuel cells, and span the gap between high levels of power and energy density, as can be seen in Figure 1-1 [1].

Supercapacitors (also known as ultracapacitors, electric double-layer capacitors, and electrochemical capacitors) share some similarities with parallel plate capacitors. The devices are both composed of two parallel and opposing electrodes, and store energy between those two electrodes. But while a parallel plate capacitor contains a dielectric structure, which separates the two opposing electrodes. A supercapacitor contains an electrolyte and separator, as shown in Figure 1-2. The separator functions

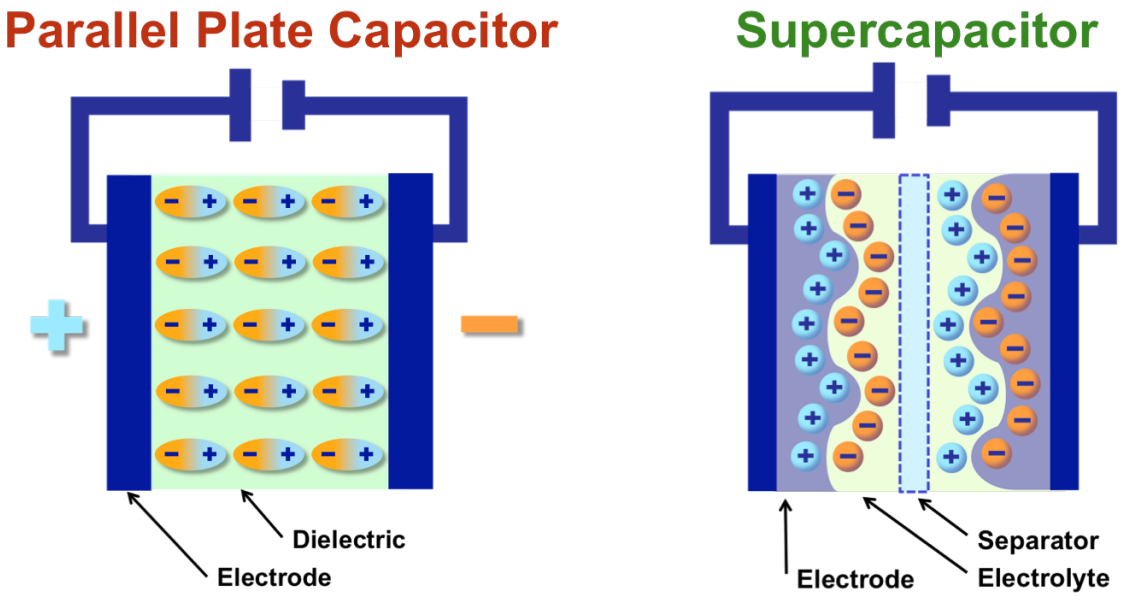

Figure 1-2: Schematic illustration of a supercapacitor (right), and how it compares to a traditional, parallel plate capacitor (left).

as an ion-permeable membrane which ensures the opposing electrodes do not make electrical contact and create a short. The electrolyte may be a liquid or solid ion-conducting medium, and must be able to wet or coat the working electrodes. Upon the application of a voltage across the parallel plate capacitor, an electric field forms across the dielectric material between the plates, and charge accumulates at each plate. In contrast, when a voltage is applied across a supercapacitor, the electrolyte between the two electrodes becomes polarized, and ions accumulate at the surface of both electrodes, while charge accumulates within the electrode material. The ion accumulation at the interface between the electrode surface and the electrolyte is called the electrical double layer, or EDL. It is this layer that is responsible for storing charge in a supercapacitor. As the size of the EDL increases, more charge may be stored. Thus, as the surface area of the supercapacitor increases, more energy may be stored. This same information is given by [2]:

$$C = \frac{\varepsilon_0 \varepsilon_r A}{d} \qquad (1)$$

where C is capacitance, ε_0 and ε_r are the electric and dielectric constants, A is the surface area of the electrodes, and d is the thickness of the EDL. Compared to the parallel plate capacitor, supercapacitor has a much smaller value for d. The separation between the parallel plates of a traditional capacitor is on the order of microns, while the thickness of the EDL is on the order of molecular dimensions. In addition, the surface area of the supercapacitor is much greater than that of a parallel plate capacitor, due to the electrodes being textured and normally nanostructured. The upshot of the supercapacitor having a large surface area and smaller charge separation is that its capacitance is several orders of magnitude larger than that of a parallel plate capacitor [3].

The very quick charge and discharge capability of supercapacitors gives them a good deal of desirability for use in portable electronics and electric vehicles. They are currently used in camera flashes, rechargeable screwdrivers (which retain 85% of their charge after three months of being idle on a shelf, and can be recharged in 90 s [4]), recoverable energy from vehicle braking, hybrid buses, and as buffer power and voltage stabilizers. Supercapacitors may be used in just about anything that batteries are used in, and in even more applications that batteries cannot. According to IDTechEx, a market research company looking at emerging technologies, the global supercapacitor market is said to grow to $6.5 Billion by the year 2024 [5]. Another research firm predicts a market size of $3.5 Billion by 2020 – an increase of almost 1500% to 800% over 2013's market size of $446 million [6,7]. Supercapacitors are said to be improving at a faster rate than lithium ion batteries, and a gradual increase in supercapacitors combined with a decrease in lithium-ion batteries leads to these much-improved market values [8]. Out of the various rechargeable or secondary battery systems, lithium ion has the highest growth and is obtaining the most investment [9].

While supercapacitors can charge and discharge very quickly (on the order of seconds), secondary, or rechargeable batteries, can take hours to recharge. This is due to the physical differences in the energy storage mechanism. The charge storage mechanism of supercapacitors is one where no electrons or material is exchanged between the electrode and electrolyte – electrolyte ions adsorb onto the surface of the electrode, while electrons within the electrode align at the surface, matching the electrolyte ions in an electric double layer. Rechargeable batteries, however, depend on the transfer of ions between the electrolyte and electrodes to store charge. In the case of lithium-ion batteries, lithium ions are exchanged between the opposing electrodes and the electrolyte, as can be seen in Figure 1-3. This mechanism takes a much longer time to complete to reach a full electrode charge – sometimes on the order of several hours. If the battery is pushed to charge too fast, lithium alloying at the electrode occurs, leading to a reduced cycle life, degradation in performance, and safety issues [10].

In addition, supercapacitors have cycling lifetimes of millions of cycles, compared to just thousands for rechargeable batteries. Instead of replacing burnt-out lithium ion batteries, supercapacitors will simply outlive the device in which they are placed.

Notwithstanding the clear advantages of supercapacitors, lithium ion batteries are still

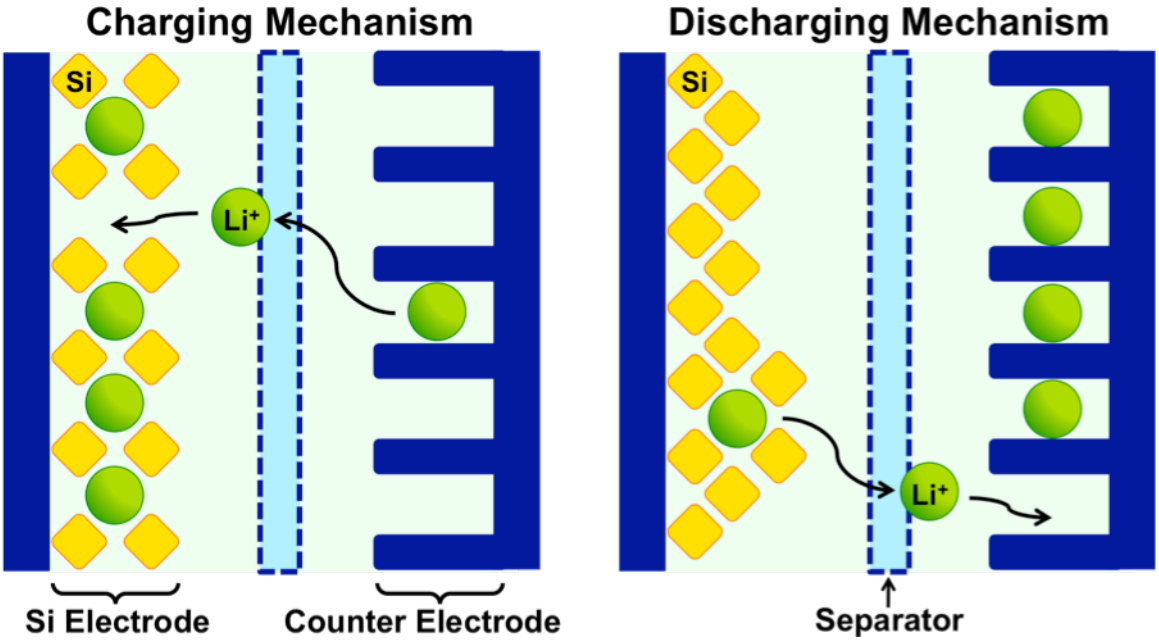

Figure 1-3: Charging and discharging mechanism of a lithium-ion battery.

needed in applications where the amount of energy stored in a small space (e.g. energy density) is important, such as in full-electric vehicles. After all, supercapacitors store only about one-tenth the amount of energy that a lithium ion battery does for the same weight. With ongoing research, lithium ion battery technology continues to improve. Since Sony introduced the first commercial Li-ion battery in 1991 for a portable phone, these batteries have infiltrated cell phones, video cameras, laptops, and more [11].

Carbon Nanotubes

So what do we make these things out of? In both cases – for supercapacitors as well as Li-ion batteries – surface area is a factor of high importance. As mentioned previously, surface area directly relates to the size of the electric double layer of the supercapacitor electrode, which is a measure of the electrode's capacitance, or how much energy it can store. Thus, in order to increase the amount of energy stored in a supercapacitor electrode, one may increase the surface area of that electrode. Commercial supercapacitors typically use activated carbon as their electrode material, due to its stability, good electrical conductivity, and high surface area [3].

However, activated carbon is limited by its relatively low effective pore area, the high internal resistance between the carbon particles, and the low ion transport rates through its microporous structure [3]. Carbon nanotubes (CNTs), on the other hand, possess outstanding electrical conductivities as well as mechanical strength and high surface areas. In addition, forests of CNTs innately grow in a vertically aligned fashion, which allows the ions within the electrolyte to pass freely between the individual CNTs

from electrode to electrode, unlike in activated carbon, where the electrolyte ion paths are tortuous [12]. Due to these advantages, carbon nanotubes have been studied by various research groups as a material for use in supercapacitor electrodes [3,13-16]. An SEM image is included in Figure 1-4 showing a CNT forest growing on a wafer's edge.

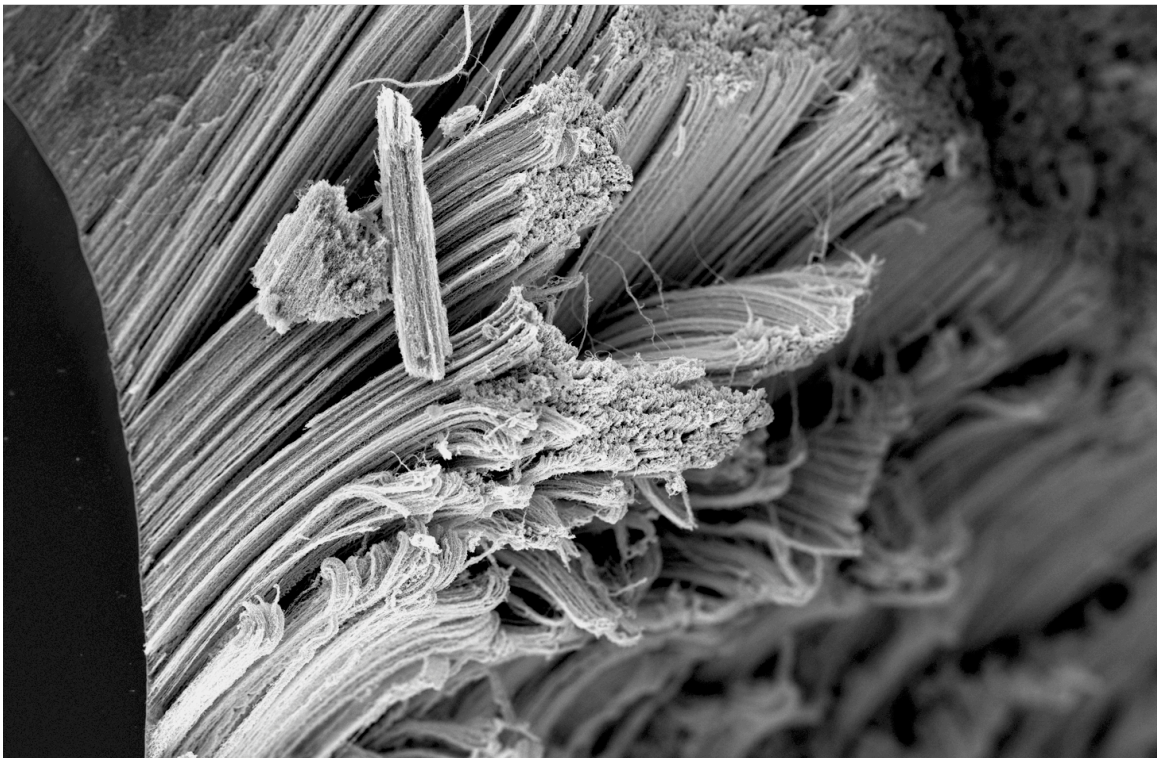

Figure 1-4: SEM image of the edge of a carbon nanotube forest. The carbon nanotubes are about 100 nm tall.

A number of various approaches to fabricate CNT supercapacitor electrodes have been reported to meet various design requirements in modern electronics. Since CNTs are grown at high temperatures, typically around 700°C, a transfer process is required to move the CNTs from their growth substrate to a fragile, flexible, or temperature-sensitive functional substrate. This transfer process often involves cleaving the CNTs from their growth substrate and drop casting them onto the receiving substrate, creating a mesh or network of CNTs [17-20]. An additional step is then often necessary to add a current collector layer, since the conductivity of CNT forests is affected by the orientation of the CNTs. The conductivity parallel to the tubes (or perpendicular to the growth substrate in the case of CNT forests) is about 60 times higher than the conductivity perpendicular to the tube [16]. This is understandable since electrons mostly travel within individual tubes when flowing parallel to the tubes, but must jump from tube to tube frequently when they flow in a perpendicular direction to the tubes, thus facing numerous contact resistances. By using an aligned CNT forest grown on a current collector, the electrode minimizes the system internal resistance,

and, as a result, increases the maximum output power, decreases the time it takes to charge and discharge the device, and reduces internal losses.

The vertically aligned CNT forest electrode has a good deal of utility as a lithium ion battery electrode as well, due to the aforementioned properties of the CNTs – high mechanical strength, excellent conductivity, and high surface area. However, the capacity of CNTs for storing lithium ions is significantly smaller than that of the highest capacity material, silicon (372 mAh/g for CNTs versus 4200 mAh/g for silicon). Silicon is abundant and safe, but bulk silicon tends to pulverize after just a few charge-discharge cycles in a lithium ion battery [21-23]. However, utilizing flexible CNTs as a supportive scaffolding for the silicon has been shown to relieve somewhat the stresses undergone by silicon during the charging and discharging processes, and improves the battery's cycling life [24,25].

Dissertation Goals and Structure

The goals of this dissertation are to provide a simple yet excellent architecture for the electrodes of energy storage devices – specifically for supercapacitor and lithium ion battery applications, as seen in Figure 1-5. This architecture is a vertically aligned carbon

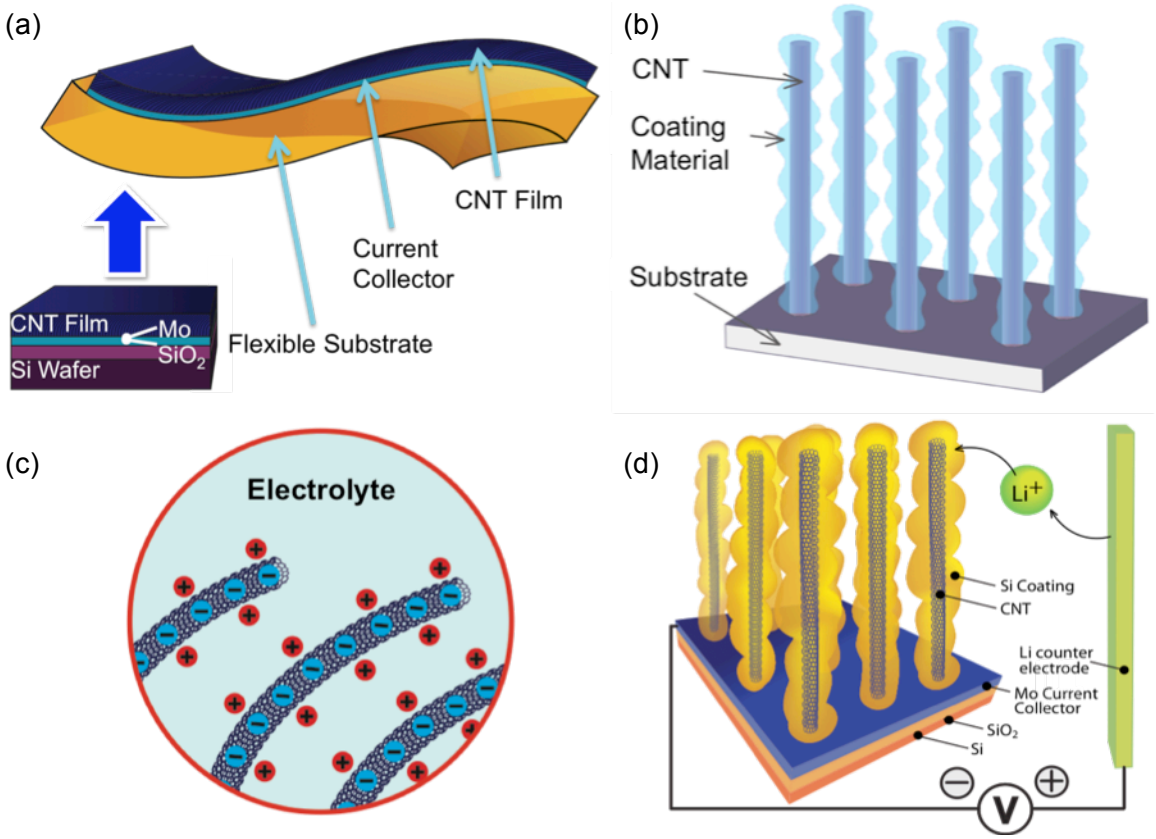

Figure 1-5: Goals of this work: (a) a flexible energy storage electrode with supercapacitor applications, (b) supercapacitor electrode with increased surface area, (c) increased supercapacitor voltage window using an ionic liquid electrolyte, and (d) a lithium-ion battery electrode.

nanotube forest with an innate thin film current collector to which each CNT is attached. Specific capacitance, voltage window, cycling performance, and charge-discharge performance are assessed, as well as the rate of LPCVD silicon deposition onto the CNT forest.

Chapter 2 describes the growth of vertically aligned carbon nanotube forests on an electrically conductive metal thin film (molybdenum), and the facile way in which the CNT-Mo film may be lifted from its growth substrate and placed onto a flexible or thermally fragile substrate for use as a supercapacitor electrode.

Chapter 3 details a simple manner by which to increase the surface area of an energy storage electrode. A thin, conformal coating of amorphous silicon is deposited onto a vertically aligned carbon nanotube forest using low pressure chemical vapor deposition (LPCVD). Various silicon film thickness depositions are tested as supercapacitor electrodes, and shown to improve the specific capacitance.

Chapter 4 shows how the electrochemical window of a supercapacitive device may be increased by tailoring the electrolyte used. In this chapter, an ionic liquid electrolyte (1-ethyl-3-methylimidazolium tetrafluoroborate, or EMIM-BF_4) is chosen and tested – improving the voltage window from 1 V (in aqueous electrolyte) to 4 V.

Chapter 5 presents how the architecture used in the above chapters may also be utilized in a lithium ion battery electrode. A silicon coating throughout the CNT forest creates a high surface area electrode, with some promising results.

Finally, chapter 6 concludes this dissertation, reviewing the energy storage applications of aligned carbon nanotube films discussed in this work, as well as some remarks and possible future works going forward.

References

[1] M Winter and R J Brodd, "What Are Batteries, Fuel Cells, and Supercapacitors?," *Chemical Reviews*, vol. 104, no. 10, pp. 4245-4269, Nov 2004.

[2] J R Miller, "Capacitors - Overview," *Encyclopedia of Electrochemical Power Sources*, pp. 587–599, Nov 2009.

[3] A G Pandolfo and A F Hollenkamp, "Carbon properties and their role in supercapacitors," *Journal of Power Sources*, vol. 157, pp. 11-27, May 2006.

[4] E Sofge, "Coleman's FlashCell: Yes, a Cordless Screwdriver That Really Charges in 90 Seconds," *Popular Mechanics*, Oct 2009. [Online]. http://www.popularmechanics.com/technology/gadgets/4223118

[5] P Harrop, V Zhitomirsky, and F Gonzalez, "Electrochemical Double Layer Capacitors: Supercapacitors," *IDTechEx*, Nov 2014. [Online]. http://www.idtechex.com/research/reports/electrochemical-double-layer-capacitors-supercapacitors-2014-2024-000378.asp?viewopt=showall

[6] "Ultracapacitor Market Forecast 2015-2020," *Market Research Media*, Nov 2014. [Online]. http://www.marketresearchmedia.com/?p=912

[7] C Jacques, "Market for Supercapacitors to Grow 128% to $836 Million in 2018," *Lux Research*, Oct 2013. [Online]. http://www2.luxresearchinc.com/news-and-events/press-releases/201.html

[8] T Henry, "Supercapacitors can destroy the lithium-ion battery market," *IDTechEx*, Jun 2014. [Online]. http://www.idtechex.com/research/articles/supercapacitors-can-destroy-the-lithium-ion-battery-market-00006649.asp

[9] C Pillot, "The Worldwide Battery Market 2011-2025," *Batteries 2012 Conference*, Oct 2012.

[10] Aurelien Du Pasquier, Irene Plitz, Serafin Menocal, and Glenn Amatucci, "A comparative study of Li-ion battery, supercapacitor and nonaqueous asymmetric hybrid devices for automotive applications," *Journal of Power Sources*, vol. 115, no. 1, pp. 171-178, Mar 2003.

[11] W Schalkwijk and B Scrosati, "Advances in Lithium Ion Batteries," pp. 481 - 505, Nov 2002.

[12] K Hata, "Water-Assisted Highly Efficient Synthesis of Impurity-Free Single-Walled Carbon Nanotubes," *Science*, vol. 306, pp. 1362-1364, Nov 2004.

[13] P Simon and Y Gogotsi, "Materials for electrochemical capacitors," *Nature Materials*, vol. 7, pp. 845-854, Oct 2008.

[14] E Frackowiak and F Begui, "Carbon materials for the electrochemical storage of energy in capacitors," *Carbon*, vol. 39, pp. 937-950, Apr 2001.

[15] C Peng, S Zhang, Jewell D., and G Z Chen, "Carbon nanotube and conducting polymer composites for supercapacitors ," *Progress in Natural Science*, vol. 18, pp. 777-788, May 2008.

[16] H Zhang, G Cao, and Y Yang, "Electrochemical properties of ultra-long, aligned, carbon nanotube array electrode in organic electrolyte," *Journal of Power Sources*, vol. 172, no. 1, pp. 476-480, 2007.

[17] J.N Barisci*, G.G Wallace*, and R.H Baughman, "Electrochemical studies of single-wall carbon nanotubes in aqueous solutions," *Journal of Electroanalytical Chemistry*, vol. 488, no. 2, pp. 92-98, 2000.

[18] E B Sansom, D Rinderknecht, and M Gharib, "Controlled partial embedding of carbon nanotubes within flexible transparent layers," *Nanotechnology*, vol. 19, p. 035302, Dec 2008.

[19] Po-Chiang Chen, Guozhen Shen, Saowalak Sukcharoenchoke, and Chongwu Zhou, "Flexible and transparent supercapacitor based on In[sub 2]O[sub 3] nanowire/carbon nanotube heterogeneous films," *Applied Physics Letters*, vol. 94, no. 4, p. 043113, Jan 2009.

[20] Shan Hu, Rajesh Rajamani, and Xun Yu, "Flexible solid-state paper based carbon nanotube supercapacitor," *Applied Physics Letters*, vol. 100, no. 10, p. 104103, Jan 2012.

[21] T L Kulova, Y V Pleskov, A M Skundin, E I Terukov, and O I Kon'kov, "Lithium Intercalation into Amorphous-Silicon Thin Films: An Electrochemical-Impedance Study," *Russian Journal of Electrochemistry*, vol. 42, no. 7, pp. 708-714, Nov 2006.

[22] Uday Kasavajjula, Chunsheng Wang, and A. John Appleby, "Nano- and bulk-silicon-based insertion anodes for lithium-ion secondary cells," *Journal of Power Sources*, vol. 163, no. 2, pp. 1003-1039, Jan 2007.

[23] I Lahiri et al., "High Capacity and Excellent Stability of Lithium Ion Battery Anode Using Interface-Controlled Binder-Free Multiwall Carbon Nanotubes Grown on Copper," *ACS nano*, vol. 4, no. 6, pp. 3440-3446, 2010.

[24] L.F Cui, L Hu, J.W Choi, and Y Cui, "Light-Weight Free-Standing Carbon Nanotube-Silicon Films for Anodes of Lithium Ion Batteries," *ACS nano*, vol. 4, no. 7, pp. 3671-3678, 2010.

[25] K Evanoff et al., "Ultra Strong Silicon-Coated Carbon Nanotube Nonwoven Fabric as a Multifunctional Lithium-Ion Battery Anode," *ACS nano*, vol. 6, no. 11, pp. 9837-9845, Oct 2012.

[26] M. F. L De Volder, S. H Tawfick, R. H Baughman, and A. J Hart, "Carbon Nanotubes: Present and Future Commercial Applications," *Science*, vol. 339, pp. 535-539, Feb 2013.

[27] H Zhang, G Cao, and Y Yang, "Electrochemical properties of ultra-long, aligned, carbon nanotube array electrode in organic electrolyte," *Journal of Power Sources*,

vol. 172, no. 1, pp. 476-480, 2007.

[28] H Lin et al., "Twisted Aligned Carbon Nanotube/Silicon Composite Fiber Anode for Flexible Wire-Shaped Lithium-Ion Battery," *Advanced Materials*, vol. 26, pp. 1217-1222, Nov 2014.

[29] K Evanoff et al., "Ultra Strong Silicon-Coated Carbon Nanotube Nonwoven Fabric as a Multifunctional Lithium-Ion Battery Anode," *ACS nano*, vol. 6, no. 11, pp. 9837-9845, Oct 2012.

[30] Jung-Keun Yoo, Jongsoon Kim, Yeon Sik Jung, and Kisuk Kang, "Scalable Fabrication of Silicon Nanotubes and their Application to Energy Storage," *Advanced Materials*, vol. 24, no. 40, pp. 5452-5456, Jul 2012.

[31] Hui Wu et al., "Stable cycling of double-walled silicon nanotube battery anodes through solid-electrolyte interphase control," *Nature Nanotechnology*, vol. 7, no. 5, pp. 310-315, Mar 2012.

[32] K H An et al., "Supercapacitors using single-walled carbon nanotube electrodes," *Advanced Materials*, vol. 13, no. 7, pp. 497-500, Nov 2001.

[33] Y Fang et al., "Self-supported supercapacitor membranes: Polypyrrole-coated carbonnanotube networkse nabled by pulsed electrodeposition," *Journal of Power Sources*, vol. 195, pp. 674-679, Aug 2010.

[34] Y Fan, Q Zhang, Q Xiao, X Wang, and K Huang, "High performance lithium ion battery anodes based on carbon nanotube–silicon core–shell nanowires with controlled morphology," *Carbon*, vol. 59, pp. 264-269, Nov 2013.

[35] X Su et al., "Silicon-Based Nanomaterials for Lithium-Ion Batteries: A Review," *Advanced Energy Materials*, vol. 4, p. 1300882, Jan 2014.

Chapter 2: A Mechanically Flexible CNT/Mo Supercapacitor Electrode

Chapter Summary

In this chapter a physically flexible energy storage device is developed. Aligned carbon nanotube (CNT) forests with inherent bottom metal current collector layers are used to construct the flexible electrodes. Using a lift-off and CNT forest densification process, the thin CNT forests along with their current collector are placed onto an easily bendable substrate. The flexible CNT structure is fabricated and tested as a supercapacitor electrode with the following characteristics: (1) excellent transfer of charge from the aligned CNTs to the bottom contact metal layer, (2) a simple and straightforward fabrication process, and (3) easy integration with a variety of surfaces and topographies. Experimental results have shown that a 5 mm by 10 mm electrode with a 40 µm-thick CNT forest and a 50 nm-thick molybdenum bottom metal contact is transferred from a silicon growth substrate onto a 200 µm-thick Al/Thermanox^{TM} plastic substrate. The attached film can withstand a bending of at least as large as 180°. A measured specific capacitance of 7.0 mF/cm^2 has been achieved. Repeated mechanical bending tests followed by electrochemical cyclic voltammogram measurements have shown good device stability. As such, flexible energy storage devices composed of CNT forests with built-in metal electrodes may have broad applications in modern systems that demand components with adaptable shapes to fit into small form factors and ergonomic designs.

Introduction

As the demand for energy continues to rise, and as portable and small electronics pervade every corner of our daily lives, the need for energy storage devices with high power and energy densities becomes vitally important. Not only did one-third off all American households own a tablet computer in 2013, but 91% off American adults owned a mobile phone as well. And now that the market for wearables is exploding (set to quintuple in size within the next decade), the necessity of small but powerful and long-lasting energy storage devices is evident [1-3]. Furthermore, due to the decreasing size and weight of these electronics, the energy storage devices must also shrink. Hence it is desirable to have energy storage devices of adjustable shape, such that they may conform to small form factors. Thus, mechanically flexible electrodes within these storage devices may be an attractive prospect.

The research and development of energy storage devices has been progressively cultivated through these past decades. Two devices of note are especially intriguing – supercapacitors [4-7] and rechargeable (or secondary) batteries [4,8-10], as both have good power and energy densities. Supercapacitors and rechargeable batteries are both good solutions to our energy storage needs, however, their use needs to be tailored to the specific application in mind. First, these devices differ in a number of ways. A charged supercapacitor stores its charge at the interface of the electrode and electrolyte. This layer is known as the electrochemical double layer (EDL), is

nanometers-thick, and extends across the entire accessible surface area of the supercapacitor electrode [4]. In contrast, a rechargeable battery stores charge by employing a redox reaction during the charging process. In order to accommodate the intercalation of ions, the electrode material of a battery undergoes large volumetric changes. These large changes in volume can pulverize the electrode material, and further decrease charge and discharge speeds. For instance, the charge-discharge process in lithium ion (Li-ion) batteries tends to deposit residual material within the battery electrolyte, which then slows ion transport and in effect increase overall resistance and decreasing battery life. Li-ion batteries, for this reason, have lifetimes in the thousands of cycles. However, the electrostatic charge storage mechanism of supercapacitors enables them to charge and discharge quickly, with lifetimes in the millions of cycles.

As mentioned previously in Chapter 1, supercapacitors benefit greatly from a large electrode surface area. And while activated carbon is commonly used in industrial supercapacitors, this material is limited by relatively low effective pore areas, high internal resistances between its constituent carbon particles, and low ion transport rates [7]. CNTs, however, have excellent electrical conductivities as well as mechanical strength and good flexibility, and vertically aligned CNT forests provide an easy transfer of electrolyte ions and could be useful in flexible supercapacitor applications [11]. In addition, CNT forests can be synthesized by several facile chemical vapor deposition (CVD) methods [12-14]. Because of these advantageous properties, supercapacitor electrodes based on CNTs have been studied by various research groups [5-7, 15-18].

A number of methods to arrive at flexible CNT electrodes have been reported that meet various design needs in modern electronics. CNTs are typically grown at high temperatures (around 700°C), which is high enough to damage many substrates such as polymers. Hence, a transfer process is needed. Because CNT forest conductivity is anisotropic (conductivity parallel to the CNTs is 60X greater than across the CNTs), a current collector needs to be added as well [19]. These issues can be easily addressed by utilizing a vertically aligned CNT forest grown atop a conductive metal layer. This will minimize the system internal resistance, and, as a result, lower the time to charge and discharge, and hence increase the maximum output power.

There have been a few methods used to build flexible CNT electrodes. One approach makes use of printing or electrodeposition techniques, which result in networks, or mats, of CNTs [20-22]. For instance, Kaempgen et al. sprayed suspensions single-walled CNTs onto polyethylene-terephthalate substrates, and realized CNT networks with randomly entangled CNTs networks [20]. In this case, the CNT network functioned as both the electrode and current collecting layer, but had a large system resistance as well as a fixed electrode thickness. Some direct transfers of entire CNT forests onto flexible substrates also appears in previous work [23-25]. The usual production process of these electrodes is made up of several steps. First, the forests are usually partially embedded in a somewhat melted polymer substrate. Then, the polymer is dried, and finally the substrate that the CNT forest was originally attached to is removed, leaving the

embedded CNTs in the cured polymer substrate. However, a current collector still needs to be added, and normally is applied using a metal deposition process [23].

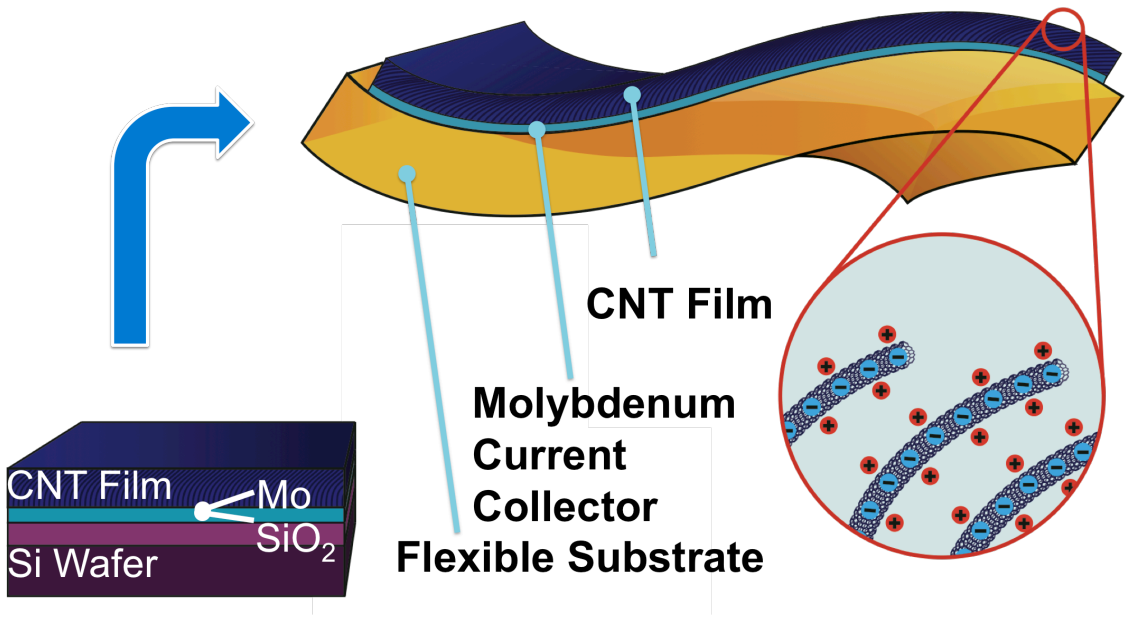

Figure 2-1: Schematic illustration of the flexible supercapacitor electrode using a water assisted, lift-off process. (Top) After the CNT forest–Mo film has been placed onto a flexible substrate. (Bottom) After the growth of CNTs on top of an oxidized silicon substrate and the separation from the substrate. Circular inset shows the electrical double layer effect upon charging of the CNT forest electrode in electrolyte.

The concept for the work in this chapter is illustrated in Figure 2-1 – an active CNT forest atop a flexible substrate for use in energy storage devices. This offers unique advancements over prior works. First, the CNT forests herein are directly grown atop a conductive metal layer so that each CNT is electrically connected to the molybdenum metal current collector. Second, both the current collector layer as well as the CNT forest remain whole and intact during the transfer of the CNT-Mo film to its target substrate. The current collector layer (Mo) obviates the need to deposit a metal contact after the liftoff and transfer have occurred. Finally, the CNTs are well aligned before the transfer process, and remain so after as well. This alignment allows for low electrical contact resistance, unlike CNT networks fabricated in a random fashion [26]. Both the metal current collector and the densified CNT forest are thin (tens of nanometers, and single-digit microns, respectively), which lends the CNT-Mo film the ability to be bent, or mechanically deformed, after transfer to a flexible substrate. Furthermore, the densification process allows the electrode to achieve high volumetric energy density, which are useful for supercapacitor applications [27].

Design and fabrication

The fabrication process of the CNT-Mo flexible supercapacitor electrode is illustrated in Figure 2-2. First, a vertically aligned CNT forest is fabricated. To this end, a silicon wafer is thermally oxidized, after which a molybdenum current-collecting layer is deposited onto the wafer using electron-beam evaporation, yielding a Mo thickness of 50 nm.

Next, the CNT catalyst is evaporated (also using electron-beam evaporation, although thermal evaporation may also be used) onto the Mo layer. Namely, 10 nm of aluminum and 5 nm of iron. Whereas iron may be used by itself at times for CNT growth, aluminum is added here as a buffer layer between the Fe and Mo layers, to help prevent

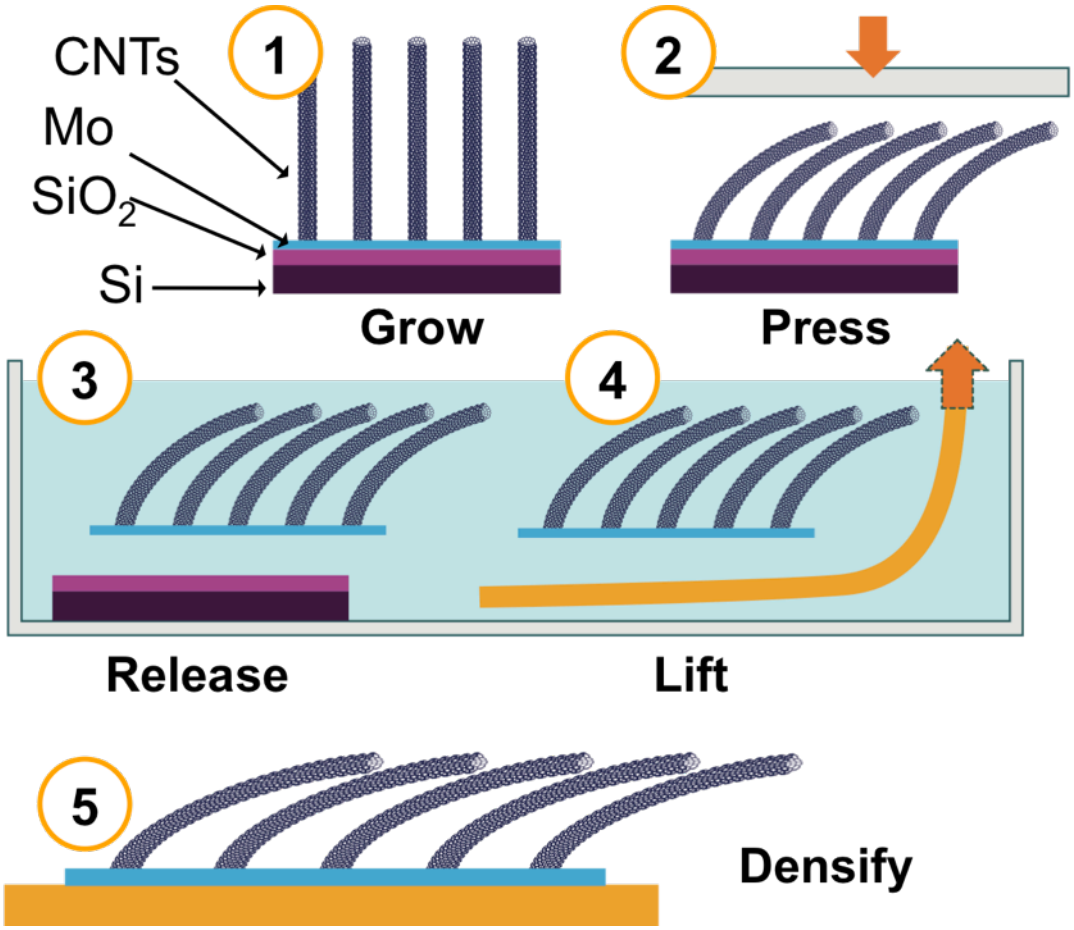

Figure 2-2: Fabrication steps of the flexible CNT-Mo film electrode: (1) a vertically self-aligned CNT forest is grown after thermal oxidation of a silicon wafer and subsequent metal layer deposition; (2) The CNT forest is mechanically pre-pressed; (3) the CNT–Mo film is released by submerging the specimen in DI water; (4) the film is lifter out of the liquid onto a flexible substrate; and (5) The CNT forest is densified during the drying process.

the Fe from alloying with the underlying Mo. If the Fe were to alloy with the Mo layer, it would not be able to properly act as a catalyst for CNT growth. After these steps, the CNT forest may finally be grown. The metal-layered silicon wafer is placed into a vacuum

quartz tube furnace (Lindberg/Blue M® three-zone tube furnace, Thermo Electron Corp., Asheville, NC), and the quartz holding tube is evacuated then purged with hydrogen gas until the pressure inside the tube reaches atmospheric pressure. Next, the temperature is increased 720°C. Once the temperature is stabilized, hydrogen (carrier gas) and ethylene (carbon precursor) are passed through the quartz tube at volumetric flow rates of approximately 7:1, respectively. The chemical vapor deposition (CVD) growth process continues for 10 minutes, after which the quartz tube furnace is powered off. The quartz holding tube is then allowed to cool to room temperature, and the gas inside the tube is evacuated, then purged back to atmospheric pressure using argon gas. This process (all encompassed in step 1 in the schematic in Figure 2-2), yields a vertically self-aligned CNT forest grown on a metal contact layer. As shown in previous work, the contact resistance between the Mo current collector and the CNT forest film is 5×10^{-3} Ωcm^2 [28].

Now that the CNT forest has been fabricated, the CNT-Mo film may be transferred. In order to do this, the forest must first be mechanicall pre-pressed, as depicted in figure 2-2(2). This pre-pressing guides the individual CNTs of the forest to bend in a direction that is more parallel to their growth substrate [27]. Any number of items may be used to pre-press the CNT forest, from a planar surface, a roller, or another custom device, as long as care is taken that the CNTs do not end up sticking to the pressing surface, and leaving their Mo current collector.

In the third step, the CNT-Mo film is released by submerging the entire wafer in deionized (DI) water until the desired film detaches from the substrate and floats to the top of the liquid. This water-assisted lifting process is gentle, and causes little degradation to the connections between the CNTs and their Mo current collecting layer. Since no adhesive layers were deposited between the Mo and SiO_2 layers, and the adhesion between Mo and SIO_2 is not very strong, the Mo detaches from the SiO_2 over time as water infiltrates the space between the Mo and SiO_2. For an electrode area of 5 mm by 10 mm, it takes about 96 hours to complete the lift-off process. However, if 5 nm of titanium is deposited onto the SiO_2 before Mo as an adhesion layer, the CNT-Mo film will not release from the SiO_2 substrate beneath.

Fourthly, the CNT–Mo film is lifted out of its aqueous environment atop a flexible substrate (Kapton ® or Thermanox™ film, in this case). Finally, in step 5, the CNT-Mo film now on a flexible substrate is air-dried, which further pulls the CNTs downward toward their substrate (with the help of the pre-pressing step before), due to the capillary forces of water evaporating from in between the individual CNTs [29]. In order to electrically connect to the fabricated electrode, a metal contact layer may be deposited (or affixed) onto the flexible target substrate before the CNT-Mo film is lifted out of the water with said substrate. In these prototype tests, Thermanox™, Kapton®, and various metal contact layers including gold, molybdenum, copper, and aluminum have been demonstrated to work successfully. The CNT–Mo film has been found to attach to all of these surfaces and to remain securely in place after the process due to strong Van der Walls forces.

The mechanical pre-pressing utilized in step 3 above makes sure that the CNT forest does not densify unpredictable as water evaporates from between the CNTs in step 5 above. Instead, the pre-press step helps maintain the integrity of the CNT–Mo film during the transfer process, and allows the CNTs to densify in a predictable, organized manner. In fact, if no pre-press step is incorporated into the above fabrication process, the CNTs tend to adhere to one another in random clumps, as seen in Figure 2-3(a) and (b).

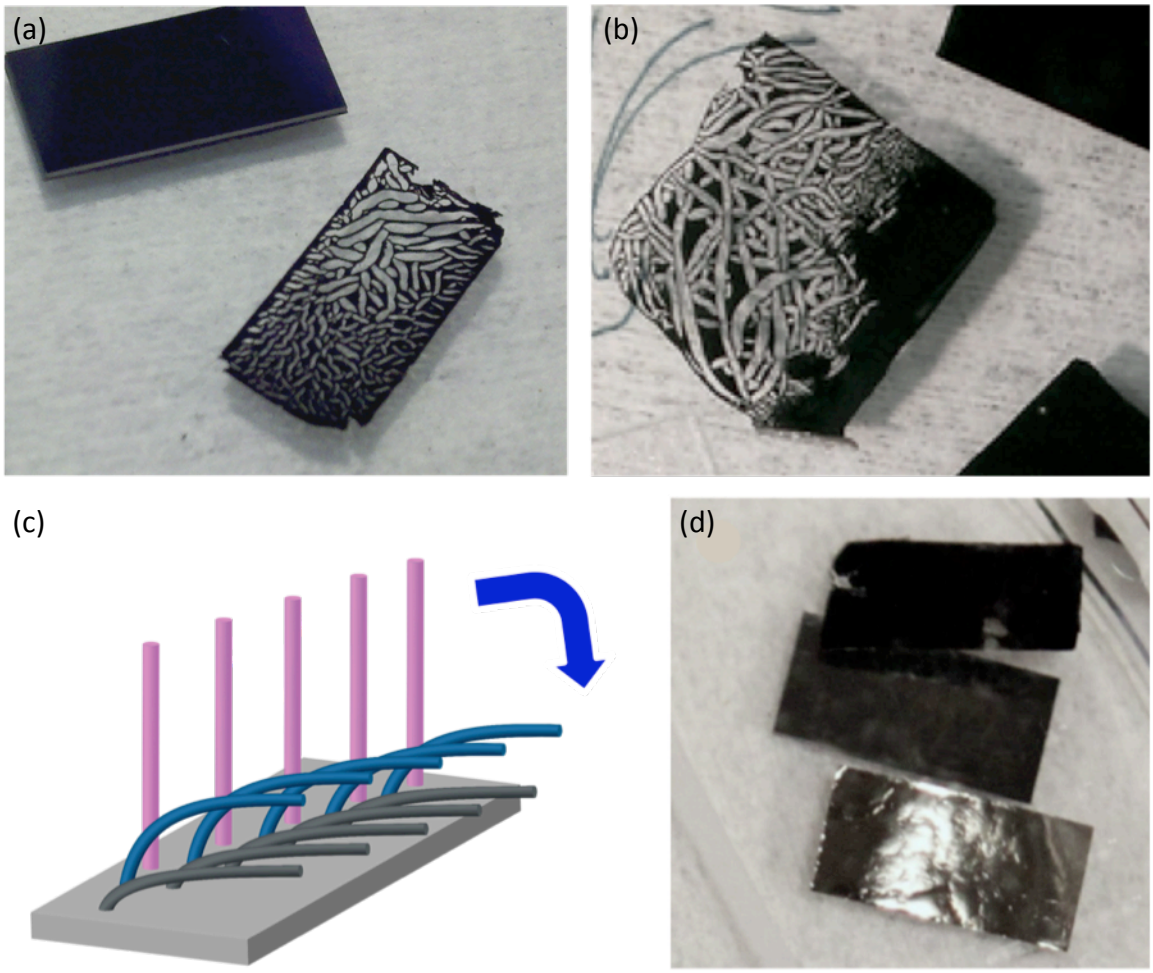

Figure 2-3: (a) Digital photograph showing randomly-coalesced CNTs after densification (bottom right), as well as the film's growth substrate (upper left), (b) another instance of random CNT clumping, (c) illustration showing the beding of the CNTs after pre-pressing (blue), and densification (dark gray), (d) a properly pre-pressed CNT-Mo film (top), it's original clean growth substrate (center), and the shiny Mo backside layer of an upside-down CNT-Mo film.

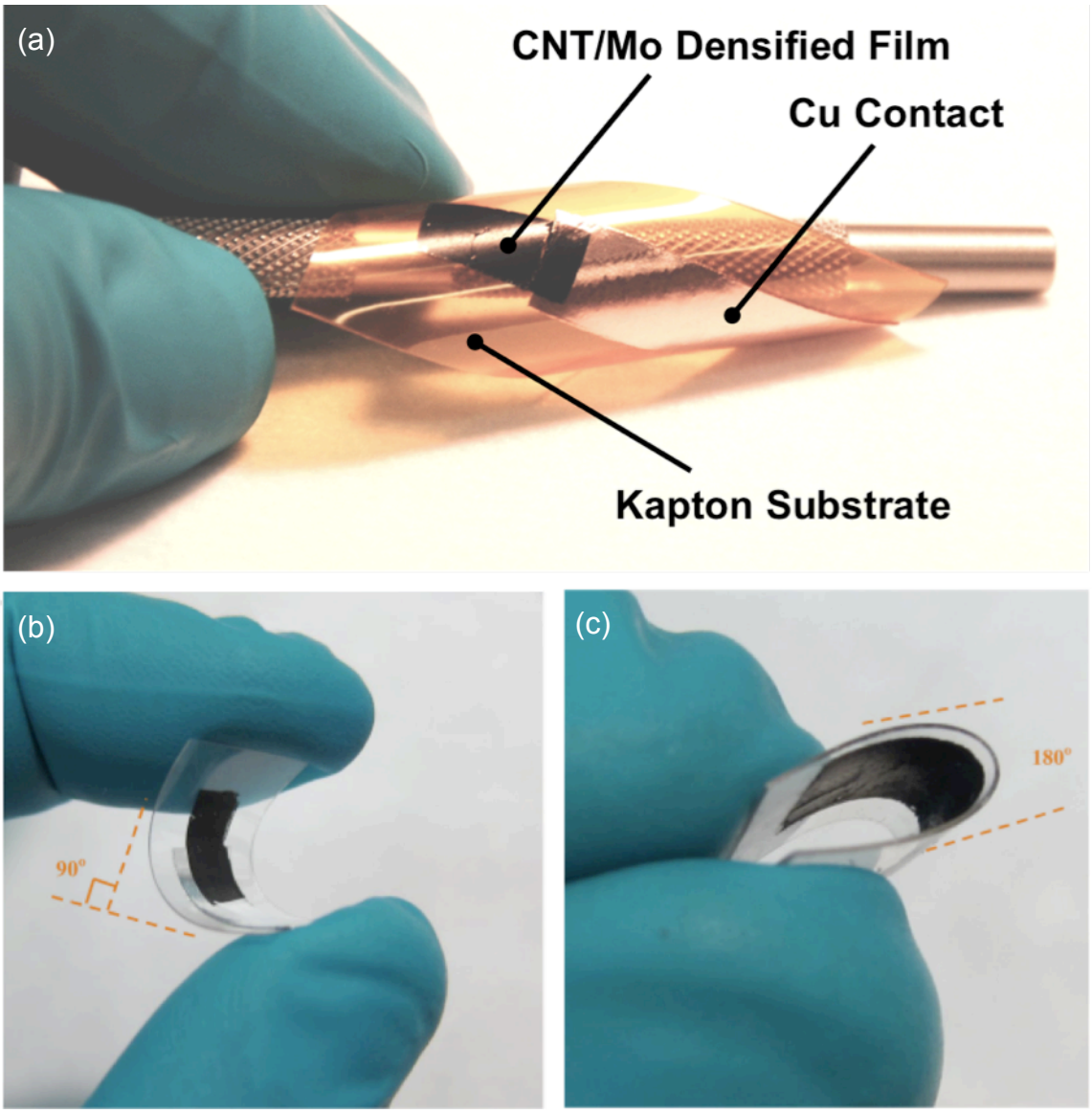

Figure 2-4: Digital photographs displaying the mechanical flexibility of the CNT–Mo film supercapacitor electrode. Figure (a) shows the CNT-Mo film contacted with a Cu contact on Kapton® film, and (b) and (c) on an Al/Thermanox™ film surface, being bent at a tangent-to-tangent angle of about 90°, and about 180°, respectively. The CNT–Mo electrodes in the images have areas of 5 mm by 10 mm.

Even though the unpressed CNT-Mo film does release from its growth substrate, randomly collapsed CNT patterns can clearly be seen. However, if the film is pre-pressed before liftoff, the CNT forest remains intact and uniform, as seen in Figure 2-3(d), since the individual CNTs are predisposed to bend vertically (down towards the substrate, as depicted in Figure 2-3(c)), instead of horizontally (towards one another in clumps). Furthermore, as evidenced by Figure 2-3(d), a reflective metal layer may be seen on the upside-down CNT-Mo film lifted electrode, which shows the Mo film is still present after the release step.

After the fabrication process is complete, a useable supercapacitor electrode is complete. Figure 2-4 shows digital photographs of two such flexible electrodes – one composed of a CNT-Mo film atop a Cu/Kapton® substrate (Figure 2-4(a)), and another atop an Al/Thermanox™ film surface (Figure 2-4(b) and (c)). Figure 2-4 also shows how the electrode bends – angles up to 180° were tested, and no breakage or delamination of the film has been observed for any of the angles tested. This shows that that the adhesion force is strong, and the CNT-Mo film extends when its substrate is bent. All of the the CNT-Mo film electrodes in the figures above have CNT forest areas of 5 mm by 10 mm, but larger area flexible supercapacitor electrodes may also be fabricated. Samples such as those below in Figure 2-5 below can be used in simple pouch cells for testing or implementation in devices. Continuous CNT-Mo films have been lifted off onto Mo-coated flexible Kapton® film, with active electrode areas of 4 cm^2.

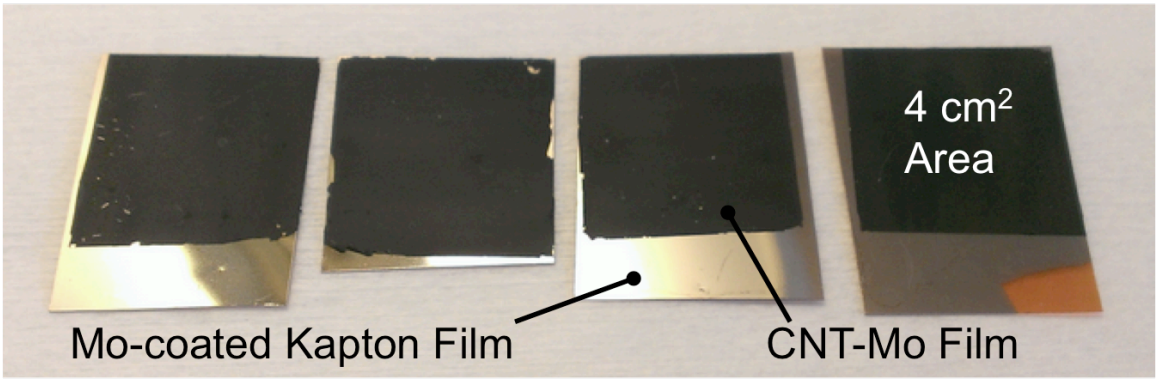

Figure 2-5: Digital photograph of larger area flexible supercapacitor electrodes. A 4cm2 area CNT-Mo film has been lifted off and placed onto a molybdenum-coated flexible Kapton® film.

Results and Discussion

The height of the CNT forest used in the flexible energy storage electrode has an original (just after growth) height of 41 µm, as can be seen in the SEM image of Figure 2-6(a). Once steps 2 through 5 in the fabrication process have been performed (as seen in Figure 2-2), the total height of the CNT film decrease to 1.1 µm, as seen in Figure 2-6(b) and 2-6(c). This is a factor of 37 X in height reduction, and increases the volumetric capacitance of the electrode, as well as allowing the electrode to pack more tightly in a rolled or layered configuration, due to its more compact size. Specifically, this means that if the measured capacitance does not degrade after the pre-press, lift-off, and densification steps, then the capacitance by volume may increase by up to 37, and as demonstrated in previous literature [27].

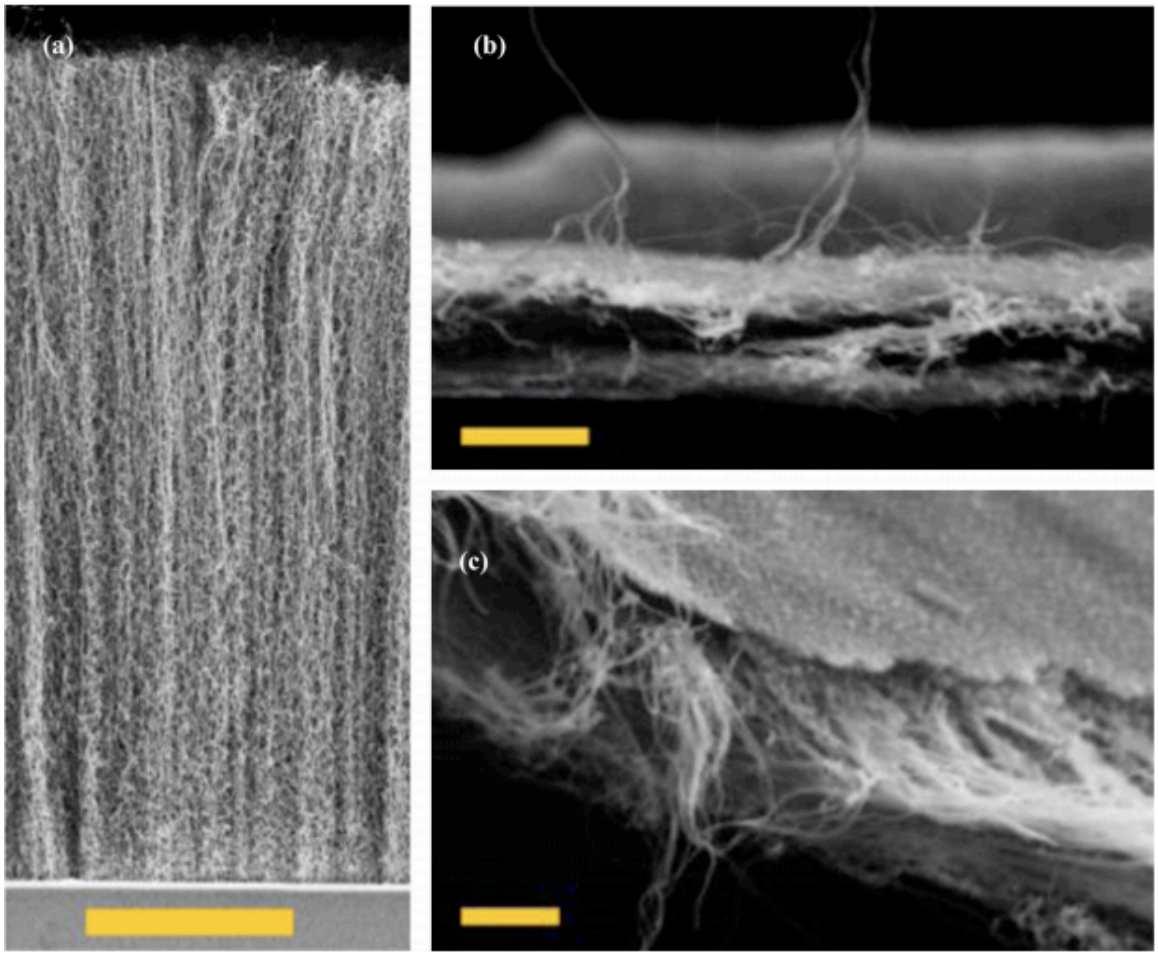

Figure 2-6: SEM images of the CNT forest after (a) growth, (b) release and densification in liquid, and (c) 40 electrochemical cycling tests. Scale bars are 10 μm, 1 μm, and 500 nm for (a), (b), and (c), respectively.

In order to characterize and test the supercapacitive performance of the fabricated electrode, three-electrode electrochemical tests are performed. In addition, to see if these tests had any further impact on the thickness or morphology of the CNT film, an SEM image of a cross section of the film was taken after 40 electrochemical cycling tests. As can be seen in Figure 2-6(c), there is no obvious change in either the morphology or the thickness of the CNT-Mo film.

During electrochemical testing of this electrode, an aqueous electrolyte is used - specifically 0.1 M K_2SO_4. As this is a three-electrode test, a reference and counter electrode are needed. In this case, the reference used is an Ag/AgCl electrode, with a counter electrode of platinum. The CNT-Mo film is 5 mm by 10 mm in area with an originally 41 μm-tall CNT forest (before pressing, release, and densification). The flexible plastic substrate upon which the CNT-Mo film is placed is Kapton® film having a copper film contact layer on top, as well as a Thermanox™ plastic with an aluminum contact layer. Once dipped into the electrolyte, half of the electrode area is in contact with the

solution. In other words, the active contact area of the CNT-Mo film with the electrolyte is 5 mm by 5 mm.

A good starting point for electrochemical supercapacitive testing is a cyclic voltammogram. Here, an increasing voltage is applied to the electrode, then reversed, as current is measured. Figure 2-7 shows the cyclic voltammetry curve (CV) of the flexible CNT-Mo film on Kapton® electrode. Here, the applied voltage starts at −0.7 V,

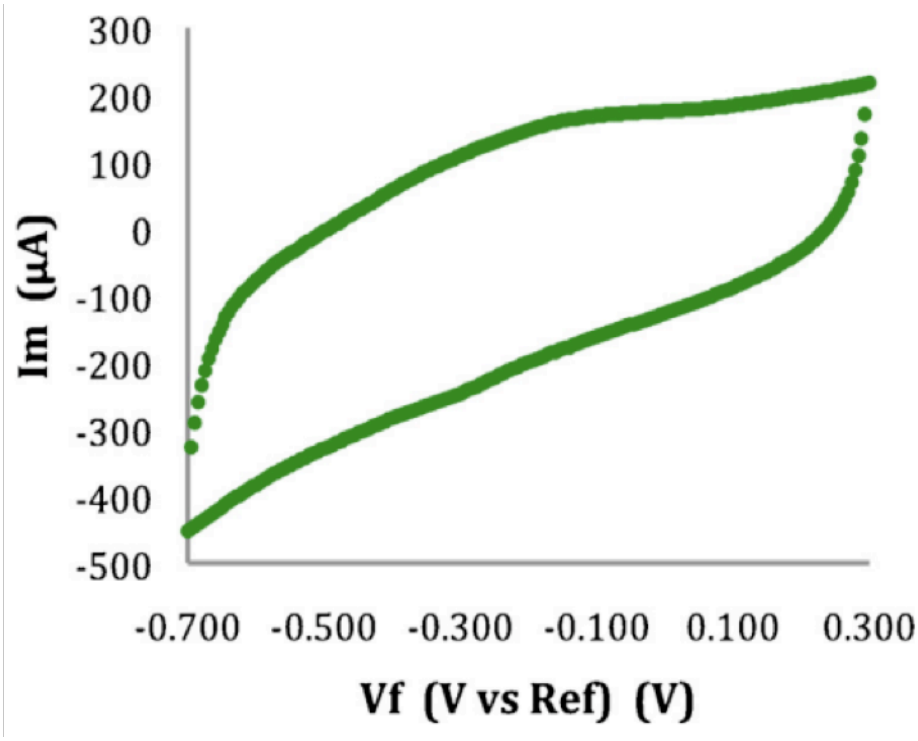

Figure 2-7: Cyclic voltammetry curve of the densified, flexible CNT–Mo film electrode cycled from −0.7 V to 0.3 V at a rate of 100mV/s in 0.1 M K_2SO_4 electrolyte. An Ag/AgCl reference electrode and Pt counter electrode were used in the experiments.

ends at 0.3 V, and reverses to complete a cycle. The voltage is increased (then decreased) at a rate of 100 mV/s. The specific capacitance of the device is calculated as 7.0 mF/cm^2 using the equation:

$$C_{sp} = \frac{I}{dV/dt \cdot A} \qquad (1)$$

Where C_{sp} is the specific capacitance of the CNT supercapacitor in terms of the electrode area, I is the sweeping current (equal to 174 µA, or one-half of the current difference at −0.2 V between the CV curve in Figure 2-7), dV/dt is the voltage scanning rate (100 mV/s), and A is the active physical area of the CNT electrode (in other words, the area of

the electrode which is submerged in electrolyte) – 5 mm by 5 mm. The capacitance of this device may be increased by either increasing the height of the CNT forest, or by adding a coating of another material to increase surface area. Indeed, it will be shown in the next chapter that coating a CNT forest with a low pressure CVD coating of amorphous silicon yields an increase in the total surface area of the electrode, and increases the capacitance.

A typical charge-discharge chronoamperometry curve may be seen in Figure 2-8. A voltage of -0.2 V is applied for 1 s, then set to 0 V. This is repeated in the figure for 5 cycles. The response of the current is measured at the same time, and can be seen in the blue curve of Figure 2-8. The voltage input is in the graph below, in purple.

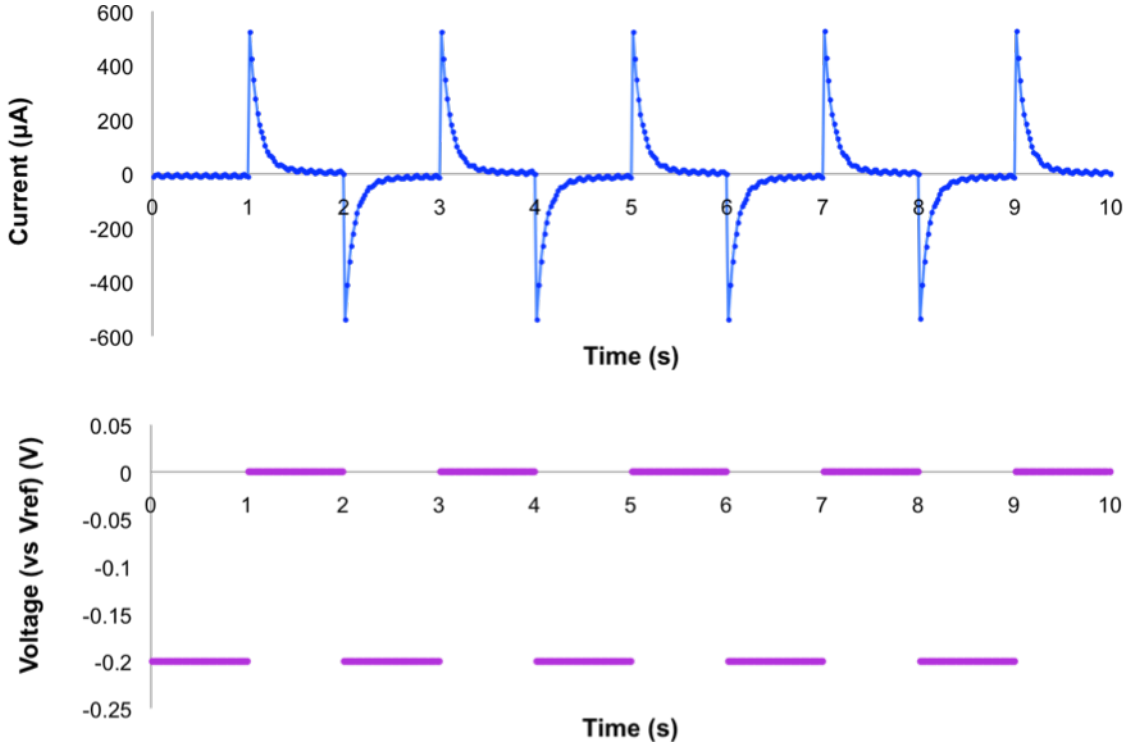

Figure 2-8: A chronoamperometry curve (blue) of a CNT–Mo film on a flexible Al/Thermanox™ substrate. The time period of each cycle is 2 s, while the charging voltage is set to -0.2 V. The voltage is set to 0 V during discharge.

In order to ensure that the flexible supercapacitor electrode is stable over cycling, the capacitance of each cycle can be measured and compared over time. Figure 2-9 depicts the capacitance of the electrode in terms of the percentage of the first cycle's capacitance over 300 charge-discharge cycles. The capacitance values are gathered at a voltage value of −0.2 V in measured cyclic voltammetry curves. It should be noted that the standard deviation in capacitance over the entirety of the 300 cycles tested is only 3%. Furthermore, some of this variation may be attributed to noise within the measurement device as well as the environment.

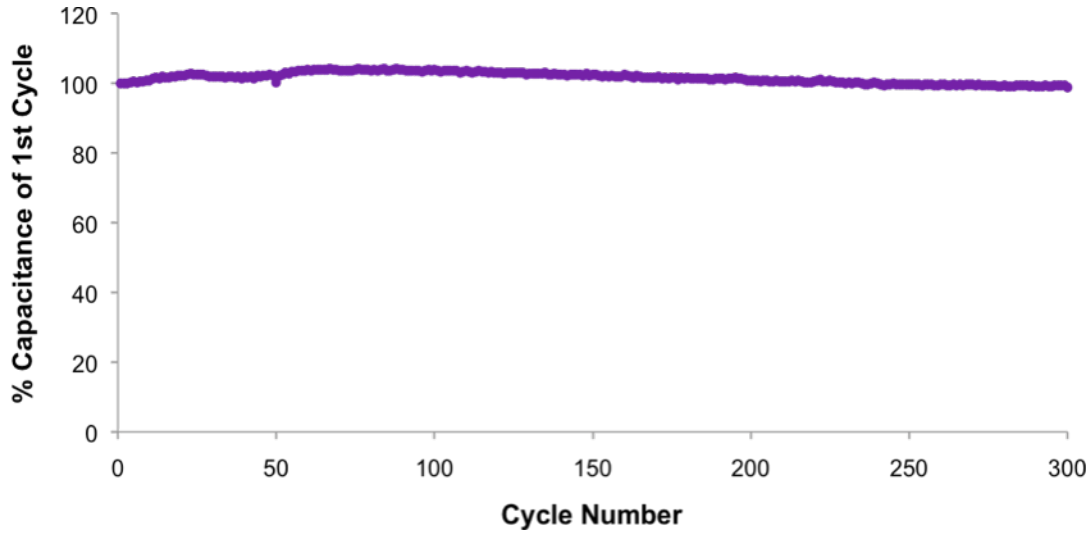

Figure 2-9: Cycling performance of the flexible CNT-Mo supercapacitor electrode measured through 300 cycles, normalized to the capacitance of the first cycle. Capacitance values are represented by the voltage value of −0.2 V in measured cyclic voltammetry curves.

As one of the main advantages of this electrode is its flexibility (where it is proposed that it may be used as a mechanically flexing energy storage device in potential future applications such as flexible readers and mobile phones), the integrity of the electrode as it undergoes bending is also tested. The way in which this is achieved here is by

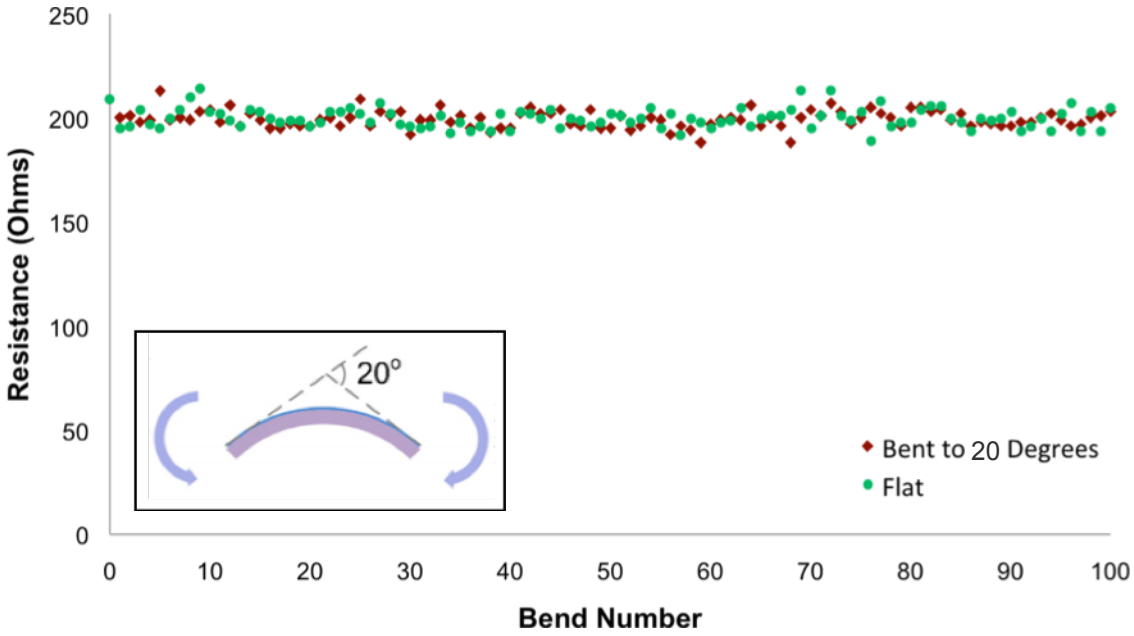

Figure 2-10: Electrode resistance vs. bending cycle of the flexible CNT-Mo electrode, normalized to the original resistance before the sample had been bent. One bending cycle is comprised of one bend to 20°(shown as red data points), and a re as illustrated in the inset, and then one release to 0°(shown as green data points).

recording the resistance of the flexible CNT-Mo (placed onto Thermanox plastic) electrode as it is bent to a certain angle – in this case 20° - then releasing the electrode until it lies flat again, and recording the electrode resistance at this point as well. The illustration of the measured angle may be seen in the inset of Figure 2-10. The release to 0° is almost instantaneous for this specific electrode, as the Thermanox plastic substrate used is elastic in this bending region. Due to the excellent adhesion of the CNT-Mo film to the Thermanox substrate after the completion of the drying process, as the plastic substrate bends, the attached CNT–Mo film does as well. As can be seen in Figure 2-10, this bend-testing is repeated over 100 bend, with resistance measured at each bend. The resistance values are obtained through a two-probe resistance measurement method. The resistance of the CNT-Mo film on the Thermanox plastic substrate remains stable with bending, and has a range of 199 Ω ± 4 Ω. The reason for this variation in resistance may be due to the physical slight movement of the electrical contact between the probes and the film.

In addition, the adhesion of the CNT-Mo film to the plastic substrate tested seems to be excellent. For instance, over the course of all of the above electrochemical tests in the aqueous electrolyte, the electrode film was not seen to show evidence of delamination from its plastic substrate. In fact, once the CNT–Mo film has been dried and densified atop the flexible substrate which it has been placed on, it is impossible to remove the CNT-Mo film from the substrate in air without completely annihilating the film. The film may be scraped off of its plastic substrate, but is then not functional as an electrode. This strong adhesion is due to strong Van der Waals forces, without any adhesives or extra manipulation involved.

Conclusions

To conclude, a mechanically flexible carbon nanotube supercapacitor electrode with an inherent metal current collector layer is developed and tested. A thin and flexible CNT-Mo electrode is fabricated using a water-assisted lift-off and drying and densification process. Once the vertically aligned CNT forest is grown, a pre-press step is utilized to predispose the individual CNTs within the forest to lie in a more flattened orientation parallel to the substrate. This pre-press step is important for the fabrication of a uniformly densified CNT forest for use in the flexible electrode. After the pre-press step, a lift-off process using DI water gently releases the thin CNT forest film with its current collecting molybdenum layer intact. This released CNT-Mo film may then be transferred to a flexible substrate, or to a different surface of choice. The prototype experimental results show that the CNT-Mo film densifies during the drying process from an original height of 41 μm to 1.1 μm – a factor of 37 X. The supercapacitor electrode thus fabricated has a specific capacitance of 7.0 mF/cm^2. The electrode was also found to be stable through 300 charge-discharge cycles, as well as through 100 mechanical bending cycles.

References

[1] K Zickuhr, "Tablet Ownership 2013," *Pew Research Center's Internet & American Life Project*, Jun 2013. [Online]. http://www.pewinternet.org/2013/06/10/tablet-ownership-2013/

[2] L Rainie, "Cell phone ownership hits 91% of adults," *Pew Research Center*, Jun 2013. [Online]. http://www.pewresearch.org/fact-tank/2013/06/06/cell-phone-ownership-hits-91-of-adults/

[3] P Harrop, R Das, and G Chansin, "Wearable Technology 2014-2024: Technologies, Markets, Forecasts," *IDTechEx*, Dec 2014. [Online]. http://www.idtechex.com/research/reports/wearable-technology-2014-2024-technologies-markets-forecasts-000379.asp

[4] B E Conway, *Electrochemical Supercapacitors- Scientific Fundamentals and Technological Applications*., Mar 1999, vol. New York, USA.

[5] P Simon and Y Gogotsi, "Materials for electrochemical capacitors," *Nature Materials*, vol. 7, pp. 845-854, Oct 2008.

[6] E Frackowiak and F Begui, "Carbon materials for the electrochemical storage of energy in capacitors," *Carbon*, vol. 39, pp. 937-950, Apr 2001.

[7] A G Pandolfo and A F Hollenkamp, "Carbon properties and their role in supercapacitors," *Journal of Power Sources*, vol. 157, pp. 11-27, May 2006.

[8] Gianfranco Pistoia, "Batteries for Portable Devices," vol. Elsevier Science B.V., no. Amsterdam, The Netherlands, 2005.

[9] Seung Woo Lee et al., "High-power lithium batteries from functionalized carbon-nanotube electrodes," *Nature Nanotechnology*, vol. 5, no. 7, pp. 531-537, Jun 2010.

[10] Daniel T Welna, Liangti Qu, Barney E Taylor, Liming Dai, and Michael F Durstock, "Vertically aligned carbon nanotube electrodes for lithium-ion batteries," *Journal of Power Sources*, vol. 196, no. 3, pp. 1455-1460, Feb 2011.

[11] H Zhang, G Cao, and Y Yang, "Electrochemical properties of ultra-long, aligned, carbon nanotube array electrode in organic electrolyte," *Journal of Power Sources*, vol. 172, no. 1, pp. 476-480, 2007.

[12] M Endo, M S Strano, and P M Ajayan, "Potential Applications of Carbon Nanotubes," *Topics in Applied Physics*, vol. 111, pp. 13-62, Dec 2008.

[13] A M Cassell, J A Raymakers, J Kong, and H Dai, "Large Scale CVD Synthesis of Single-Walled Carbon Nanotubes," *Journal of Physical Chemistry B*, vol. 103, pp. 6484-6492, Aug 1999.

[14] K Hata, "Water-Assisted Highly Efficient Synthesis of Impurity-Free Single-Walled Carbon Nanotubes," *Science*, vol. 306, pp. 1362-1364, Nov 2004.

[15] C Peng, S Zhang, Jewell D., and G Z Chen, "Carbon nanotube and conducting polymer composites for supercapacitors ," *Progress in Natural Science*, vol. 18, pp. 777-788, May 2008.

[16] K H An et al., "Supercapacitors using single-walled carbon nanotube electrodes," *Advanced Materials*, vol. 13, no. 7, pp. 497-500, Nov 2001.

[17] R Warren, F Sammoura, A Kozinda, and L Lin, "ALD Ruthenium Oxide-Carbon Nanotube Electrodes for Supercapacitor Applications," *IEEE MEMS Conference 2014, San Francisco*, pp. 167-170, Nov 2014.

[18] M. F. L De Volder, S. H Tawfick, R. H Baughman, and A. J Hart, "Carbon Nanotubes: Present and Future Commercial Applications," *Science*, vol. 339, pp. 535-539, Feb 2013.

[19] A E Aliev et al., "Thermal transport in MWCNT sheets and yarns," *Carbon*, vol. 45, pp. 2880-2888, Nov 2007.

[20] M Kaempgen, C K Chan, J Ma, and G Gruner, "Printable Thin Film Supercapacitors Using Single-Walled Carbon Nanotubes ," *Nano letters*, vol. 9, no. 5, pp. 1872-1876, May 2009.

[21] Po-Chiang Chen, Guozhen Shen, Saowalak Sukcharoenchoke, and Chongwu Zhou, "Flexible and transparent supercapacitor based on In[sub 2]O[sub 3] nanowire/carbon nanotube heterogeneous films," *Applied Physics Letters*, vol. 94, no. 4, p. 043113, Jan 2009.

[22] Y Fang et al., "Self-supported supercapacitor membranes: Polypyrrole-coated carbonnanotube networkse nabled by pulsed electrodeposition," *Journal of Power Sources*, vol. 195, pp. 674-679, Aug 2010.

[23] V.L Pushparaj et al., "Flexible energy storage devices based on nanocomposite paper," *Proceedings of the National Academy of Sciences*, vol. 104, no. 34, p. 13574, 2007.

[24] T. Y Tsai, C. Y Lee, N. H Tai, and W. H Tuan, "Transfer of patterned vertically aligned carbon nanotubes onto plastic substrates for flexible electronics and field emission

devices," *Applied Physics Letters*, vol. 95, no. 1, p. 013107, Jan 2009.

[25] E B Sansom, D Rinderknecht, and M Gharib, "Controlled partial embedding of carbon nanotubes within flexible transparent layers," *Nanotechnology*, vol. 19, p. 035302, Dec 2008.

[26] H Zhang, G Cao, Y Yang, and Z Gu, "Comparison Between Electrochemical Properties of Aligned Carbon Nanotube Array and Entangled Carbon Nanotube Electrodes," *Journal of the Electrochemical Society*, vol. 155, no. 2, pp. K19-K22, Dec 2008.

[27] Yingqi Jiang and Liwei Lin, "A two-stage, self-aligned vertical densification process for as-grown CNT forests in supercapacitor applications," *Sensors & Actuators: A. Physical*, vol. 188, pp. 261-267, Dec 2012.

[28] Y Jiang, P Wang, and L Lin, "Characterizations of contact and sheet resistances of vertically aligned carbon nanotube forests with intrinsic bottom contacts," *Nanotechnology*, vol. 22, p. 365704, Aug 2011.

[29] D Futaba, K Hata, T Yamada, and T Hiraoka…, "Shape-engineerable and highly densely packed single-walled carbon nanotubes and their application as super-capacitor electrodes," *Nature Materials*, vol. 5, pp. 987-984, Jan 2006.

[30] A Kozinda, Y Jiang, T Chang, and L Lin, "Flexible energy storage devices based on carbon nanotube forests with built-in metal electrodes," *Sensors and Actuators A: Physical*, vol. 195, pp. 224-230, Sep 2013.

[31] A Kozinda, Y Jiang, and L Lin, "Amorphous Silicon-Coated CNT Forest For Energy Storage Applications," *Proceedings of IEEE Transduers'11 Conference, Beijing, China, June 5–9*, pp. 723-726, May 2011.

[32] B E Conway, V Birss, and J Wojtowicz, "The role and utilization of pseudocapacitance for energy storage by supercapacitors," *Journal of Power Sources*, vol. 66, pp. 1-14, Nov 1997.

Chapter 3: Supercapacitor Electrode with Enhanced Surface Area

Chapter Summary

This chapter introduces the development of an amorphous silicon-coated, vertically aligned carbon nanotube (CNT) forest with increased surface area for energy storage applications. The architecture of the electrode has three valuable features: (1) an enhanced charge transfer via aligned CNTs to the underlying substrate, (2) excellent charge storage capability via amorphous silicon, and (3) the preservation of a high surface area and porosity with an enhanced energy storage capacity. As such, this could offer a new type of nanomaterial for energy storage applications. A supercapacitor electrode is used in this chapter for the energy storage demonstration.

Introduction

As high energy density storage materials are crucial for numerous applications, from their use in hybrid electric vehicles, to applications in the aerospace and defense industries, as well as in autonomous sensing devices, there has been a strong interest to increase the amount of electrochemical storage of energy in supercapacitors and secondary (rechargeable) batteries [1]. This increase may be achieved in a few ways, including through the development and employment of new materials for use in electrodes, as well as by the structural design of those electrodes [2-6]. For instance, Kou et al. used coaxially wet-spun fibers composed of sodium carboxymethyl cellulose and CNTs as well as graphene oxide, while Kim et al. pyrolized commercial photoresist to fabricate flexible micro supercapacitor electrodes [4,6]. As mentioned before, the mechanism of charge storage differs between that of a supercapacitor and lithium ion (Li-ion) battery. Charging and discharging a supercapacitor polarizes the electrolyte between the electrodes, creating a charge separation between the electrolyte and electrode surfaces, forming an electrochemical double layer that electrostatically stores charge [7]. In contrast, in the charged state of the Li-ion battery, the anode stores the lithium ions within its lattice. During discharge, the lithium ions migrate toward and intercalate into the cathode lattice, by way of the electrolyte [8].

Despite these differences, a larger electrode surface area is a key element for high energy storage in both supercapacitors as well as in Li-ion batteries. In the former, the capacity for storing charge in the electrochemical double-layer is augmented, while in the latter, the lithium ion intercalation capability is increased [9,10]. Another key to high energy storage is utilizing a material capable of storing a large amount of lithium ions, for the Li-ion battery aspect of the electrode. To date, the largest known lithium ion intercalation specific capacity of a material is that of silicon (4,200 mAh/g). However, if used in a Li-ion battery, bulk silicon pulverizes as it is cycled due to the large volumetric changes (from 300% to 400%) caused by the intercalation of the lithium ions [11]. Work has been done to solve this issue using silicon nanowires as electrodes, but the high resistivity of silicon nanowires hinders the energy storage capability [12]. A core-shell

structure of carbon nanofibers (CNFs) with a silicon coating has also been used to alleviate the resistivity issue with limited success, as the nanofibers have been randomly deposited on a charge-collecting substrate with expectable poor contacts [11]. Similar work has been done using a film of CNTs, also randomly deposited onto a substrate, and then coated with Si [2, 13-16]. Not only do CNTs have excellent conductivity and a high lithium ion intercalation capacity, they also afford the silicon that coats them a large measure of mechanical strength and stress release [13,15,16]. Thus, as lithium ions intercalate within the deposited silicon, the silicon will expand in volume, while the CNT within the silicon casing will accommodate some of the mechanical stresses induced by charging and discharging the lithium ion battery electrode.

In contrast, with the CNT forest grown here as illustrated in Figure 3-1(a), each CNT has an inherent contact with the underlying substrate from which the CNTs have grown. Furthermore, with a smaller diameter than CNFs, yet having a vertically aligned conformation, a CNT forest provides a better platform for silicon coating. Finally, the CNT forest shape is easily controllable by patterning the catalyst, making it ideal for a variety of MEMS applications. Two of the possible energy storage applications are illustrated in Figures 3-1(b) and 3-1(c) – as a supercapacitor and a Li-ion battery electrode, respectively.

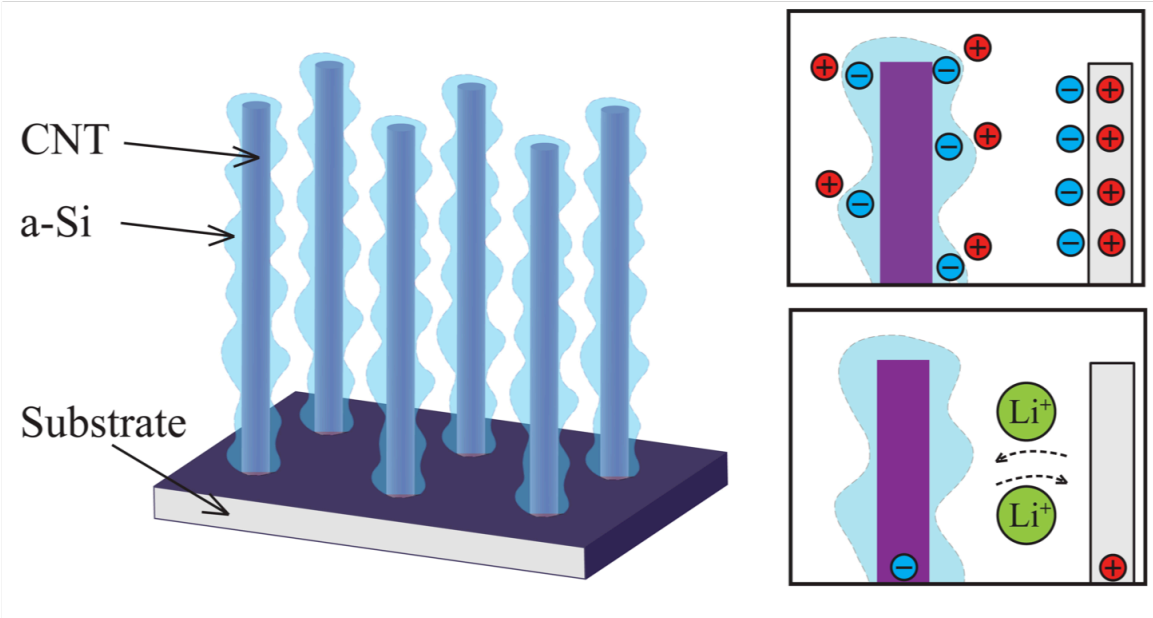

Figure 3-1: (a) Schematic illustrating a silicon coating on vertically aligned carbon nanotubes (CNTs). (b) The usage of the architecture in electrochemical double layer capacitor (i.e., supercapacitor) electrodes. (c) The usage of the architecture in lithium ion battery electrodes.

Design and Fabrication

A supercapacitor electrode is developed and analyzed in this chapter as an energy storage application of the amorphous-silicon coated CNT forest. The fabrication process of the electrode is summarized in Figure 3-2.

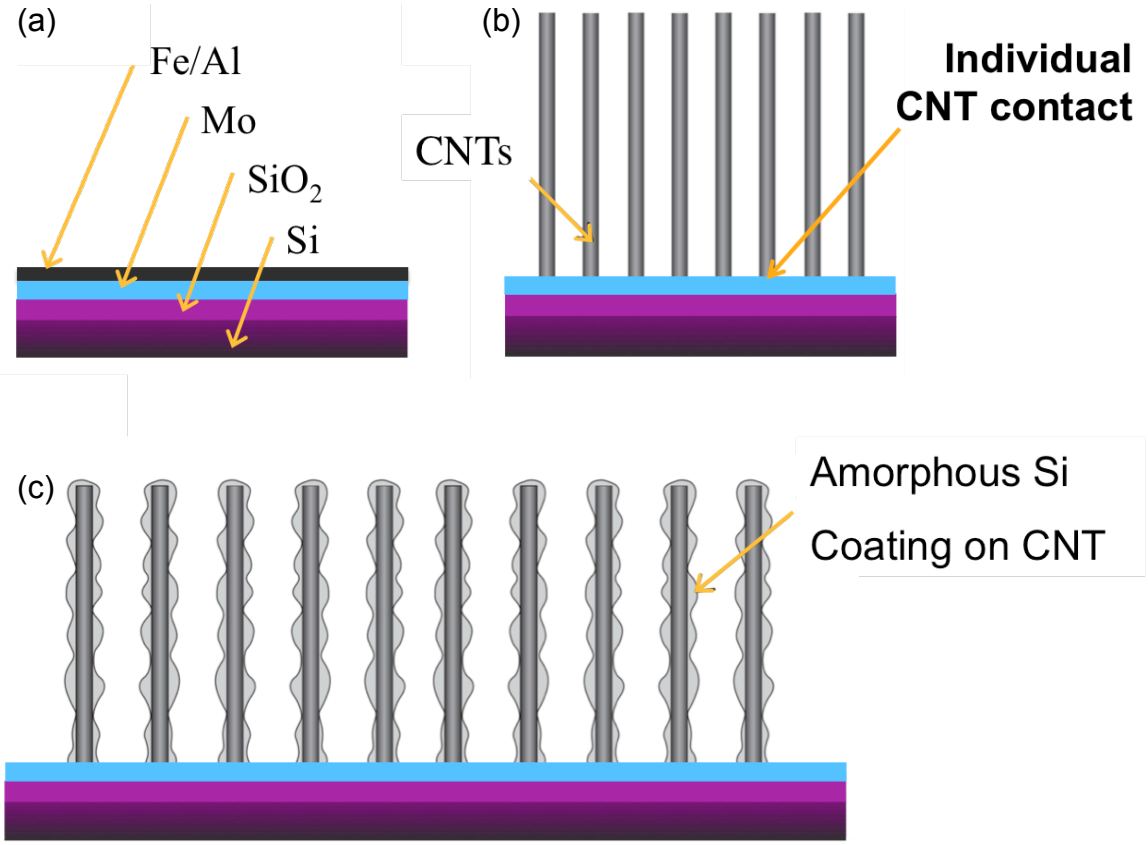

Figure 3-2: A schematic illustration of the main steps used to fabricate the CNT/Si-coated electrode: (a) Current collector and catalyst deposition, (b) CVD CNT growth, and (c) timed LPCVD silicon deposition.

The fabrication process begins with the cleaning and thermal oxidation of a silicon wafer, which provides a substrate for the CNT forest. Next, a thin film molybdenum current collector is deposited onto the wafer using e-beam evaporation, followed by the thin film depositions of the catalyst for CNT growth (Al and Fe), also using e-beam evaporation. The thicknesses of the deposited metals are 50 nm of Mo, 10 nm of Al, and 5 nm of Fe. After scribing individual 5 mm by 10 mm sample areas using a wafersaw into the wafer containing the evaporated layers, the wafer is transferred into a vacuum quartz tube furnace (Lindberg/Blue M® threezone tube furnace, Thermo Electron Corp., Asheville, NC). The CNT growth follows the process developed by Y. Jiang et al [17]. Once the quartz tube is evacuated and purged with hydrogen, and the furnace is

stabilized to a temperature of 720°C in a hydrogen gas environment, the process gases (hydrogen and ethylene) are flown through the tube at volumetric flow rates of ratios of approximately 7:1, respectively. The chemical vapor deposition (CVD) growth process proceeds for ten minutes, during which the temperature and gas flow rates are held constant. Once the growth process is complete, the tube is cooled to room temperature. This process results in a vertically self-aligned CNT forest. A small amount of amorphous silicon is then deposited onto the CNT forest using a Tystar low pressure CVD furnace. A pump/purge sequence and a temperature stabilization process leads to a deposition temperature of 500°C and a process pressure of 375 mTorr. At this temperature and pressure, silane gas is flown through the chamber at a volumetric flow rate of 120 sccm for time durations of 5 to 35 minutes. The silicon film deposition results from the migration and reaction of the process gas (silane) with the surfaces it encounters.

After cooling and venting the chamber to atmosphere, the samples can be investigated using a scanning electron microscope. Figure 3-3(a) shows SEM imaging of the electrode with vertically self-aligned CNTs of 50 µm in length, after a 15-minute LPCVD amorphous silicon deposition. The silicon deposits onto the individual CNTs by first nucleating on certain areas of the CNTs, then growing larger in size as further silane gas is introduced into the growth chamber. It should be noted that the silicon completely penetrates and coats the entire height of the CNT forest – every CNT is coated with silicon. This may be

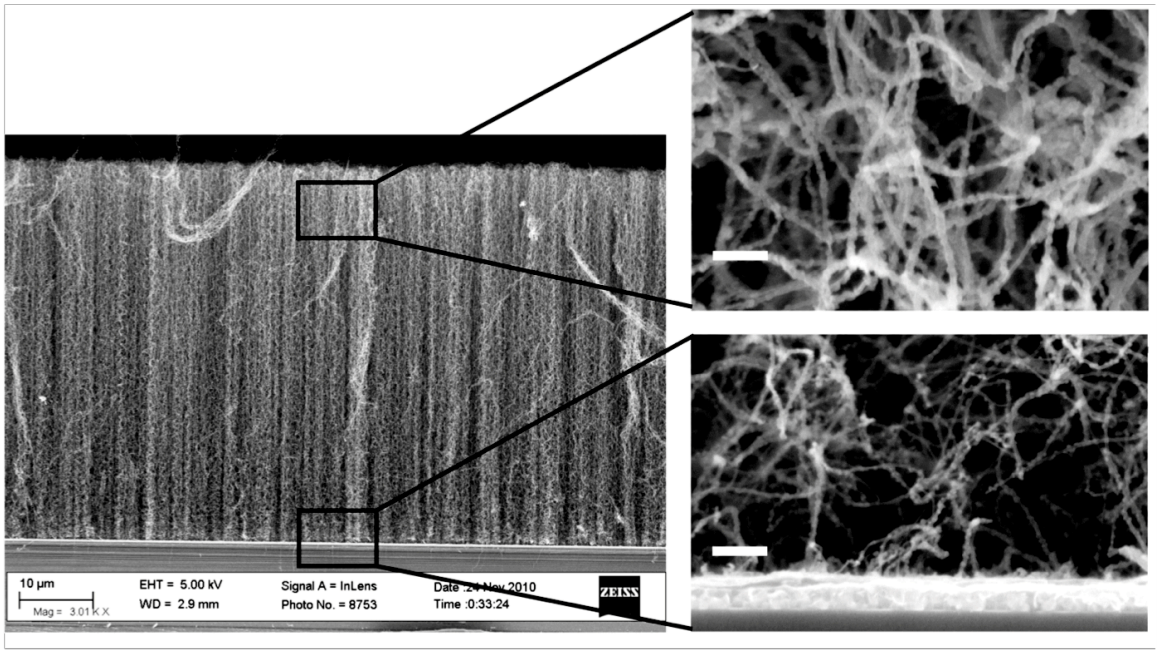

Figure 3-3: SEM images of (a) a cross-section of the Si-coated CNT forest, (b) a zoomed view of Si deposition near the top and (c) bottom of the forest. Scale bars in (b) and (c) are 200 nm. The total height of the forest pictured is 50 µm.

seen by the uniform coating seen on both the top (Figure 3-3(b)) and bottom (Figure 3-3(c)) portions of the CNT forest in the SEM images taken. The upper portion of the CNT forest has a slightly heavier coating of silicon, due to the large aspect ratio of the CNTs, and the depth that the silane gas must penetrate. However, silicon does reach to the very bottom of the CNT forest, and coats each CNT. Meanwhile, it is also clearly seen that the surface area of the electrodes has not been compromised by the addition of this coating.

Furthermore, additional samples were deposited with amorphous silicon for various deposition times in order to determine the growth rate of the silicon particles as deposited onto the CNTs. After investigation, the amount of silicon coating on the individual CNTs was found to steadily increase over deposition time. The relation between the overall size of the particles and the deposition time in the Tystar furnace is plotted in Figure 3-4. The corresponding SEM images of the silicon coatings after 5, 15, 25, and 35 minutes are also shown. The growth rate was found to be approximately 0.8 nm/min.

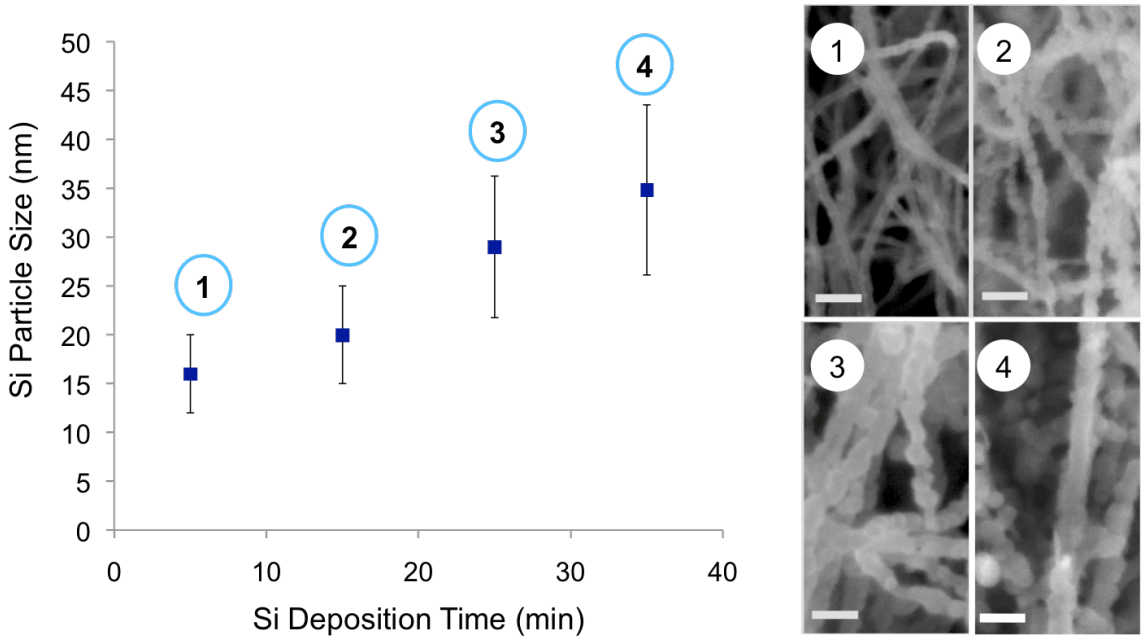

Figure 3-4: (a) Si particle size over time of deposition, and (b) SEM images of forest after (1) 5 min (2) 15 min (3) 25 min and (4) 35 min of LPCVD Si deposition. Scale bars in SEM images are 100 nm.

Results and Discussion

As the demonstrative energy storage application, a 3-electrode supercapacitor test setup is employed. The aqueous electrolyte used in the electrochemical analysis is 1M H_2SO_4, with an Ag/AgCl reference electrode and Pt counter electrode to complete the

three-electrode test setup. The supercapacitor electrodes tested are each 5 mm by 10 mm in area, with a 70 µm–high CNT forest structure. Each electrode contains a CNT forest with a different silicon coating thickness – 0 nm (bare), 15 nm, and 35 nm-think

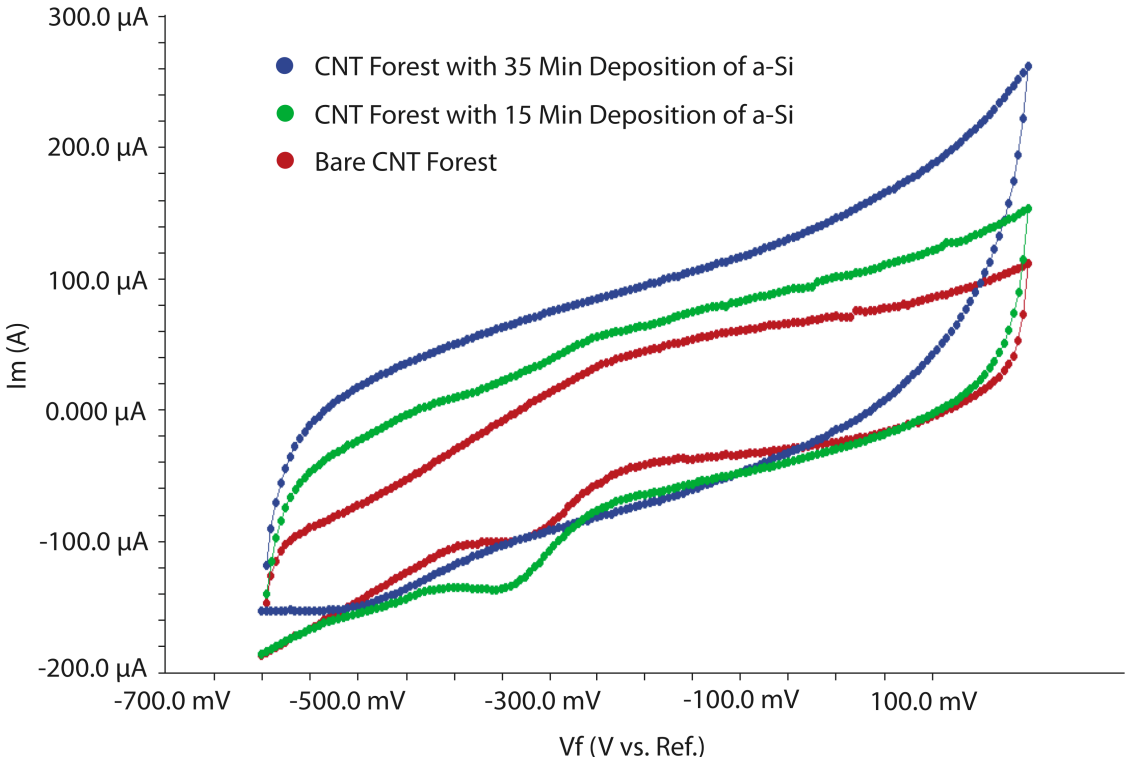

Figure 3-5: Measured cyclic voltammetry data of electrodes before (red) and after 15 minute (green) and 35 minute (blue) depositions of amorphous silicon, correlating to 15 nm and 35 nm-thick coatings, respectively. This data is collected at a voltage scanning rate of 100 mV/s. The electrodes are tested in 1M H_2SO_4 electrolyte.

coatings, in order to compare the performance of the variably amorphous silicon-coated electrodes to an electrode with no silicon coating. All of these electrodes are cycled from -0.6 V to 0.2 V, at a voltage scanning rate of 100 mV/s. The cyclic voltammetry curves for the three electrodes are shown in Figure 3-5. The red curve depicts the as-grown CNT forest without any silicon deposition, while the green and blue curves show data from the same CNT forest with 15-minute and 35-minute depositions of amorphous silicon, correlating to 15 nm and 35 nm-thick coatings of amorphous silicon, respectively. There is a clear improvement in performance of the silicon-coated electrodes over the bare CNT electrode. The improvement in energy density of the coated samples over the bare samples may be seen in Table 3-1 – there is a clear improvement in specific capacitance as the thickness of the silicon coating increases,

which validates the fundamental working principle that silicon imparts an increase to the energy density of the electrode. For the 35 nm-thick silicon coating, the specific capacitance may be seen to almost double compared to that of the same electrode with

Table 3-1: Specific capacitance of supercapacitor electrodes increases with an increasing thickness of amorphous silicon coating.

a-Si Depostion Time (min)	a-Si Coating Thickness (nm)	Specific Capacitance (mF/cm^2)
0	0	2.6
15	15	3.7
35	35	4.9

no silicon coating. Also, this increase surely could not have been achieved if the porosity of the forest was compromised.

Next, the stability of the silicon-coated electrode is analyzed, in terms of the percentage of the initial capacitance value. Figure 3-6 shows the measured cycling performance of the electrode with a 35 nm-thick coating of silicon over 200 charge/discharge cycles. The structure consistently demonstrates over 90% efficiency, which implies that the

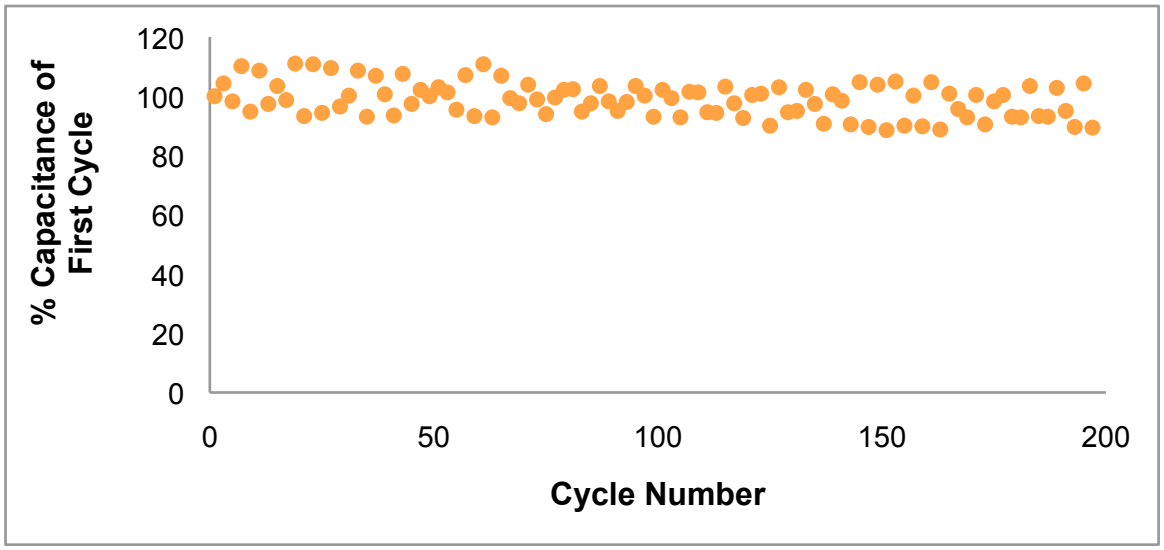

Figure 3-6: Measured cycling performance of anode cycled from -0.4 to 0 V for 200 cycles in 1M H_2SO_4 electrolyte at 100 mV/s. The structure consistently demonstrated over 90% efficiency.

enhanced electrode is indeed stable in capacitance, and thus energy density, over cycling.

In order to further increase the capacitance of the electrode, a taller CNT forest may be grown and the coated with amorphous silicon. For instance, a 430 µm-high CNT forest is coated with 20 nm of amorphous silicon and tested in a three-electrode supercapacitor setup. The cyclic voltammetry results may be seen in Figure 3-7, where the blue graph denotes the data for the bare 430 µm-high CNT forest, and the red graph shows the improved cyclic voltammetry performance of the same CNT forest coated with amorphous silicon. The capacitance of the coated electrode is improved by 16% to 50 mF/cm^2.

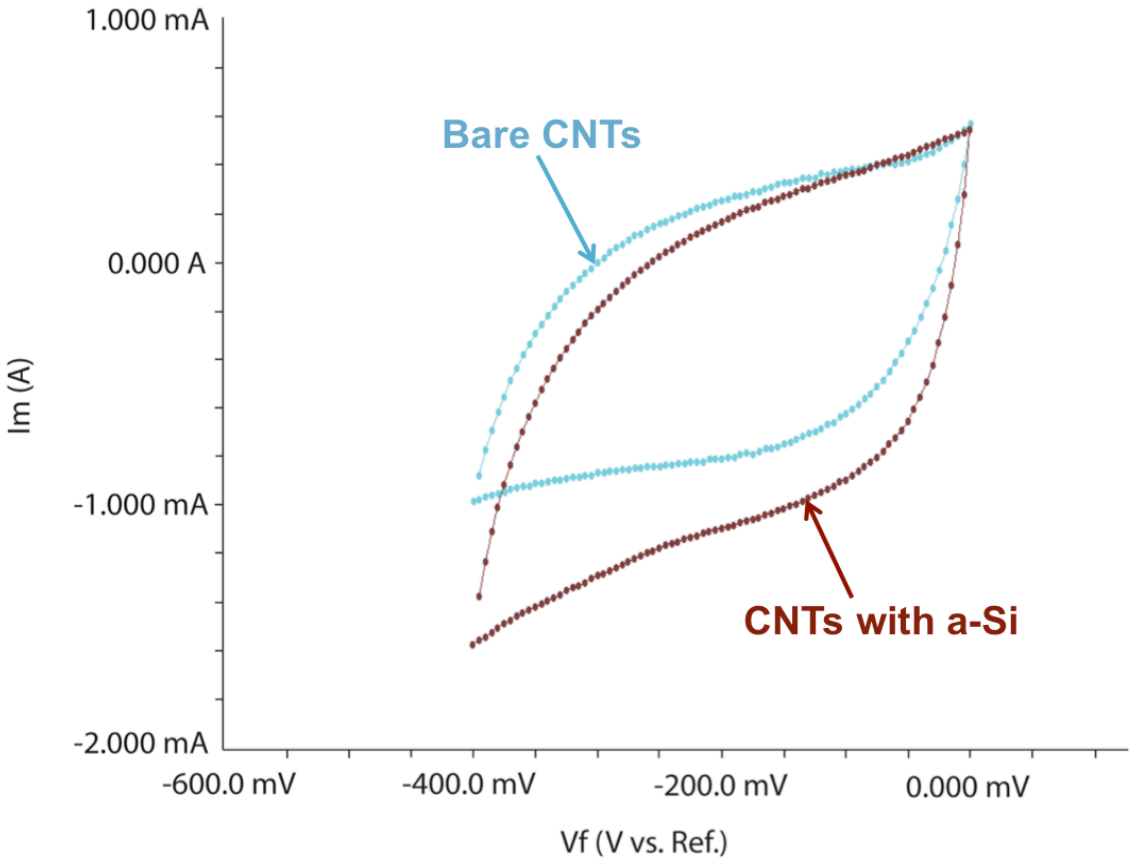

Figure 3-7: Measured cyclic voltammetry data of supercapacitor electrodes before (blue) and after (dark red) a 20 nm amorphous silicon deposition onto a 430 µm-high vertically aligned CNT forest, collected at a scanning rate of 50 mV/s. The electrodes were tested in 1M H_2SO_4 electrolyte.

In order to determine the charge/discharge characteristics of the supercapacitor electrode, a chronopotentiometry scan of the same electrode is also performed, and may be seen in Figure 3-8. Here, a constant current is applied to the electrode for a certain amount of time, which charges the electrode. Then, the current is set to zero for 1s. This cycle is repeated 5 times, and the voltage response of the electrode is recorded. As evidenced in the chronopotentiometry scan, there is some internal resistance within

the supercapacitor setup. It should be noted that these last two electrodes do not contain a specific current-collecting layer. Instead, the underlying substrate is a thermally oxidized silicon wafer with no Mo thin film.

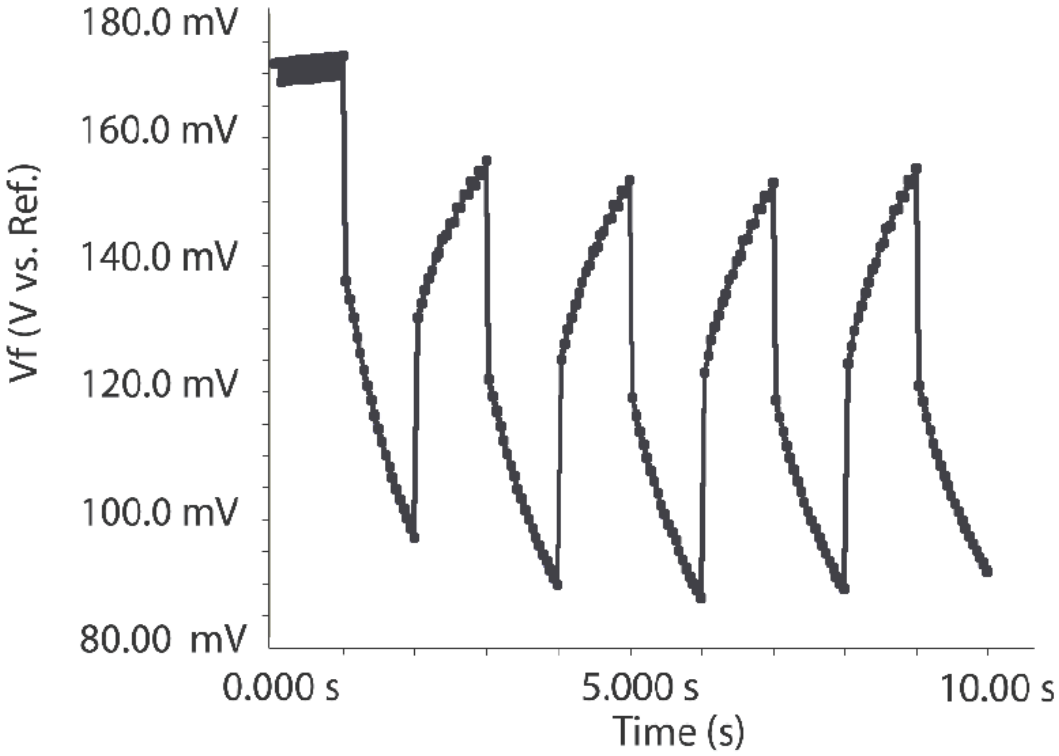

Figure 3-8: Charge/discharge curves of voltage over time for tall CNT forest supercapacitor electrode with an amorphous silicon coating.

Conclusions

A supercapacitor electrode has been demonstrated in this chapter to realize the high energy storage potential of an amorphous-silicon coated CNT forest. The electrode is fabricated by cleaning and thermally oxidizing a silicon wafer, depositing thin films of Mo (a current collector), Al, and Fe, then growing a vertically self-aligned CNT forest using CVD with hydrogen and ethylene gases, followed by a low-pressure CVD of amorphous silicon. This results in an electrode with three promising characteristics. First, the charge transfer to the substrate via the aligned CNTs was improved over conventional supercapacitor electrodes. Second, the coating of amorphous silicon provides for excellent charge storage. Thirdly, the large amount of surface area and porosity of the CNT forest is preserved. The electrode is also compared to one with a tall CNT forest. The tall CNT forest also benefits from the deposition of a layer of amorphous silicon, but has a larger overall capacitance due its increase in CNT length, which also effectively increases the surface area of the electrode. Electrochemical testing indicated

that the electrodes are stable in capacitance over cycling, with over 90% efficiency, and hence stable in energy density.

References

[1] V.L Pushparaj et al., "Flexible energy storage devices based on nanocomposite paper," *Proceedings of the National Academy of Sciences*, vol. 104, no. 34, p. 13574, 2007.

[2] L.F Cui, L Hu, J.W Choi, and Y Cui, "Light-Weight Free-Standing Carbon Nanotube-Silicon Films for Anodes of Lithium Ion Batteries," *ACS nano*, vol. 4, no. 7, pp. 3671-3678, 2010.

[3] B G Choi, M Yang, W H Hong, J W Choi, and Y S Huh, "3D Macroporous Graphene Frameworks for Supercapacitors with High Energy and Power Densities ," *ACS nano*, vol. 6, no. 5, pp. 4020-4028, Apr 2012.

[4] Mun Sek Kim, Ben Hsia, Carlo Carraro, and Roya Maboudian, "Flexible micro-supercapacitors with high energy density from simple transfer of photoresist-derived porous carbon electrodes," *Carbon*, vol. 74, pp. 163-169, Apr 2014.

[5] X Lu et al., "High Energy Density Asymmetric Quasi-Solid-State Supercapacitor Based on Porous Vanadium Nitride Nanowire Anode," *Nano letters*, vol. 13, pp. 2628-2633, Jun 2013.

[6] Liang Kou et al., "Coaxial wet-spun yarn supercapacitors for high-energy density and safe wearable electronics," *Nature Communications*, vol. 5, pp. 1-10, Apr 2014.

[7] M. Mastragostino, F. Soavi, and C. Arbizzani, "Ch. 16: Electrochemical Supercapacitors," in *Advances in Lithium Ion Batteries*. US: Springer, Kluwer Academic Publishers, Nov 2002, pp. 481 - 505.

[8] D. Berndt, "Electrochemical Energy Storage," in *Battery Technology Handbook*, 2nd ed.: CRC Press, Nov 2003.

[9] I Lahiri et al., "High Capacity and Excellent Stability of Lithium Ion Battery Anode Using Interface-Controlled Binder-Free Multiwall Carbon Nanotubes Grown on Copper," *ACS nano*, vol. 4, no. 6, pp. 3440-3446, 2010.

[10] M Inagakia, Hidetaka Konno, and Osamu Tanaike, "Carbon materials for electrochemical capacitors," *Journal of Power Sources*, vol. 195, no. 24, pp. 7880-

7903, Dec 2010.

[11] L.F Cui, Y Yang, C.M Hsu, and Y Cui, "Carbon− Silicon Core− Shell Nanowires as High Capacity Electrode for Lithium Ion Batteries," *Nano letters*, vol. 9, no. 9, pp. 3370-3374, 2009.

[12] Candace K Chan et al., "High-performance lithium battery anodes using silicon nanowires," *Nature Nanotechnology*, vol. 3, no. 1, pp. 31-35, Jan 2008.

[13] W Wang and P.N Kumta, "Nanostructured hybrid silicon/carbon nanotube heterostructures: Reversible high-capacity lithium-ion anodes," *ACS nano*, vol. 4, no. 4, pp. 2233-2241, 2010.

[14] Y Fan, Q Zhang, Q Xiao, X Wang, and K Huang, "High performance lithium ion battery anodes based on carbon nanotube–silicon core–shell nanowires with controlled morphology," *Carbon*, vol. 59, pp. 264-269, Nov 2013.

[15] K Fu et al., "Aligned Carbon Nanotube-Silicon Sheets: A Novel Nano-architecture for Flexible Lithium Ion Battery Electrodes," *Advanced Materials*, vol. 25, pp. 5109-5114, Nov 2013.

[16] L Hu, H Wu, Y Gao, A Cao, and H Li…, "Silicon–Carbon Nanotube Coaxial Sponge as Li-Ion Anodes with High Areal Capacity," *Advanced Energy Materials*, vol. 1, pp. 523-527, Jan 2011.

[17] Y.Q Jiang, Q Zhou, and L Lin, "Planar MEMS Supercapacitor Using Carbon Nanotube Forests ," *Micro Electro Mechanical Systems, MEMS Conference 2009*, pp. 587-590, Mar 2009.

Chapter 4: Supercapacitor Electrode with Enhanced Voltage Window

Chapter Summary

This chapter introduces the performance and benefits of an ionic liquid electrolyte in place of an aqueous electrolyte in conjunction with two symmetric aligned carbon nanotube forest electrodes possessing high surface areas. Compared to aqueous electrolytes used in the previous chapters, the ionic liquid electrolyte EMIM-BF_4 [citations] is capable of producing a considerably larger voltage (4 V vs 1 V), which improves the power performance of the supercapacitive device, and yields a good power density in the range of 19 to 53 kW/kg. In addition, the EMIM-BF_4/VACNT forest combination retains charge well over more than 7000 charge and discharge cycles, and has good specific capacitance values of 5 mF/cm^2 to 11.5 mF/cm^2 for a symmetric two-electrode supercapacitor. Finally, the capacitance by volume of the EMIM-BF_4/VACNT forest supercapacitor outperforms an EMIM-BF_4/AC supercapacitor of similar area by a factor of 12.

Introduction

The previous two chapters have detailed the important role that surface area plays in the energy storage of a supercapacitive electrode. The larger the surface area, the more expansive the electrochemical double layer, and hence the larger the amount of energy that can be stored within the electrode becomes. Energy density is a crucial factor for energy storage devices. With increased energy density, lightweight energy storage becomes a possibility. For applications such as recovering energy from a car wheel during braking, and powering electric vehicles, energy density in terms of weight as well as size must be taken into account. But if the goal is to charge up a device and discharge it quickly, power density must also be a concern. A larger power density allows these devices to charge and discharge quickly, such that energy may be more efficiently recovered from a braking car wheel, and charging electric vehicle batteries in a matter of minutes instead of hours becomes a possibility. High power density storage materials are not only needed in the automotive industry, but also in applications in the aerospace and defense industries, as well as in consumer electronics.

One way to increase the power density capability in a supercapacitor is to increase the maximum available voltage, where power is proportional to the square of the voltage [1]:

$$P_{\max} = \frac{V_{\max}^2}{4(ESR)} \qquad (1)$$

Here P_{max} is the maximum possible power output by the supercapacitor, V_{max} is the maximum available voltage, and *ESR* is the equivalent series resistance of the device. The maximum voltage is governed by the breakdown potential of the electrolyte [2]. Whereas in the last two chapters aqueous electrolytes were used, whose breakdown

potentials are equivalent to that of water (about 1 V), electrolytes with higher breakdown potentials may be used. For instance, room temperature ionic liquid electrolytes, which are composed of a combination of large inorganic anions and asymmetrical organic cations (in other words, are room-temperature salts in liquid form), possess breakdown voltages of 4 to 6 V [3,4]. These ionic liquids are also known to have further beneficial properties, including high ionic conductivity, great thermal stability (due to their extremely low vapor pressures), and nonvolatility [4-7]. However, the use of ionic liquids is still beginning in supercapacitor research, and more study needs to be made to fully explore all of the possible advantageous properties. Furthermore, the architecture of the supercapacitor electrodes is important when considering which ionic liquid to use for best performance, since the wetting of the electrode surface must be excellent in order to utilize the combined properties of high surface area electrodes and high electrochemical window of ionic liquids [4].

In essence, using these ionic liquid electrolytes in place of the aqueous electrolytes from previous chapters gives us the possibility of increasing the voltage window of the supercapacitor devices, and further improving their performance. Tsai et al. used

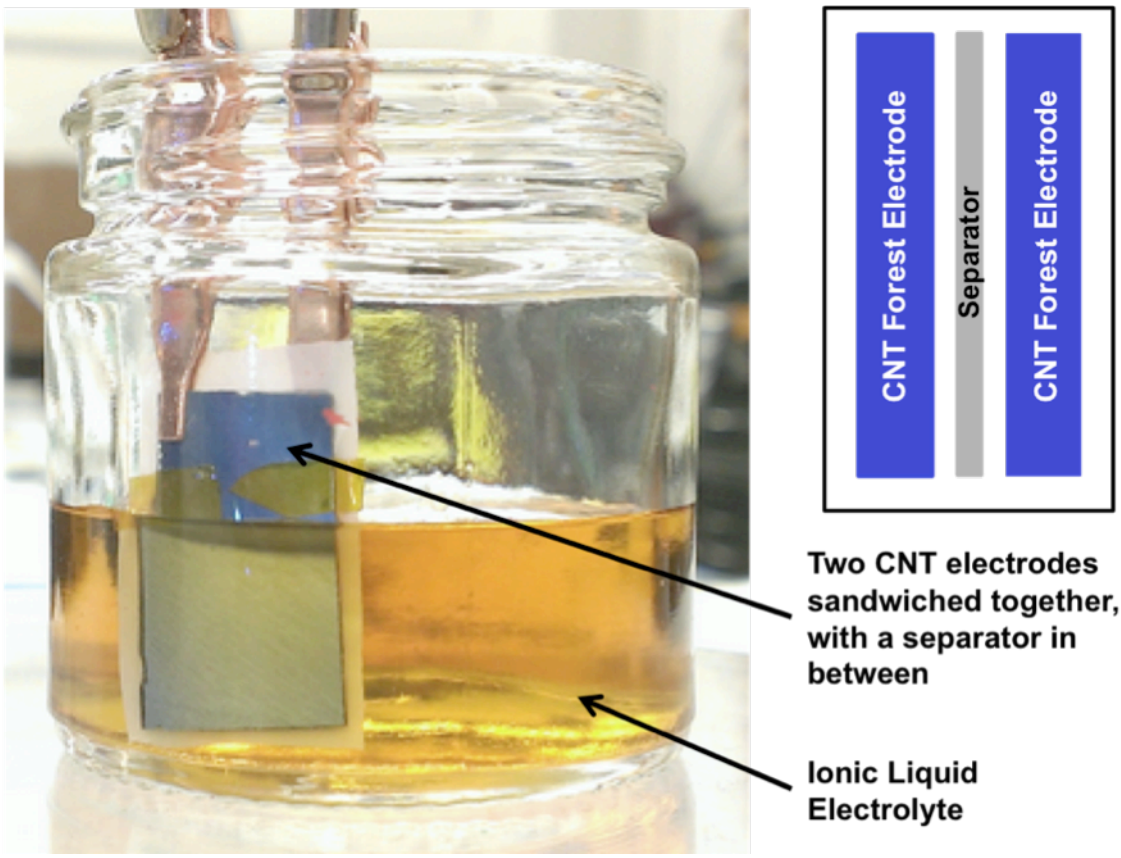

Figure 4-1: Electrochemical 2-electrode test setup used for supercapacitor tests in this chapter. The 2 electrodes consist of two symmetric VACNT forest electrodes, with a separator sandwiched in between them to prevent electrical shorting. A schematic of the separator placement may be seen in the inset.

mixtures of ionic liquids with graphite oxide electrodes to form supercapacitors with excellent thermal properties and high energy densities, while Balducci et al. used a microporous activated carbon electrode in conjunction with an ionic liquid to create a supercapacitor than can withstand a high temperature working environment [8,9]. The safety of ionic liquid supercapacitors has also been demonstrated in the literature. For instance, Arbizzani et al. determined that ionic liquid electrolytes can meet the energy and power requirements necessary for hybrid electric vehicles (HEVs), while still remaining safe to use in HEVs [10].

The ionic liquid electrolyte used for the work in this chapter is unadulterated 1-ethyl-3-methylimidazolium tetrafluoroborate (EMIM-BF_4). The testing setup for the 2-electrode electrochemical tests used to quantify the performance of the CNT forest electrodes within the ionic liquid electrolyte may be seen in Figure 4-1. The two electrodes are sandwiched together with a polymer (polypropylene) separator, which ensures that the opposing electrodes do not short during testing.

Design and Fabrication

The fabrication process of the supercapacitor electrodes used in this chapter follows the same process as outlined in chapter 2, but stopping at step 2 with the growth of the vertically aligned carbon nanotube (VACNT) forest. In essence, the fabrication process

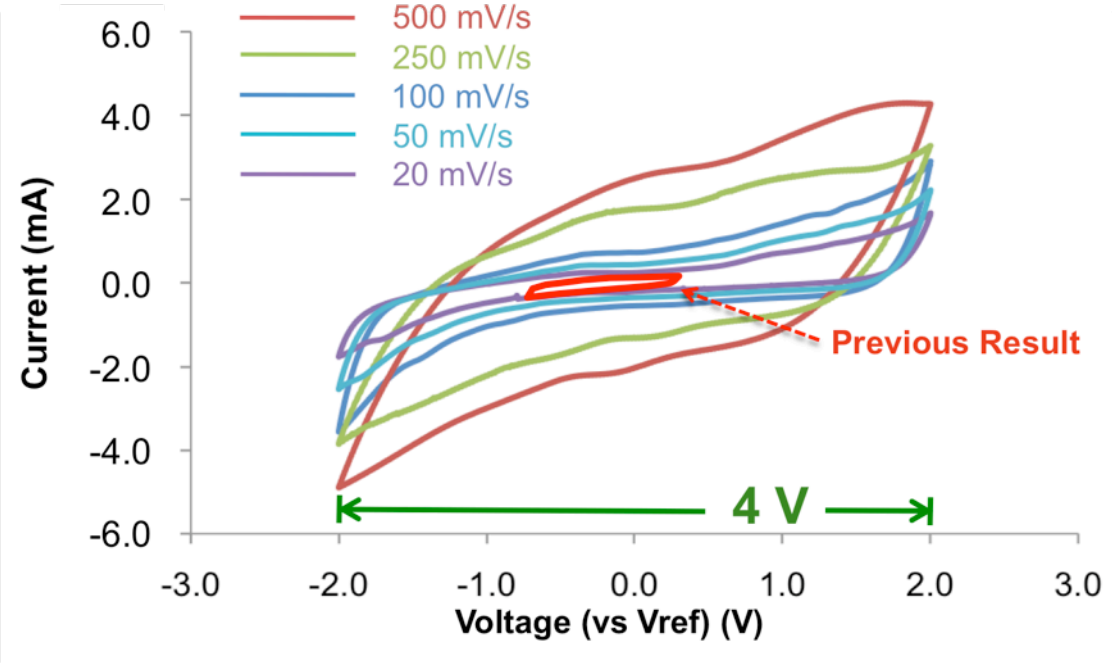

Figure 4-2: Cyclic voltammetry data of two CNT forest supercapacitor electrodes tested in ionic liquid electrolyte EMIM-BF_4, taken at various voltage scan rates ranging from 20 mV/s to 500 mV/s. The previous result (of a bare CNT forest of similar height in aqueous electrolyte) may be seen overlaid in bright red.

begins with the cleaning and thermal oxidation of a silicon wafer. Then, a thin film molybdenum current collector is deposited onto the wafer using e-beam evaporation, followed by the thin film depositions of the catalyst for CNT growth (Al and Fe). The thicknesses of the deposited metals are 50 nm of Mo, 10 nm of Al, and 5 nm of Fe. After scribing individual 5 mm by 10 mm sample areas using a wafersaw into the wafer containing the evaporated layers, the wafer is transferred into a vacuum quartz tube furnace (Lindberg/Blue M® threezone tube furnace, Thermo Electron Corp., Asheville, NC). The CNT growth follows the process developed by Y. Jiang et al [11]. Once the quartz tube is evacuated and purged with hydrogen gas, and the furnace is stabilized to a temperature of 720°C in a hydrogen gas environment, the process gases (hydrogen and ethylene) are flown through the tube at volumetric flow rates of ratios of approximately 7:1, respectively. The chemical vapor deposition (CVD) growth process proceeds for ten minutes, during which the temperature and gas flow rates are held constant. Once the growth process is complete, the tube is cooled to room temperature. This process results in a vertically self-aligned CNT forest. This CNT forest electrode is then used to test the improved voltage window of the ionic liquid electrolyte, EMIM-BF_4.

Results and Discussion

A 2-electrode test setup is employed, where each half is comprised of a 1 cm by 1 cm area supercapacitive electrode utilizing a vertically aligned CNT forest atop a silicon

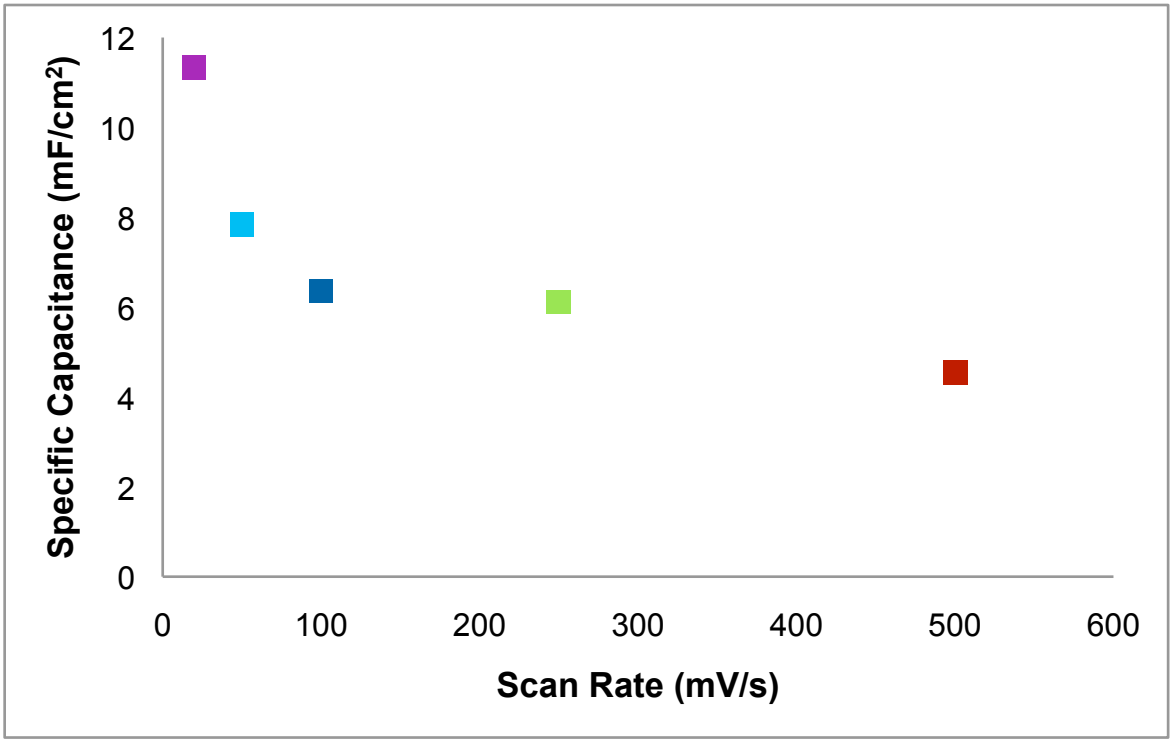

Figure 4-3: Specific capacitance of the two-electrode supercapacitor device in ionic liquid EMIM-BF_4 as a function of voltage scanning rate.

growth substrate. To ensure that electrical shorting between the two electrodes does not occur, a 25 µm thick polypropylene Celgard® separator was secured between the two CNT forests. In order to assess how the electrodes perform in the new ionic liquid electrolyte (EMIM-BF_4), a series of cyclic voltammetry curves are recorded at varying voltage scan rates from 20 mV/s to 500 mV/s, as seen in Figure 4-2. This data is compared to that of the previous result – the cyclic voltammogram of a bare CNT forest of similar height in aqueous electrolyte - which may be seen overlaid in bright red.

It can be clearly seen that the voltage window has dramatically increased over the past result, leading to a potential of as much as a 16X improvement in maximum power as well as energy stored. However, this improvement is likely smaller, as the resistance of the system is slightly increase by switching from an aqueous to an ionic liquid electrolyte.

The specific capacitance of the device has been determined for each scanning rate, and is graphed in Figure 4-3. The specific capacitance of the device decreases from 11.5 mF/cm^2 to 5 mF/cm^2 as scanning rate increases from 20 mV/s to 500 mV/s. This is expected since at very high scan rates the electrolyte ions do not have time to fully adsorb onto the entire surface of the CNTs, leading to a smaller amount of energy stored, and a smaller capacitance [12].

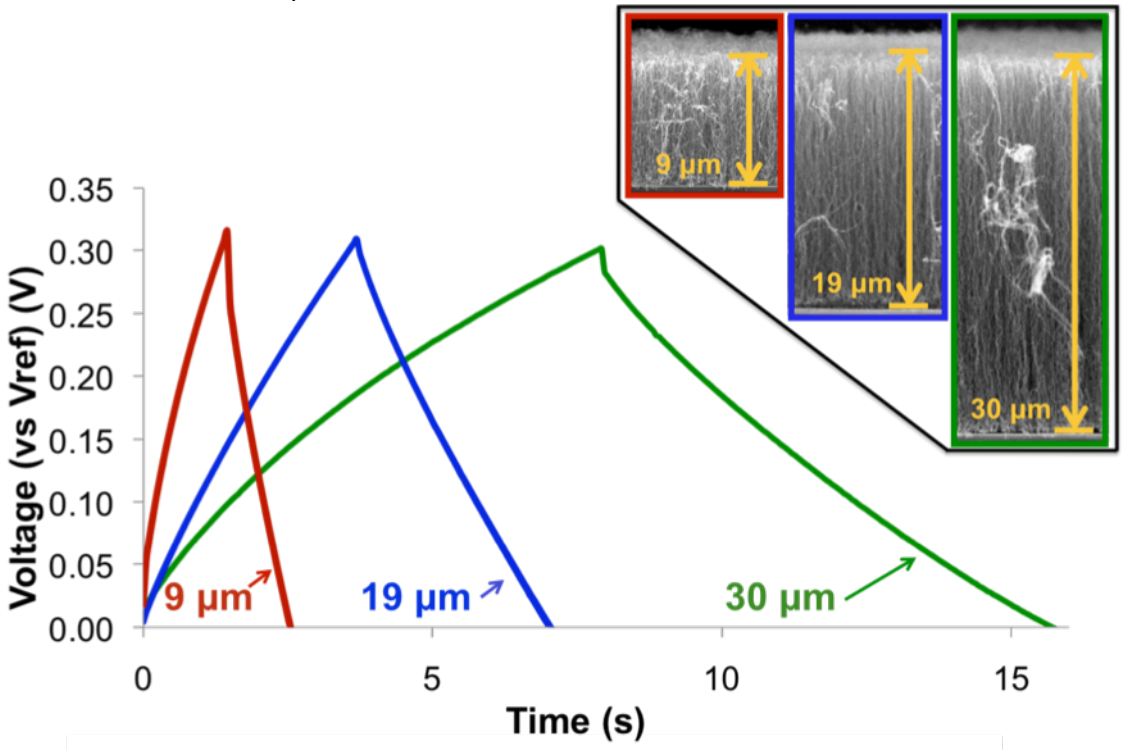

Figure 4-4: Charge-Discharge curves of the aligned CNT forest electrodes in ionic liquid, EMIM-BF4, taken with a 2-electrode testing setup, with electrode areas of 1 cm by 1 cm. Three CNT forest heights are tested – the red curve denotes the 9 um forest, pictured in the red-outlined inset, and the blue and green curves similarly match the blue and green outlined CNT forests, respectively.

On a similar note, the larger the capacitance of a supercapacitor device, the longer it will take to charge it. To show this, and the compromise that is taken between a larger capacitance and a shorter charge time, three supercapacitor devices were fabricated and tested using three different CNT forest heights – 9 µm, 19 µm, and 30 µm. Cross-sectional SEM images for each forest height may be seen in the inset in Figure 4-4. Each test conducted uses the same electrode area sizes, in the same ionic liquid electrolyte EMIM-BF_4. Each device is charged to 0.3 V at a constant current, then discharged at a constant current equal to the negative of the charging current. As seen in Figure 4-4, the time to charge to 0.3 V increases as the CNT forest height increases. An increase in CNT height yields to an increase in total electrode surface area, and hence the capacitance of the electrode.

In order to see how the aligned CNT forest supercapacitor electrode measures up to activated carbon, which is used in commercial supercapacitor devices, a sample of activated carbon (AC) was obtained and tested. Two-electrode cyclic voltammetry tests are conducted on both the CNT forest supercapacitor electrodes and the AC supercapacitor electrodes in EMIM-BF_4, using a scanning rate of 100 mV/s – the results are shown in Figure 4-5. Each electrode in this test has an area of 1 cm by 1 cm. Compared to the AC electrodes, the CNT electrodes have a capacitance that is 2.5 X

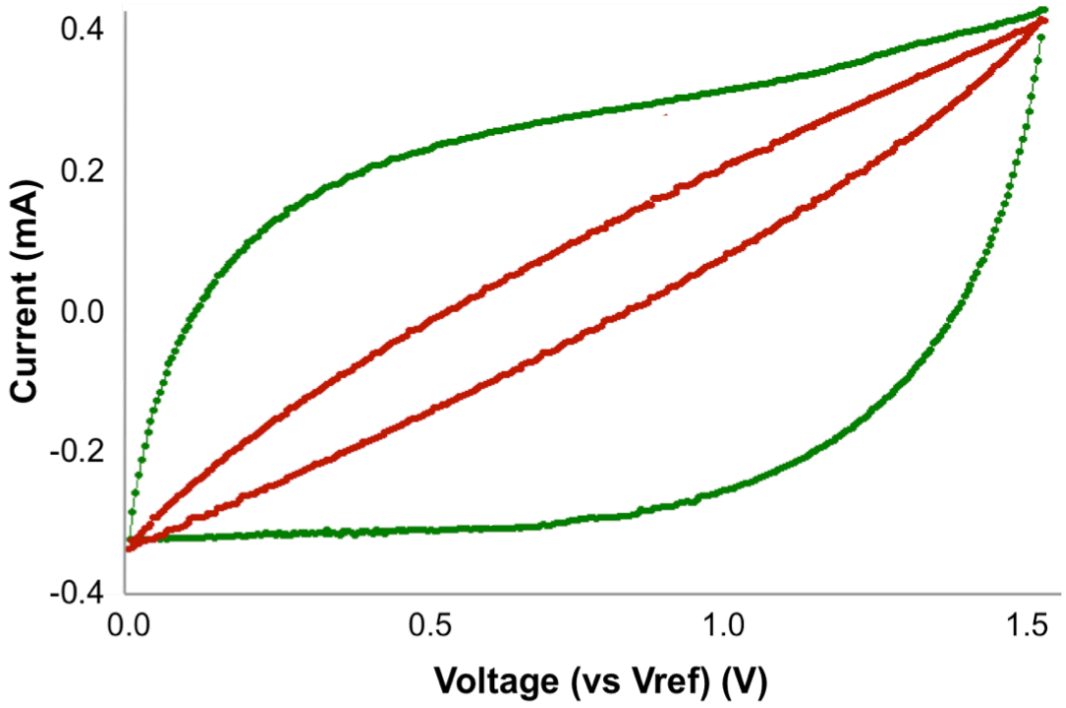

Figure 4-5: Cyclic voltammetry scans comparing aligned CNT forest electrode (green) performance to that of an AC electrode (red). Both scans were performed using a two-electrode test setup in ionic liquid electrolyte EMIM-BF_4 at a scan rate of 100 mV/s. All electrodes had equivalent areas of 1 cm by 1 cm.

larger. It should be noted that the capacitance of the CNT supercapacitor is larger despite the AC carbon electrode being much thicker. The CNT forest used for this testing is 80 µm tall, while the AC is 385 µm thick, and can be seen in Figure 4-6. This means that the specific capacitance of the CNT electrode by volume is 12 X larger than that of the AC electrode – 388 mF/cm^3 versus 31 mF/cm^3 for the AC electrode. A factor that may be contributing to the smaller capacitance of the AC electrode is the difference in pore structure between the AC and CNT electrode materials. The randomly arranged

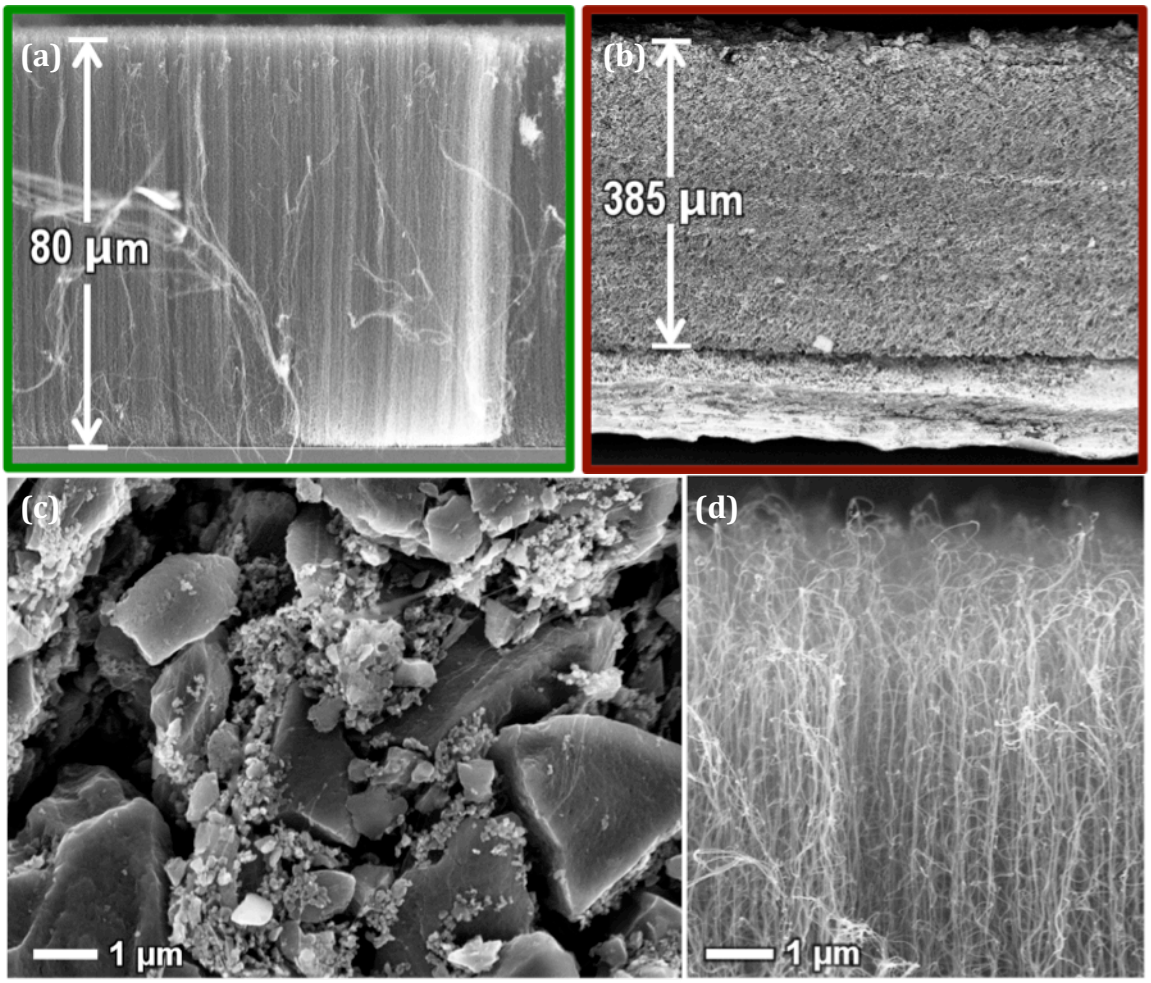

Figure 4-6: SEM images showing cross sections of supercapacitive electrodes. An 80 µm tall vertically aligned CNT forest in (a) is compared to a 385 µm thick AC electrode in (b). Further magnification reveals the pore structure of the two electrode materials – (c) for AC, and (d) for the CNT forest.

carbon particles in the AC electrode yield uneven pores – some of which may be difficult for the electrolyte ions to access [8,2]. In addition, in order for the electrolyte ions to reach the bottom of the AC electrode, they must travel along a tortuous path. A CNT electrode material, however, allows for a more direct ion path, and leaves no pores closed off from the ions [13].

In addition, the specific power of the CNT forest supercapacitor was calculated to be in the range between 19 and 53 kW/kg. This is a range due to the range in CNT mass loading data that was collected – of a given cubic centimeter of volume, the CNTs grown weigh between 33 and 92 mg.

Since it is also important to note the stability of the CNT forest electrodes in the ionic liquid over charge-discharge cycling, the cyclic performance of the 1 cm^2 area two-electrode device is also assessed. Three current densities are applied to the device - 0.5 µA, 1 µA (twice), and 5µA, in succession – the results of which may be seen in Figure 4-7. Each current is applied first for 5 s as its positive value (for instance, 1 µA) then applied for 5 s as its negative value (for instance, - 1 µA). These 10 seconds comprise one charge-discharge cycle. The device has good stability for over 7000 charge-discharge cycles.

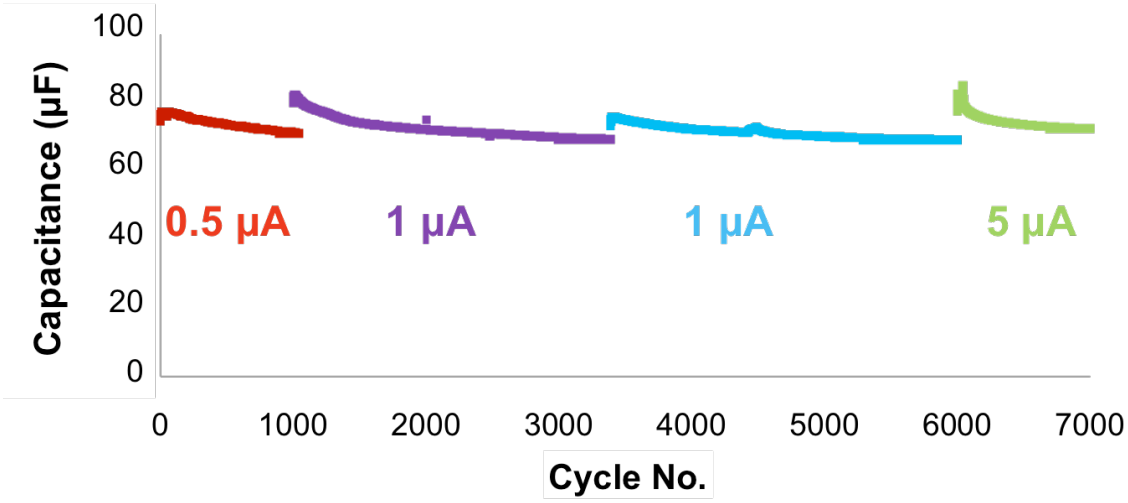

Figure 4-7: Cycling performance of the vertically aligned CNT supercapacitor electrode measured over 7000 cycles, at 3 charging currents. Measurements of the 1cm^2 are electrodes were taken using a two-electrode test setup in ionic liquid electrolyte EMIM-BF_4. Capacitance values are represented by the discharge portion of a charge-discharge curve associated with the particular current, over the 5 s of discharge.

Conclusions

This chapter has reviewed the results of using an ionic liquid electrolyte in place of an aqueous electrolyte in conjunction with two symmetric aligned carbon nanotube forest electrodes possessing high surface areas. Compared to aqueous electrolytes used, the ionic liquid electrolyte EMIM-BF_4 is capable of producing a considerably larger voltage (4 V vs 1 V), and yields good power performance in the range of 19 to 53 kW/kg. In

addition, the EMIM-BF_4/VACNT forest combination yields good stability results over charging and discharging for over 7000 cycles, as well as good specific capacitance values of 5 mF/cm^2 to 11.5 mF/cm^2 for a symmetric two-electrode supercapacitive setup. Finally, the EMIM-BF_4/VACNT forest supercapacitor outperforms an EMIM-BF_4/AC supercapacitor of similar area by 2.5 X, in terms of capacitance. Taking the volume of the supercapacitor electrodes into account, the VACNT specific capacitance is 12 X larger than that of the AC supercapacitor - 388 mF/cm^3 versus 31 mF/cm^3 for the two-electrode tests.

References

[1] H Konno, O Tanaike M Inagaki, "Carbon materials for electrochemical capacitors," *Journal of Power Sources*, vol. 195, no. 24, pp. 7880-7903, 2010.

[2] F Begui E Frackowiak, "Carbon materials for the electrochemical storage of energy in capacitors," *Carbon*, vol. 39, pp. 937-950, 2001.

[3] Marisa C Buzzeo, Russell G Evans, and Richard G Compton, "Non-Haloaluminate Room-Temperature Ionic Liquids in Electrochemistry—A Review," *ChemPhysChem*, vol. 5, no. 8, pp. 1106-1120, Aug 2004.

[4] Michel Armand, Frank Endres, Douglas R Macfarlane, Hiroyuki Ohno, and Bruno Scrosati, "Ionic-liquid materials for the electrochemical challenges of the future," *Nature Materials*, vol. 8, pp. 621-629, Jul 2009.

[5] C Angell et al., "Physical Chemistry of Ionic Liquids, Inorganic and Organic, Protic and Aprotic," *Electrochemical Aspects of Ionic Liquids*, pp. 5-23, 2005.

[6] T Y Kim et al., "High-Performance Supercapacitors Based on Poly(ionic liquid)-Modified Graphene Electrodes ," *ACS nano*, vol. 5, no. 1, pp. 436-442, Jan 2011.

[7] Chenguang Liu, Zhenning Yu, David Neff, Aruna Zhamu, and Bor Z Jang, "Graphene-Based Supercapacitor with an Ultrahigh Energy Density," *Nano letters*, vol. 10, no. 12, pp. 4863-4868, Dec 2010.

[8] R Lin, S Murali, LL Zhang, JK McDonough, RS Ruoff, P Taberna, Y Gogotsi, P Simon W Tsai, "Outstanding performance of activated graphene based supercapacitors in ionic liquid electrolyte from -50 to 80 C," *Nano Energy*, vol. 2, pp. 403-411, 2013.

[9] R Dugas, P Taberna, P Simon, D Plée, M Mastragostino, S Passerini A Balducci, "High temperature carbon–carbon supercapacitor using ionic liquid as electrolyte,"

Journal of Power Sources, vol. 165, no. 2, pp. 922-927, 2007.

[10] M Biso, D Cericola, M Lazzari, F Soavi, M Mastragostino C Arbizzani, "Safe, high-energy supercapacitors based on solvent-free ionic liquid electrolytes," *Journal of Power Sources*, vol. 185, no. 2, pp. 1575-1579, 2008.

[11] Y.Q Jiang, Q Zhou, and L Lin, "Planar MEMS Supercapacitor Using Carbon Nanotube Forests ," *Micro Electro Mechanical Systems, MEMS Conference 2009*, pp. 587-590, Mar 2009.

[12] J.N Barisci*, G.G Wallace*, and R.H Baughman, "Electrochemical studies of single-wall carbon nanotubes in aqueous solutions," *Journal of Electroanalytical Chemistry*, vol. 488, no. 2, pp. 92-98, 2000.

[13] H Zhang, G Cao, and Y Yang, "Electrochemical properties of ultra-long, aligned, carbon nanotube array electrode in organic electrolyte," *Journal of Power Sources*, vol. 172, no. 1, pp. 476-480, 2007.

[14] G Feng, S Li, V Presser, and P T Cummings, "Molecular Insights into Carbon Supercapacitors Based on Room- Temperature Ionic Liquids," *Journal of Physical Chemistry Letters*, vol. 4, pp. 3367-3376, Oct 2013.

[15] B E Conway, *Electrochemical Supercapacitors- Scientific Fundamentals and Technological Applications*., Mar 1999, vol. New York, USA.

[16] P Simon and Y Gogotsi, "Materials for electrochemical capacitors," *Nature Materials*, vol. 7, pp. 845-854, Oct 2008.

Chapter 5: Utilizing the Vertically Aligned Carbon Nanotube Forest Architecture for Lithium Ion Battery Applications

Chapter Summary

This chapter introduces the facile way in which silicon-coated vertically aligned carbon nanotube (CNT) forests may be used as architectures for lithium ion battery electrodes. A lithium ion battery electrode is fabricated and tested, and shows good promise. Testing yields a capacity plateau of 600 mAh/g, with a specific power and energy of 270 W/kg and 300 Wh/kg, respectively. The cycling life of the electrode may be improved by utilizing a thinner coating of silicon, as an overly thick coating of silicon at the bottom of the CNT forest leads to delamination of the active material from the current collector layer after 20 charge-discharge cycles.

Introduction

Whereas supercapacitors offer high rates of charge and discharge, the amount of energy they store – their energy density – is still small compared to that of rechargeable, or secondary, batteries. Supercapacitor energy densities tend to range from 2 to 86 Wh/kg (although commercially available supercapacitors possess energy densities on the low side of this – typically around 6 Wh/kg) [1]. Compared to these values, typical rechargeable batteries possess energy density values that range from 10 to 230 Wh/kg – a considerable difference [2,3]. Near the top range of these rechargeable batteries are

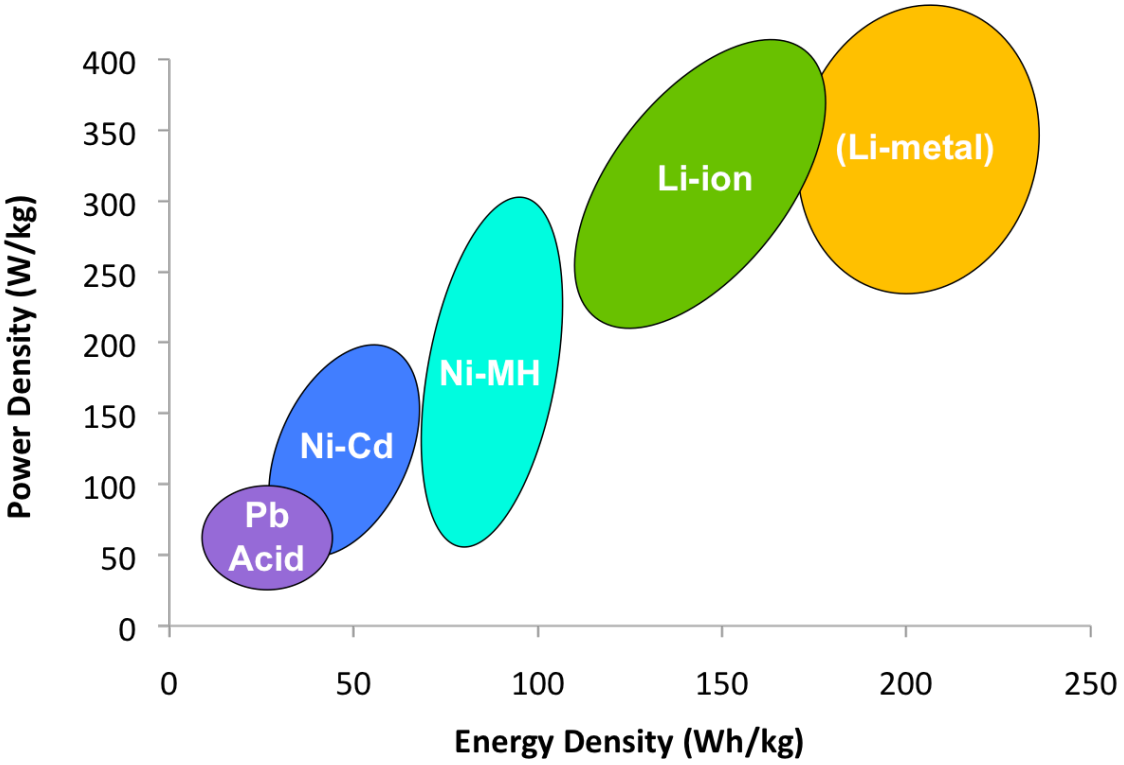

Figure 5-1: Graph comparing the energy densities and power densities of various families of rechargeable batteries: lead acid (Pb-acid), nickel-cadmium (Ni-Cd), nickel-metal-hydride (Ni-MH), lithium ion (Li-ion), and lithium-metal (Li-metal), as extracted from [3].

lithium-ion (Li-ion) batteries and lithium-metal (Li-metal) batteries, as can be seen in Figure 5-1. Li-metal batteries, though possessing larger energy densities than Li-ion batteries, are deemed unsafe due to the danger of possible explosion [2,4,5]. Li-ion batteries are considered safer than their Li-metal counterparts, since there is no dendritic Li growth emerging from the Li metal electrode (as there is no Li metal electrode), which may grow far enough as to contact the opposite electrode in the battery cell, cause a short circuit, and lead to notable local heating, fire, and explosion [4]. Instead of a Li-metal counter electrode, a Li-carrying electrolyte is used with two Li-ion host electrodes in a Li-ion battery, creating a safer energy storage device [6,7].

The host electrodes are normally composed of carbon materials, but there is growing interest in using silicon as the active Li intercalation material [8-11]. This is due to the extremely large lithium intercalation capacity of silicon: every silicon atom can accommodate 4.4 Li atoms [12-14]. To date, this yields the highest capacity for storing lithium ions, with a capacity of 4200 mAh/g [9]. Compared to the capacity of carbon to store lithium ions - 372 mAh/g. However, due to this large capacity, silicon undergoes very large volumetric changes upon charging and discharging of the Li-ion battery – from 300 to 400% [9]. If just bulk silicon were to be used, the silicon would increase in volume on the first charge, then upon discharge, would break apart and crack, as depicted in the illustration in Figure 5-2. After another few charge-discharge cycles, the silicon would become completely pulverized, separate from the current collector it was attached to, and no longer produce useable charge [8].

So what are we to do? Silicon has an amazingly high capacity for lithium ions, but becomes broken up and eventually ceases to charge after a few cycles. One way we can still make use of silicon, and avoid this pulverization, is to utilize a support architecture that allows for some strain relief as the silicon increase and decreases in volume with charge. For instance, a thin film of silicon may be evaporated onto a more flexible surface composed of a nanostructured material. The vertically aligned carbon nanotube (CNT) forest architecture that is used in the first few chapters of this work as a basis for a supercapacitor electrode is an ideal choice for a lithium-ion battery using silicon. The CNTs conduct electrons well, are flexible, have a very high surface area, and contain a bottom current collector layer that helps to increase conductivity of the forest when

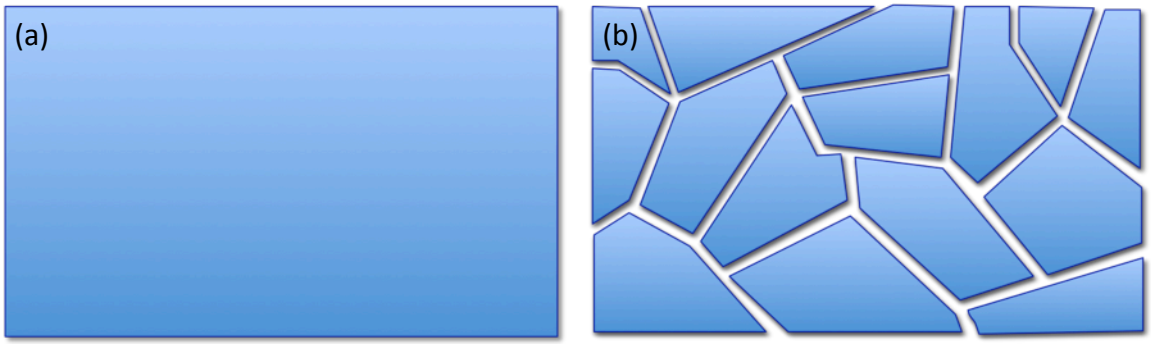

Figure 5-2: Schematic illustration of pristine, uncycled bulk film silicon (a) and (b) pulverized silicon after just one charge-discharge cycles.

configured in an electrical circuit. In addition, this work has already shown the facile method by which the CNT forests may be conformally coated with silicon (see Chapter 3). In fact, it seems that thin films of amorphous silicon are more stable upon lithium ion intercalation and discharge as compared to crystalline silicon [15-17].

Some works in literature utilizing the flexibility of carbon-based, nanostructured materials as a support structure for silicon have been performed. Cui et al. and others have used carbon nanofibers coated with amorphous silicon, as well as CNTs coated with silicon as Li-ion battery electrodes [9, 10, 18-23]. However, for the most part, these silicon/CNT electrodes are fabricated using binders, or by creating a network of CNTs and afterwards depositing silicon. The approach herein utilizes a vertically aligned CNT forest grown upon a molybdenum current collector, as discussed previously. This gives the advantage of having each CNT with inherent connection to the underlying current collector, thusly electrically connecting the entire CNT forest through this metal layer. A

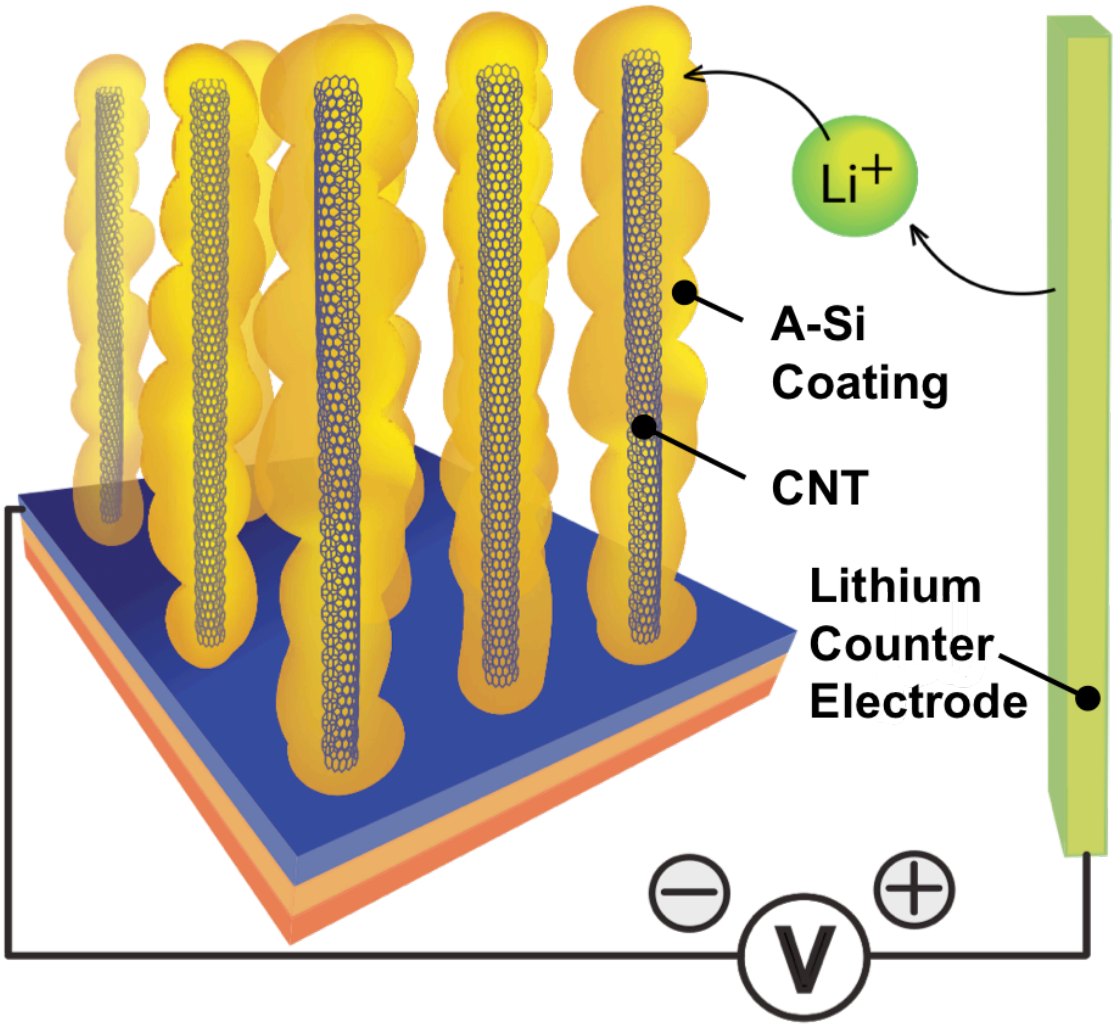

Figure 5-3: Illustration of the amorphous silicon-coated vertically aligned CNT forest Li-ion battery electrode.

schematic illustration of the Li-ion battery electrode may be found in Figure 5-3, where the blue layer corresponds to the current collector.

The overall charging and discharging mechanism of the silicon-coated CNT forest may be seen in Figure 5-4. Upon charging, the Li ions leave the host electrode, move through the electrolyte and separator, then intercalate into the silicon which coats the CNT forest. During discharge, the lithium ions leave the silicon electrode and return to their host electrode.

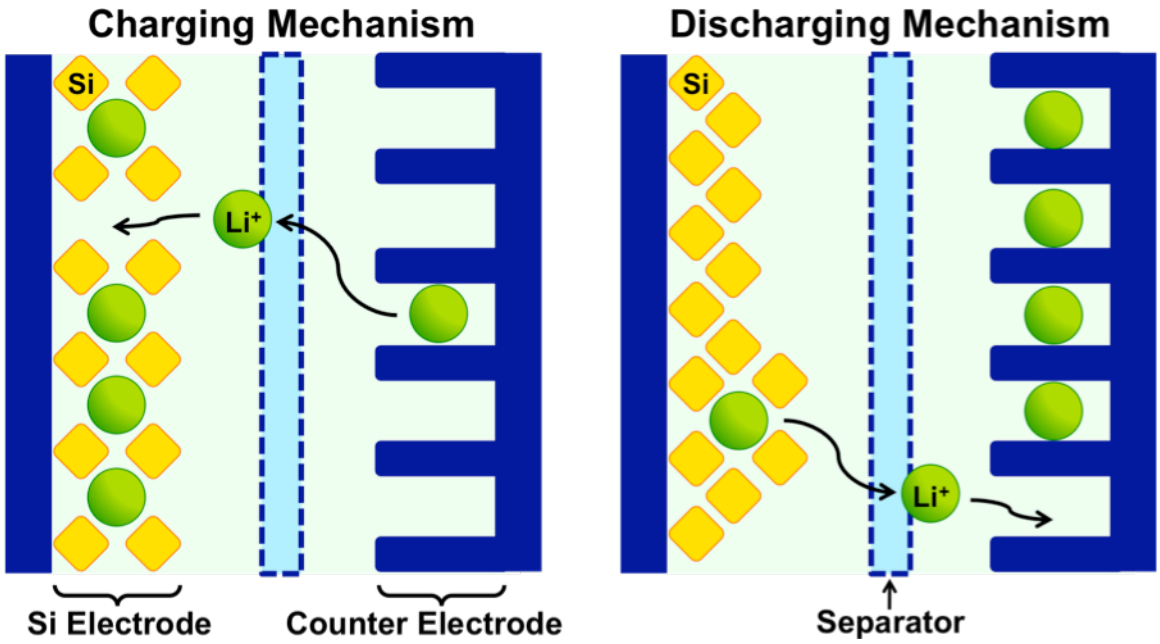

Figure 5-4: Schematic illustration of the charging and discharging mechanisms of a lithium ion battery. In charging (left), lithium ions leave the host electrode, pass through the separator, and intercalate into the silicon electrode. During discharge (right), the lithium ions leave the silicon electrode and return to their host electrode.

Fabrication

The Li-ion battery electrode fabrication process follows the fabrication process of the supercapacitor electrode in Chapter 3. Namely, the vertically aligned CNT forest is grown upon a thermally oxidized silicon wafer after thin metal film depositions using electron beam evaporation. The metal films deposited are 50 nm Mo, 10 nm Al, and finally, 5 nm of Fe. This stack of materials is then diced to the desired electrode area (1.5 cm by 1.5 cm in this case), then placed into a quartz tube furnace for the CNT growth process. The quartz tube is evacuated, then purged to atmospheric pressure with hydrogen gas. Once the furnace reaches 720°C, the process gases are flown: ethylene at 90 sccm, and hydrogen at 610 sccm. After a CVD growth time of 10 minutes, the gases

and furnace are turned off. The quartz tube furnace is cooled to room temperature, upon which the tube is once again evacuated, then purged with argon gas until atmospheric pressure is reached. The CNT forest base electrode may then be retrieved from within the quartz tube, and used in the next step. The CNT forest is then transferred to another furnace – an LPCVD silicon deposition Tystar furnace. A pump and purge sequence along with a temperature stabilization process leads to a deposition temperature of 500°C and a process pressure of 375 mTorr. At this temperature and

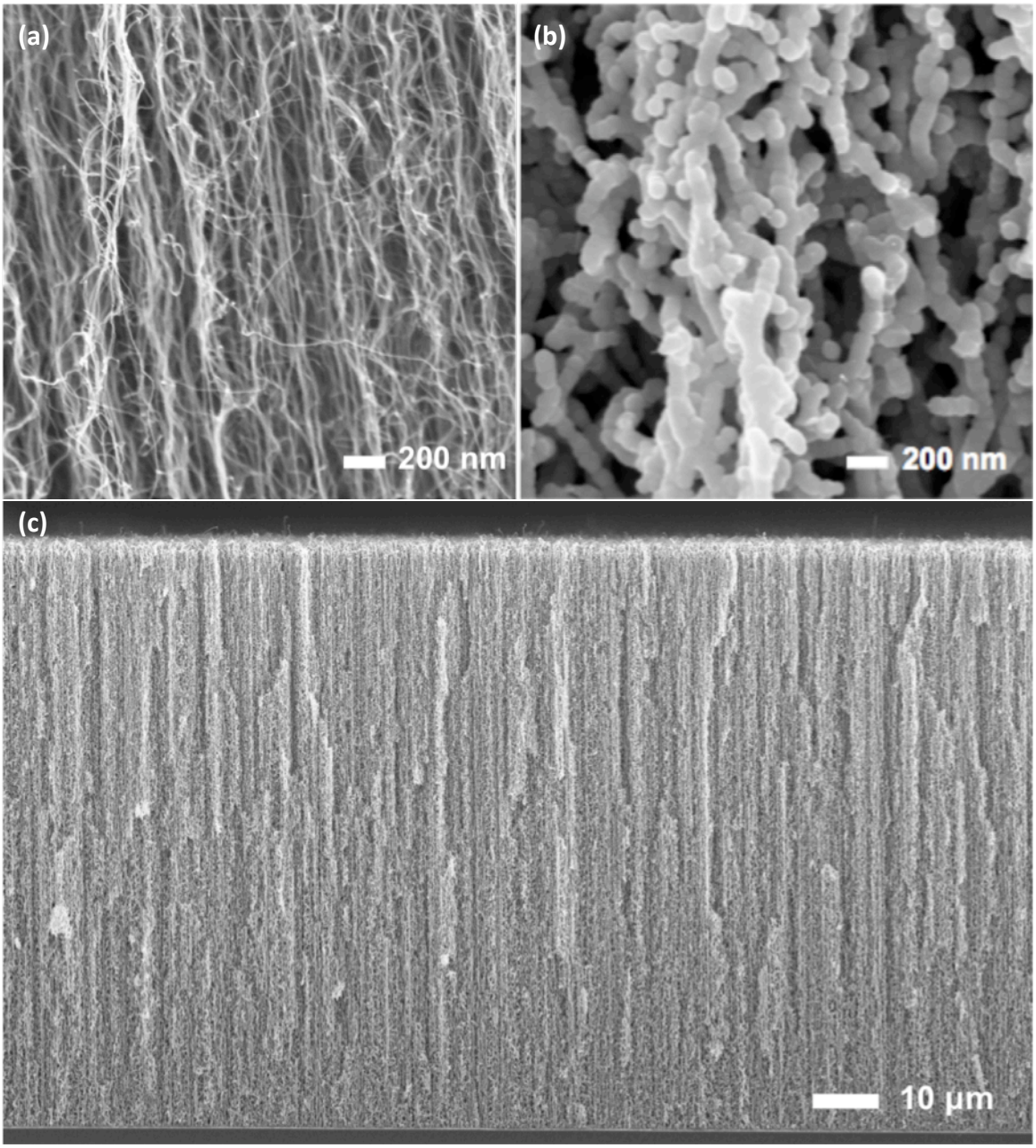

Figure 5-5: SEM images of a bare CNT forest (a) compared to a CNT forest with a 43 nm LPCVD amorphous Si coating (b). A full-height cross sectional SEM image of the silicon-coated CNT forest is shown in (c).

pressure, silane gas is flown through the chamber at a volumetric flow rate of 120 sccm for time durations of 35 minutes. The silicon film deposition results from the migration and reaction of the process gas (silane) with the surfaces it encounters.

After cooling and venting the chamber to atmosphere, the newly created silicon-coated vertically aligned CNT forest electrodes are inspected with a scanning electron microscope (SEM). The silicon coating penetrates the full depth of the CNT forest, as can be seen in the SEM image in Figure 5-5(c), and conformally coats each CNT, as seen in Figure 5-5(b). The difference between the bare CNT forest and the silicon-coated forest can be seen in the SEM images in Figure 5-5(a) and 5-5(b). The total diameter of the amorphous silicon as deposited onto the CNTs measures about 100 nm. With an average CNT diameter of 15 nm, this yields a coating thickness of approximately 43 nm.

Results and Discussion

The amorphous-coated vertically aligned CNT forest electrode is then tested as a Li-ion battery electrode. A schematic of the test setup is shown below in Figure 5-6. All of the components are assembled in an argon gas-filled glove box, with less than 1 ppm oxygen gas, and less than 1 ppm water vapor. The electrolyte used is de-aerated EC,DEC

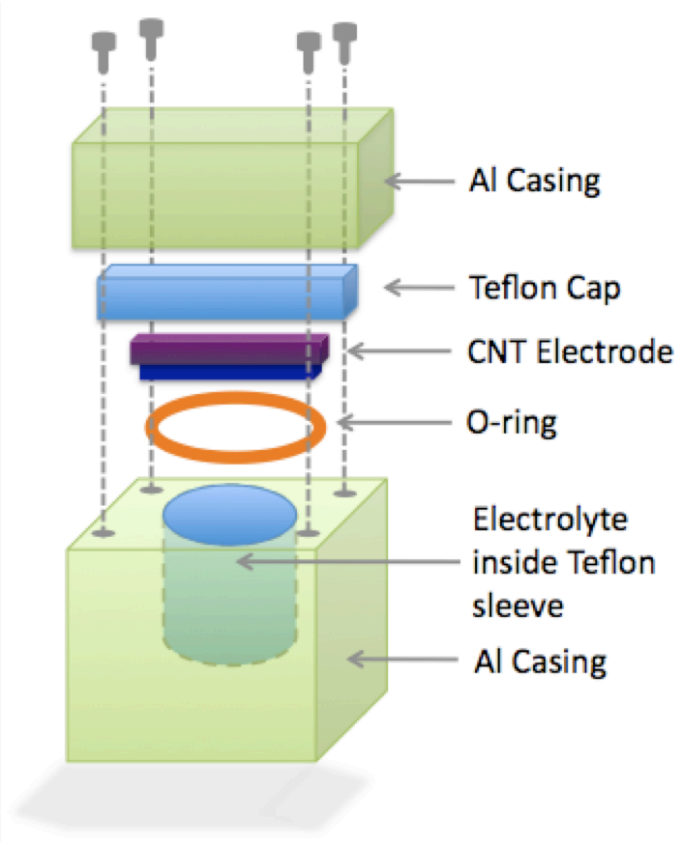

Figure 5-6: Schematic illustration of the test setup employed to test the Li-ion battery electrode. All items are assembled together in an argon-filled glove box, then attached to a potentiostat for testing.

(1:2 v/v) $LiPF_6$ (1 M), the working electrode is the silicon-coated CNT forest, and the reference/counter electrode is lithium foil. A Solartron 1480 multistat system is used to conduct the electrochemical tests.

The testing results show that the silicon-coated CNT forest electrode drops in capacity over the first 5 charge-discharge cycles, as seen in Figure 5-7, then reaches a stable plateau of 600 mAh/g for the remaining charge-discharge cycles. After 15 cycles, however, the capacity drops to almost zero, and the electrode no longer exhibits any useable capacity. The specific power and energy is calculated to be 270 W/kg and 300

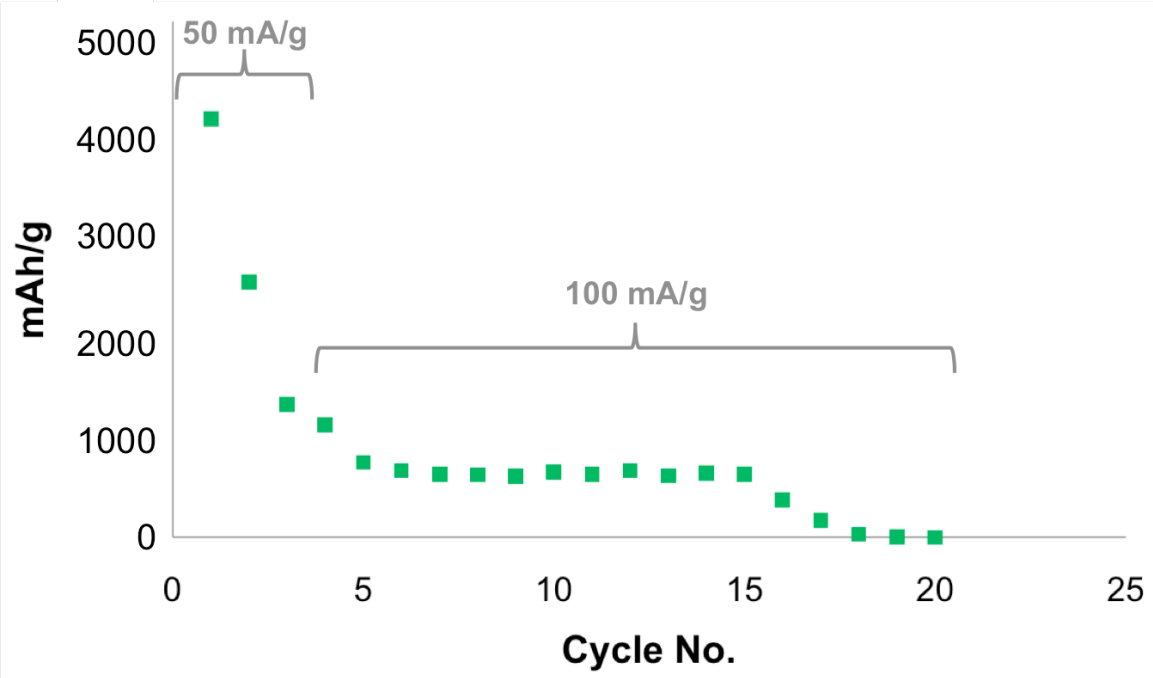

Figure 5-7: Capacity of the silicon-coated vertically aligned CNT forest Li-ion battery electrode as a function of cycle number.

Wh/kg, respectively. An in-depth look can be taken at the process of charging and discharging of the electrode in Figure 5-8, where the voltage of the electrode is read as a function of current density over time. Figure 5-8(a) shows the first three charge-discharge cycles of the electrode, using a current density of 50 mA/g, and Figures 5-8(b) and (c) show the next 17 cycles with a current density of 100 mA/g. Delamination of the active electrode material likely begins at cycle No. 16, and progresses until there is no material left attached to the current collector, and no useable capacity is left in the device. It is believed that delamination is the culprit behind the capacity fade, and not a breakdown in the silicon-coated CNT forest, since the silicon coating appears to be largely unchanged after cycling.

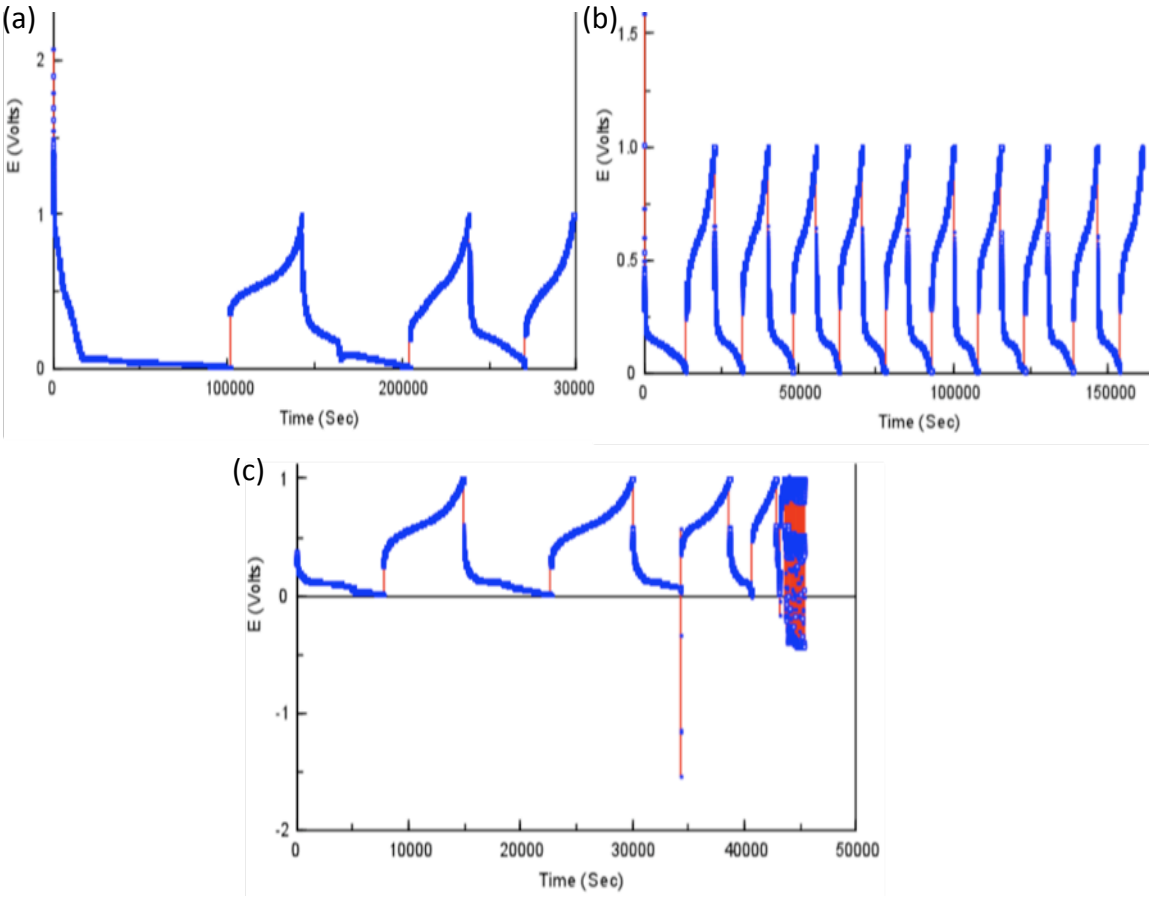

Figure 5-8: Charge-discharge cycling of the silicon-coated Li-ion battery electrode. Voltage is plotted as a function of time using a 50 mA/g current for the first three cycles (a), and using a 100 mA/g current for the next 10 cycles (b), as well as for the remaining cycles afterwards for (c).

In Figure 5-9, an SEM image of the pristine silicon-coated CNTs before any cycling has occurred, Figure 5-9(a), is compared to the same electrode's silicon-coated CNTs after the cycling from Figures 5-7 and 5-8 has occurred, Figure 5-9(b), at the same magnification. Figure 5-9(b) has some residual dried electrolyte between the silicon-coated CNTs, but the structure and integrity of the silicon coating seems much unchanged. Furthermore, after the cycling of the electrode, it can clearly be seen that the active material has delaminated from the bottom Mo current collector. This is clear in the inset digital photograph in Figure 5-9(b). An intact sample has an unbroken dark gray coloring, which corresponds to the silicon-coated CNT forest. However, the inset shows a circular shape within which there is no silicon-coated CNT forest remaining. Instead, we see the shiny metallic surface of the underlying molybdenum current collector layer.

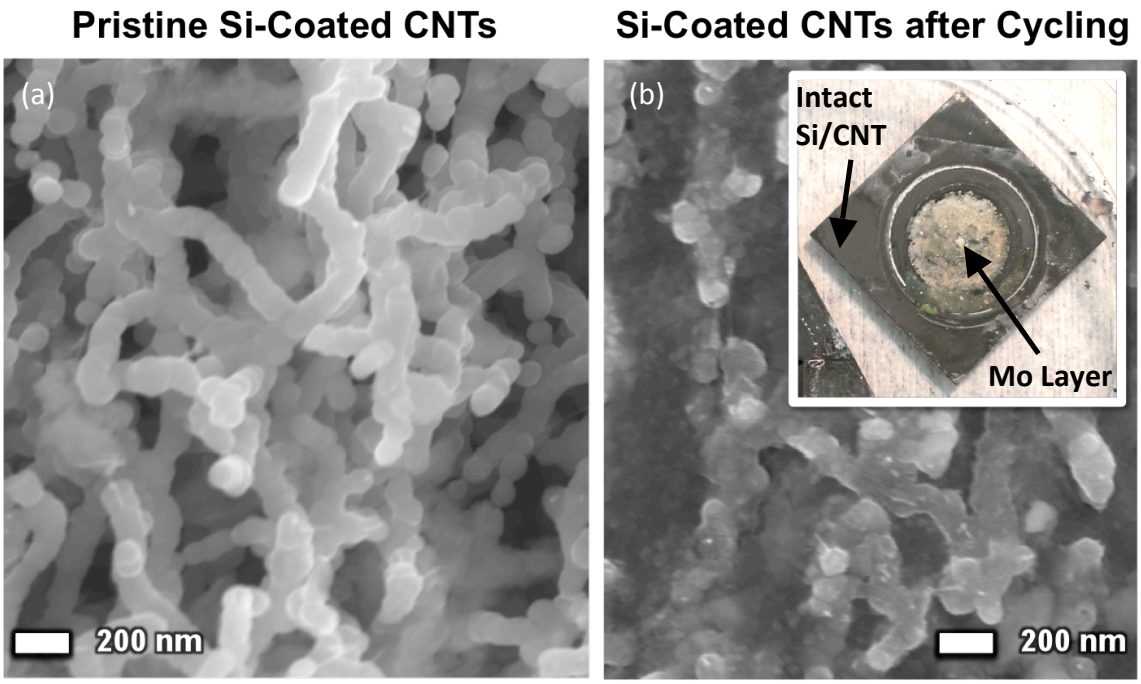

Figure 5-9: SEM images comparing a pristine, uncycled silicon-coated CNT forest in (a) to the same electrode material after cycling has occurred (b). Inset in (b) is a digital photograph of the entire sample electrode after cycling, showing the missing active material. The shiny metallic surface in the circular shape is the underlying current collector – a thin film of molybdenum evaporated onto the substrate wafer.

This Delamination is likely caused by the large volume change that silicon undergoes during the charge and discharge cycles. As the silicon coating is conformal, the silicon coats the substrate that that CNT forest is grown on as well. That is, the area on the substrate between the CNTs is also coated with a layer of silicon. With a thick enough layer, the silicon may expand and contract enough as to cleave the CNTs from their substrate – thus leaving behind only the molybdenum current collector in the inset of Figure 5-9(b). A longer cycling life and greater stability may be achieved by evaporating

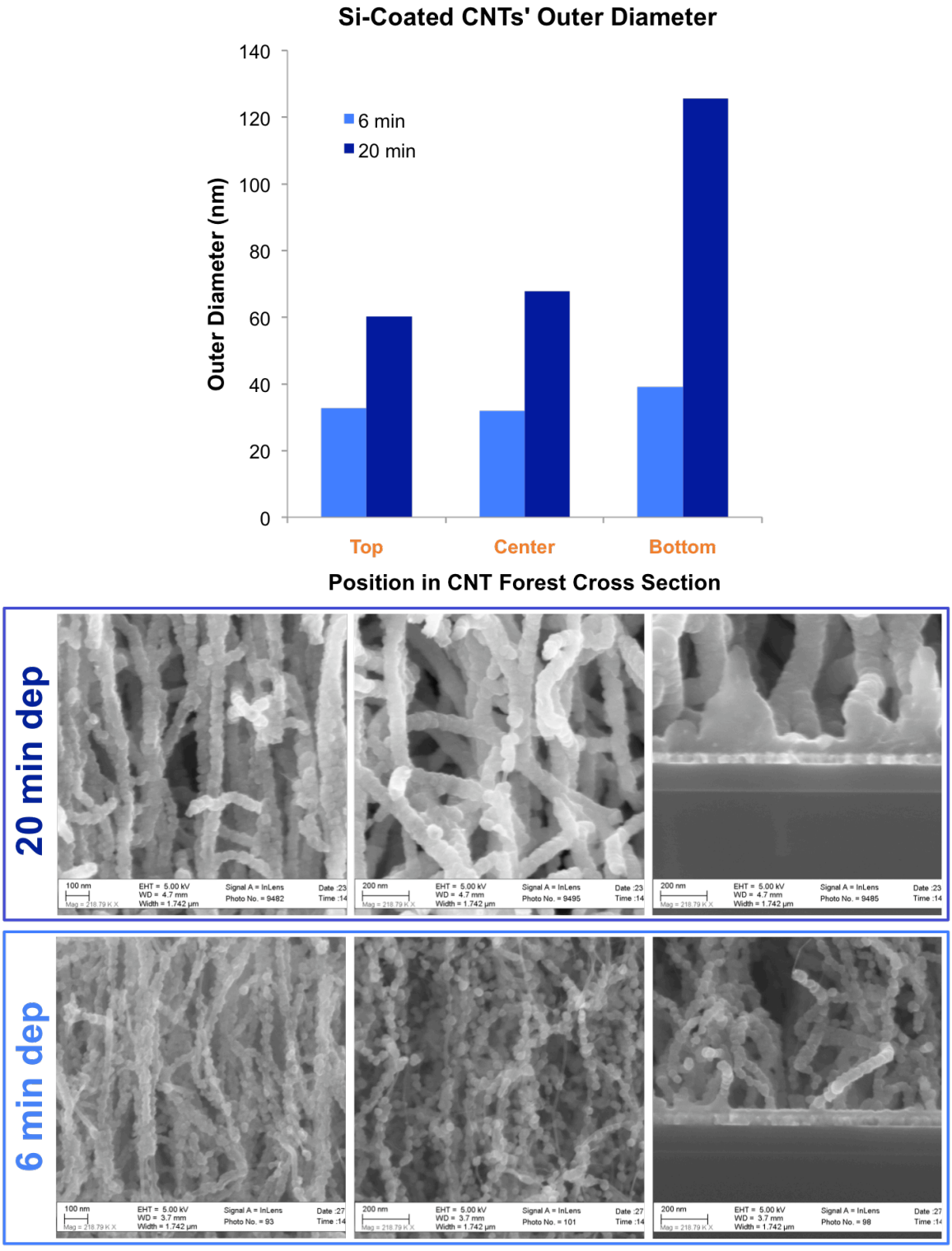

Figure 5-10: Total outer diameter of silicon coating on CNT forest electrodes, graphed for a 6 minute and 20 minute LPCVD deposition, (a). SEM images of the silicon-coated CNTs for a 20-minute deposition near the top (b), center (c), and bottom (d) of the CNT forest. Similarly, SEM images of the 6-minute deposition may be seen in (e) near the top, (f) center, and (g) bottom of the CNT forest.

a thinner layer of silicon onto the CNT forest, as this should relieve some of the stresses directed onto the CNT adhesion points on the Mo surface. This may be easily done simply by decreasing the process time during which the silane gas flows into the deposition chamber of the LPCVD furnace. Figure 5-10 shows the comparison between a 6-minute and a 20-minute silicon LPCVD deposition. A 6-minute deposition yields a 10 nm-thick coating, which may yield a longer cycling life for the silicon-coated CNT lithium ion battery electrode. However, more study needs to be made.

Conclusions

This chapter has detailed the facile way in which this body of work's vertically aligned carbon nanotube forest with an inherent connection to its underlying current collector may be used as a lithium ion battery electrode by coating the forest with a conformal layer of silicon. The electrode is fabricated and tested, and shows promise as a Li-ion battery electrode. The capacity reaches aplateau of 600 mAh/g, with a specific power and energy of 270 W/kg and 300 Wh/kg, respectively. The cycling life of the electrode may be improved by utilizing a thinner coating of silicon, as a thick coating at the bottom of the CNT forest leads to Delamination of the active material from the current collector layer after 20 charge-discharge cycles.

References

[1] Chenguang Liu, Zhenning Yu, David Neff, Aruna Zhamu, and Bor Z Jang, "Graphene-Based Supercapacitor with an Ultrahigh Energy Density," *Nano letters*, vol. 10, no. 12, pp. 4863-4868, Dec 2010.

[2] J.M Tarascon and M Armand, "Issues and challenges facing rechargeable lithium batteries," *Nature*, vol. 414, no. 6861, pp. 359-367, 2001.

[3] "BU-103: Global Battery Markets - An Overview of Battery Types," *Battery University*, Nov 2014. [Online]. http://batteryuniversity.com/learn/article/global_battery_markets

[4] P C Howlett, Douglas R Macfarlane, and A F Hollenkamp, "High Lithium Metal Cycling Efficiency in a Room-Temperature Ionic Liquid," *Electrochemical and Solid-State Letters*, vol. 7, no. 5, pp. A97-A101, Jan 2004.

[5] I Yoshimatsu, T Hirai, and J Yamaki, "Lithium Electrode Morphology during Cycling in Lithium Cells," *Journal of Electrochemical Science*, vol. 135, no. 10, pp. 2422-2427, Aug 1988.

[6] Vinodkumar Etacheri, Rotem Marom, Ran Elazari, Gregory Salitra, and Doron Aurbach, "Challenges in the development of advanced Li-ion batteries: a review,"

Energy & Environmental Science, vol. 4, no. 9, pp. 3243-3262, Jan 2011.

[7] Z Zhang, D Fouchard, and J R Rea, "Differential scanning calorimetry material studies- implications for the safety of lithium-ion cells," *Journal of Power Sources*, vol. 70, pp. 16-20, Nov 1998.

[8] Uday Kasavajjula, Chunsheng Wang, and A. John Appleby, "Nano- and bulk-silicon-based insertion anodes for lithium-ion secondary cells," *Journal of Power Sources*, vol. 163, no. 2, pp. 1003-1039, Jan 2007.

[9] L.F Cui, Y Yang, C.M Hsu, and Y Cui, "Carbon− Silicon Core− Shell Nanowires as High Capacity Electrode for Lithium Ion Batteries," *Nano letters*, vol. 9, no. 9, pp. 3370-3374, 2009.

[10] L.F Cui, L Hu, J.W Choi, and Y Cui, "Light-Weight Free-Standing Carbon Nanotube-Silicon Films for Anodes of Lithium Ion Batteries," *ACS nano*, vol. 4, no. 7, pp. 3671-3678, 2010.

[11] W Wang and P.N Kumta, "Nanostructured hybrid silicon/carbon nanotube heterostructures: Reversible high-capacity lithium-ion anodes," *ACS nano*, vol. 4, no. 4, pp. 2233-2241, 2010.

[12] R A Sharma and R N Seefurth, "Thermodynamic Properties of the Lithium-Silicon System," *Journal of the Electrochemical Society*, vol. 123, pp. 1763-1768, Sep 1976.

[13] B A Boukamp, G C Lesh, and R A Huggins, "All-Solid Lithium Electrodes with Mixed-Conductor Matrix," *Journal of the Electrochemical Society*, vol. 128, pp. 725-729, Sep 1981.

[14] C V D Marel, G J B Vinke, and W V D Lugt, "The Phase Diagram of the System Lithium-Silicon," *Solid State Communications*, vol. 54, pp. 917-919, May 1985.

[15] V Baranchugov, E Markevich, E Pollak, G Salitra, and D Aurbach, "Amorphous silicon thin films as a high capacity anodes for Li-ion batteries in ionic liquid electrolytes," *Electrochemistry Communications*, vol. 9, pp. 796-800, Mar 2007.

[16] T L Kulova, A M Skundin, Y V Pleskov, E I Terukov, and O I Kon'kov, "Lithium Intercalation in Thin Amorphous-Silicon Films," *Russian Journal of Electrochemistry*, vol. 42, no. 4, pp. 363-369, Nov 2006.

[17] T L Kulova, Y V Pleskov, A M Skundin, E I Terukov, and O I Kon'kov, "Lithium Intercalation into Amorphous-Silicon Thin Films: An Electrochemical-Impedance Study," *Russian Journal of Electrochemistry*, vol. 42, no. 7, pp. 708-714, Nov 2006.

[18] H Lin et al., "Twisted Aligned Carbon Nanotube/Silicon Composite Fiber Anode for Flexible Wire-Shaped Lithium-Ion Battery," *Advanced Materials*, vol. 26, pp. 1217-1222, Nov 2014.

[19] K Evanoff, A Magasinski, and J Yang…, "Nanosilicon-Coated Graphene Granules as Anodes for Li-Ion Batteries," *Advanced Energy Materials*, vol. 1, pp. 495-498, 2011.

[20] K Fu et al., "Aligned Carbon Nanotube-Silicon Sheets: A Novel Nano-architecture for Flexible Lithium Ion Battery Electrodes," *Advanced Materials*, vol. 25, pp. 5109-5114, Nov 2013.

[21] Y Fan, Q Zhang, Q Xiao, X Wang, and K Huang, "High performance lithium ion battery anodes based on carbon nanotube–silicon core–shell nanowires with controlled morphology," *Carbon*, vol. 59, pp. 264-269, Nov 2013.

[22] L Hu, H Wu, Y Gao, A Cao, and H Li…, "Silicon–Carbon Nanotube Coaxial Sponge as Li-Ion Anodes with High Areal Capacity," *Advanced Energy Materials*, vol. 1, pp. 523-527, Jan 2011.

[23] Wei Wang, Rigved Epur, and Prashant N Kumta, "Vertically aligned silicon/carbon nanotube (VASCNT) arrays: Hierarchical anodes for lithium-ion battery," *Electrochemistry Communications*, vol. 13, no. 5, pp. 429-432, May 2011.

[24] V.L Pushparaj et al., "Flexible energy storage devices based on nanocomposite paper," *Proceedings of the National Academy of Sciences*, vol. 104, no. 34, p. 13574, 2007.

[25] I Lahiri et al., "High Capacity and Excellent Stability of Lithium Ion Battery Anode Using Interface-Controlled Binder-Free Multiwall Carbon Nanotubes Grown on Copper," *ACS nano*, vol. 4, no. 6, pp. 3440-3446, 2010.

[26] M Inagakia, Hidetaka Konno, and Osamu Tanaike, "Carbon materials for electrochemical capacitors," *Journal of Power Sources*, vol. 195, no. 24, pp. 7880-7903, Dec 2010.

[27] L.F Cui, L Hu, J.W Choi, and Y Cui, "Light-Weight Free-Standing Carbon Nanotube-Silicon Films for Anodes of Lithium Ion Batteries," *ACS nano*, vol. 4, no. 7, pp. 3671-3678, 2010.

[28] L.F Cui, Y Yang, C.M Hsu, and Y Cui, "Carbon− Silicon Core− Shell Nanowires as High Capacity Electrode for Lithium Ion Batteries," *Nano letters*, vol. 9, no. 9, pp. 3370-3374, 2009.

[29] Candace K Chan et al., "High-performance lithium battery anodes using silicon nanowires," *Nature Nanotechnology*, vol. 3, no. 1, pp. 31-35, Jan 2008.

[30] W Wang and P.N Kumta, "Nanostructured hybrid silicon/carbon nanotube heterostructures: Reversible high-capacity lithium-ion anodes," *ACS nano*, vol. 4, no. 4, pp. 2233-2241, 2010.

[31] Y.Q Jiang, Q Zhou, and L Lin, "Planar MEMS Supercapacitor Using Carbon Nanotube Forests ," *Micro Electro Mechanical Systems, MEMS Conference 2009*, pp. 587-590, Mar 2009.

[32] M. Mastragostino, F. Soavi, and C. Arbizzani, "Ch. 16: Electrochemical Supercapacitors," in *Advances in Lithium Ion Batteries*. US: Springer, Kluwer Academic Publishers, Nov 2002, pp. 481 - 505.

[33] D. Berndt, "Electrochemical Energy Storage," in *Battery Technology Handbook*, 2nd ed.: CRC Press, Nov 2003.

Chapter 6: Concluding Remarks and Looking Forward

Chapter Summary

This chapter reviews the energy storage applications of aligned carbon nanotube (CNT) films discussed in this work, as well as some remarks on going forward.

Concluding Remarks

Not only are carbon nanotubes used in composite, lightweight structures for bicycle frames, data cables, antifouling boat hull paint, and electromagnetic shields, their excellent mechanical, thermal, and electrical properties also make them excellent candidates for use in electronics such as transistors and high power amplifiers [1]. Here, we utilize the high specific surface area characteristics of CNTs for possible applications in energy storage, such as in electrode structures within supercapacitors and secondary, or rechargeable, batteries.

Vertically aligned carbon nanotube forests are simple and quick to fabricate with a chemical vapor deposition process. The aligned structure of the forests aids in the diffusion of electrolyte ions during charging and discharging of the energy storage devices [2], and the bottom metal current collector made of a thin metallic film gives each carbon nanotube an inherent electrical connection to the current collector. When the bottom metal current collector, molybdenum, is evaporated onto a silicon dioxide substrate, the entire CNT forest that grows from the molybdenum (as well as the molybdenum itself) releases from the SiO_2 substrate in deionized water (Chapter 2). This thin, flexible carbon nanotube and Mo film can then be lifted out and transferred to a number of surfaces, to then be used as a supercapacitor electrode. A flexible supercapacitor electrode is made in this way when the CNT-Mo film is transferred to a flexible polymer substrate. This mechanical flexibility allows the energy storage device to be used in bendable electronics, as well as offering the ability to be rolled into a tight conformation for use in devices which have limited room for energy storage.

The amount of energy stored per square centimeter of device area is increased by the deposition of a conformal film of silicon onto each CNT in the forest. This is achieved by LPCVD, and doubles the energy density of the supercapacitor electrode with a 35 nm thick silicon coating (Chapter 3).

An increase in the electrochemical potential, or voltage window, of a supercapacitor can improve its power and energy density further. The widening of the potential is achieved by using a room-temperature ionic liquid electrolyte, which has a breakdown voltage of around 5 V. This is five times that of the aqueous electrolyte voltage windows (Chapter 4).

Finally, the same architecture that delivers benefits to a supercapacitor can also be utilized for a lithium ion battery. The high surface area, excellent conductivity of the CNTs, and silicon's extremely high lithium ion intercalation capacity promise long-lived

and energy-dense lithium ion electrodes. A vertically aligned carbon nanotube forest is conformally coated with silicon and electrochemically tested (Chapter 6). Further investigation into thinner silicon coatings should yield a longer cycling life.

Looking Forward

Notwithstanding the advances made in the realm of energy storage devices, there is still far more to be done. Although some devices, such as capacitors, have very high power densities, and others such as fuel cells have very high energy densities, it is difficult to manufacture a device that has both of these sought-after characteristics, and increasing one property normally comes at the expense of the other. The ultimate goal would be to have a cheap, lightweight, and environmentally friendly energy storage device that can charge in minutes, and contain a large amount of energy.

Carbon nanotubes show great promise in this area, and much research is being conducted into using these nanostructures as the active material in both supercapacitors and batteries, which cover a good deal of territory between high energy density and high power density [3-7], as well as being combined with silicon for use in lithium-ion batteries [8-10].

The work presented herein may be further improved through a number of ways. First, the speed of the lift off process may be increased by patterning through holes in the metal layers deposited upon the oxidized silicon wafer before CNT growth, as seen in Figure 6-1. This will allow the liftoff solution to penetrate between the SiO_2 and Mo layers in a more facile manner, and thus decrease process time, and allow for much larger electrodes to be fabricated.

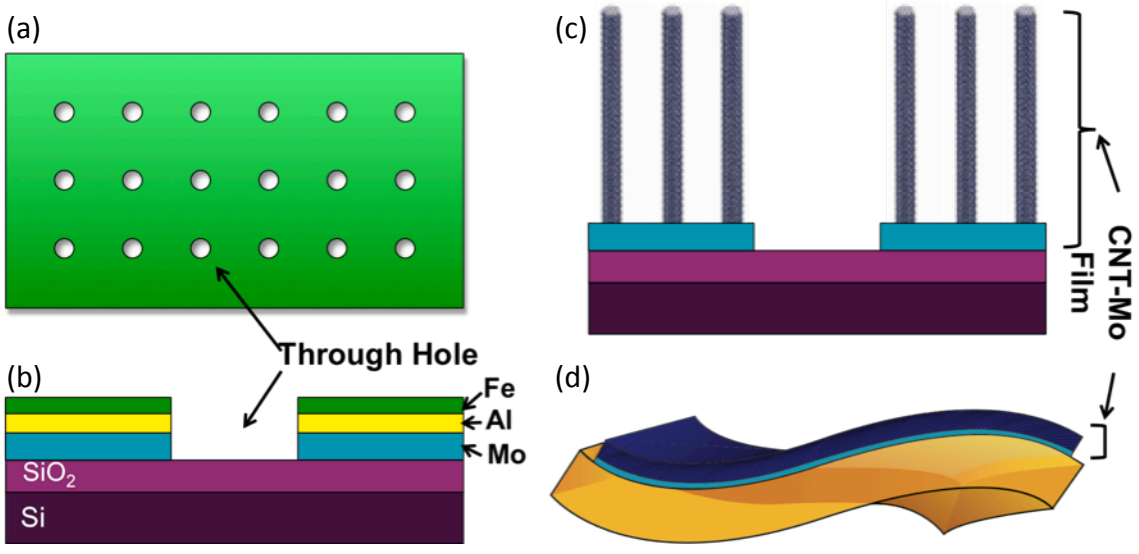

Figure 6-1: (a) Illustration of hole patterning through metal deposited layers, to increase speed of the CNT-Mo film liftoff. (b) Cross-section of hole pattern. (c) CNT growth after patterning. (d) CNT-Mo film lifted onto flexible polymer substrate.

In addition, the concepts in chapters 2 and 3 may be combined to create a silicon-coated electrode that is both flexible and has an increased surface area for supercapacitor applications. This same architecture may also be used as a flexible lithium ion battery electrode. In order to fabricate this silicon-coated flexible electrode, an LPCVD process may be used to deposit silicon onto the densified CNT forest after the CNT-Mo film has been lifted from its host substrate, as in Figure 6-2. Alternatively, for temperature-

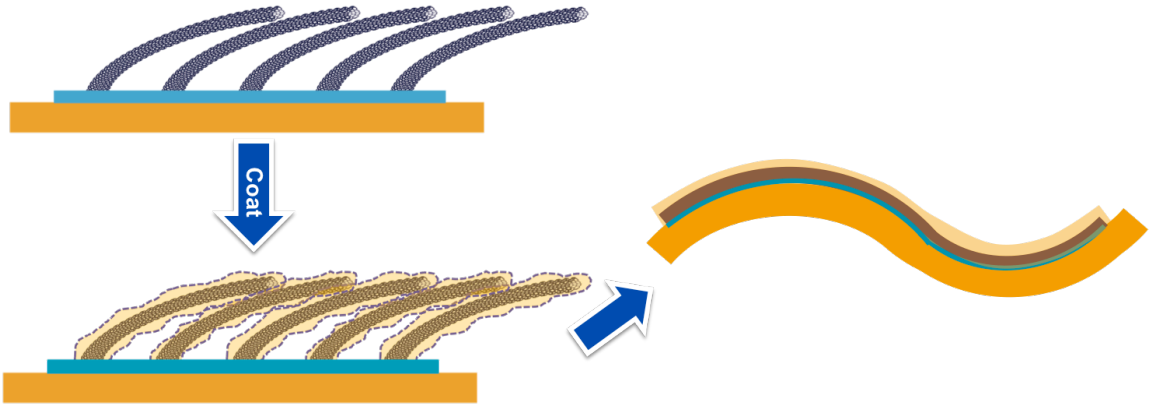

Figure 6-2: Illustration showing the sequence of events for creating a flexible silicon-coated electrode for supercapacitor and lithium ion battery applications, following the liftoff process detailed in chapter 2.

sensitive (e.g. polymer) target substrates, the CNT forest may be densified before liftoff, coated with silicon, diced into appropriate sizes, then lifted onto a polymer substrate.

Furthermore, in order to truly evaluate these electrodes for supercapacitor and lithium ion battery applications, the electrodes should be tested in the conformation in which they will be used in devices [11]. For instance, if they are to be used in flexible

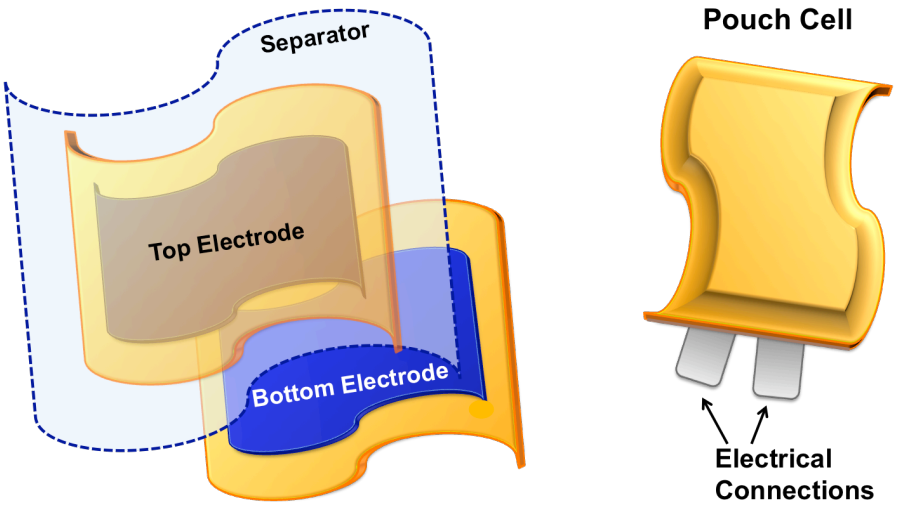

Figure 6-3: Schematic illustrating two flexible electrodes packaged into a pouch cell, with a separator in between to prevent shorting while allowing electrolyte ion transport.

electronics, flexible pouch cells may be constructed using the CNT-Mo film electrodes, as illustrated below in Figure 6-3, and thereafter tested in those conformations.

Finally, as with any new technology, a full investigation into the scalability and environmental impacts of the bare and silicon-coated carbon nanotube material should be addressed. It is one thing to yield fantastic results in a research vein, but another to scale up the production of that material or device, and retain those same characteristics.

References

[1] M. F. L De Volder, S. H Tawfick, R. H Baughman, and A. J Hart, "Carbon Nanotubes: Present and Future Commercial Applications," *Science*, vol. 339, pp. 535-539, Feb 2013.

[2] H Zhang, G Cao, and Y Yang, "Electrochemical properties of ultra-long, aligned, carbon nanotube array electrode in organic electrolyte," *Journal of Power Sources*, vol. 172, no. 1, pp. 476-480, 2007.

[3] H Lin et al., "Twisted Aligned Carbon Nanotube/Silicon Composite Fiber Anode for Flexible Wire-Shaped Lithium-Ion Battery," *Advanced Materials*, vol. 26, pp. 1217-1222, Nov 2014.

[4] Y Fang et al., "Self-supported supercapacitor membranes: Polypyrrole-coated carbonnanotube networkse nabled by pulsed electrodeposition," *Journal of Power Sources*, vol. 195, pp. 674-679, Aug 2010.

[5] K Evanoff et al., "Ultra Strong Silicon-Coated Carbon Nanotube Nonwoven Fabric as a Multifunctional Lithium-Ion Battery Anode," *ACS nano*, vol. 6, no. 11, pp. 9837-9845, Oct 2012.

[6] K H An et al., "Supercapacitors using single-walled carbon nanotube electrodes," *Advanced Materials*, vol. 13, no. 7, pp. 497-500, Nov 2001.

[7] Y Fan, Q Zhang, Q Xiao, X Wang, and K Huang, "High performance lithium ion battery anodes based on carbon nanotube–silicon core–shell nanowires with controlled morphology," *Carbon*, vol. 59, pp. 264-269, Nov 2013.

[8] X Su et al., "Silicon-Based Nanomaterials for Lithium-Ion Batteries: A Review," *Advanced Energy Materials*, vol. 4, p. 1300882, Jan 2014.

[9] Hui Wu et al., "Stable cycling of double-walled silicon nanotube battery anodes through solid-electrolyte interphase control," *Nature Nanotechnology*, vol. 7, no. 5,

pp. 310-315, Mar 2012.

[10] Jung-Keun Yoo, Jongsoon Kim, Yeon Sik Jung, and Kisuk Kang, "Scalable Fabrication of Silicon Nanotubes and their Application to Energy Storage," *Advanced Materials*, vol. 24, no. 40, pp. 5452-5456, Jul 2012.

[11] M. D., Ruoff, R. S. Stoller, "Best practice methods for determining an electrode material's performance for ultracapacitors," *Energy & Environmental Science*, vol. 3, pp. 1294–1301, 2010.